Comparison of resting state functional networks in HIV infected and uninfected children at age 9 years

by

Werner Heinrich Stoltsz

STLWER001

SUBMITTED TO THE UNIVERSITY OF CAPE TOWN

in fulfilment of the requirements for the degree:

Master of Science in Biomedical Engineering.

Faculty of Health Sciences

UNIVERSITY OF CAPE TOWN

University of Cape Town

January 2018

Supervisor:

Professor Ernesta M. Meintjes

Co-supervisor:

Dr Lindie du Plessis

The copyright of this thesis vests in the author. No quotation from it or information derived from it is to be published without full acknowledgement of the source. The thesis is to be used for private study or non-commercial research purposes only.

Published by the University of Cape Town (UCT) in terms of the non-exclusive license granted to UCT by the author.

University of Cape Town

Declaration

I, WERNER HEINRICH STOLTSZ, hereby declare that the work on which this dissertation/thesis is based is my original work (except where acknowledgements indicate otherwise) and that neither the whole work nor any part of it has been, is being, or is to be submitted for another degree in this or any other university.

I empower the university to reproduce for the purpose of research either the whole or any portion of the contents in any manner whatsoever.

Signature: Signed by candidate

Date: 13 January 2018

For Karen, my beautiful wife and my best friend.

And for Jesus Christ, the reason for this work's fruition and its significance.

Acknowledgements

My sincere thanks go to my supervisor, Professor Ernesta Meintjes, whose expertise guided this thesis, who was always willing to enter into constructive debate with patience, and from whom I have learnt much about research and research ethics. And to my co-supervisor, Dr Lindie du Plessis, who familiarised me with many of the practicalities of fMRI processing, spent many hours reviewing my writing, acted as a daily sounding board, and who was a constant encourager.

I am grateful to Dr Martha Holmes and Dr Frances Robertson, who contributed ideas and who frequently fielded my questions about the CHER clinical trial.

I would like to thank Professor Francesca Little for her consultation in Statistics.

I am also grateful to Dr Barbara Laughton, who introduced me to the basics of neuropsychological measures and frequently sourced clinical and neuropsychological measures for our sample.

Big thanks go to Dr Chris Warton, who spent not a few hours providing neuroanatomical consultation, and who, through his wonder at God's design of the human body and his talent for story-telling, has ignited my excitement about the human brain more than anyone else.

Finally, to Karen, Mamma, Pappa and Herman: thank you for your wondrously faithful love, support and grounding, which inspired the completion of this work.

Abstract

Over 2.5 million children are infected with HIV, the majority of whom reside in Sub-Saharan Africa. Treatment coverage is steadily gaining momentum, reducing mortality and morbidity. Yet little is known about brain development in HIV-infected (HIV+) children who are on highly-active antiretroviral therapy (ART), with viral load suppression from a young age. Here, we use resting state fMRI (rs-fMRI) to examine the impact of HIV and ART on the development of functional networks in 9-year-old vertically HIV-infected children compared to age-matched controls of similar socioeconomic status.

We present analyses for a sample of 40 HIV+ (9.2 ± 0.20 years; 16 males) children from the Children with HIV Early Antiretroviral (CHER) clinical trial (Cotton et al. 2013; Violari et al. 2008) and 24 uninfected (12 exposed; 12 males; 9.6 ± 0.52 years) controls from an interlinking vaccine trial (Madhi et al. 2010). Scans were performed at the Cape Universities Body Imaging Centre (CUBIC) in Cape Town, South Africa.

We investigated HIV-related differences in within- and between-network functional connectivity (FC) using independent component analysis (ICA) and seed-based correlation analysis (SCA). For SCA, seeds were placed in the structural core, in regions implicated in HIV-related between-group differences at age 7 years, and in regions associated with neuropsychological domains impaired in our cohort. In addition, we evaluated associations of past and present immune health measures with within-network connectivity using ICA.

We found no HIV-related intra-network FC differences within any ICA-generated RSNs at age 9 years, perhaps as a result of within-network connectivity not being sufficiently robust at this age. We found a positive association of CD4%, both current and in infancy, with functional integration of left lobule 7 into the cerebellum network at age 9 years. Long-term impact of early immune health supports recently-revised policies of commencing ART immediately in HIV+ neonates.

Compared to uninfected children, HIV+ children had increased FC to several seeds. Firstly, to seeds associated with the planning and visual perception neuropsychological domains. Secondly, to structural core seeds in the extrastriate visual cortex (of the medial visual network) and the right angular gyrus (of the temporoparietal network). Finally, to left paracentral (somatosensory network) and right precuneus (posterior DMN) seeds previously revealing between-group differences at age 7 years. The connections with greater FC in HIV+ children may variously indicate functional recruitment of additional brain capacity, immature excess of short-range connections, and/or immature excess of between-network connections.

In conclusion, despite early ART and early virologic suppression, HIV+ children demonstrate instances of abnormal FC at age 9 years. Disruption to visual cortex is marked, consistent with indications from neuropsychological testing that visual perception is disrupted. The profile of HIV- and/or ART-related effects on FC differs considerably between the two ages of 7 and 9 years, but both show characteristics of immature functional organisation compared with age-matched controls.

Contents

Declaration ii
Acknowledgements iv
Abstract v
List of Figures x
List of Tables xii
List of Abbreviations xiv
1 Introduction 1
2 Prior HIV Neuroimaging Research: Results and Significance 5
2.1.1 Neuroimaging in vertically infected children and adolescents 5
2.1.2 Task-based functional MRI in adults 6
2.1.3 Resting state functional MRI in children and adults 7
3 Hypotheses 10
4 Pediatric HIV: Clinical Background 12
4.1 ART: 20 years of effective treatment 12
4.2 Treatment of vertically infected children 12
4.3 Mother-to-child transmission 13
4.4 HIV pathogenesis in the periphery 14
4.5 HIV and antiretroviral drugs in the brain 15
4.5.1 Penetration of the virus 15
4.5.2 Penetration of antiretroviral drugs 16
4.5.3 Neurotoxicity of antiretroviral drugs 16
4.6 Cognitive and behavioural profile of vertically infected children on ART 17
4.7 Measures of immune health in HIV infection 19
5 Principles of Resting State Functional MRI 21
5.1 A primer on magnetic resonance physics 21
5.2 The BOLD signal and its neurobiological origins 24
5.3 Task-based and resting state functional MRI 26
5.4 Artefactual (non-neuronal) contributions to the functional MRI signal 27
5.5 Methods for extracting resting state functional connectivity 28
5.6 Interpretations of functional connectivity 29
5.7 Common resting state networks and their behavioural correlates 31
5.7.1 The default mode network 31
5.7.2 The cognitive control group 34
5.7.3 Sensory and motor networks 37
5.7.4 Resting state networks in children, and age-related changes 39

6 Methodology 41
6.1 Study cohort 41
6.2 MRI acquisition 42
6.3 Preprocessing 43
6.3.1 Pipeline overview 43
6.3.2 EPI run truncation 45
6.4 Exclusion criteria 47
6.4.1 Within-scanner motion criteria 47
6.4.2 Other criteria 49
6.5 Statistical analysis 49
6.5.1 Model design 50
6.5.2 Independent component analysis 55
6.5.3 Seed-based correlation analysis 59
7 Results 64
7.1 Sample characteristics 64
7.2 Resting state networks revealed by group independent component analysis 66
7.3 HIV+ vs. uninfected functional connectivity comparisons 69
7.3.1 ICA-revealed within-network differences 69
7.3.2 Functional connectivity with seeds related to neuropsychological domains 69
7.3.3 Functional connectivity with seeds in the structural core 75
7.3.4 Functional connectivity with seeds revealing HIV-related differences at age 7 years . 81
7.4 ICA-revealed associations of within-network connectivity with immune measures 88
7.5 Other exploratory analyses 90
8 Discussion 93
8.1 A caution on qualitative comparisons 93
8.2 ICA-generated resting state networks: reliability and developmental trajectory 93
8.2.1 Default mode network 94
8.2.2 Control and attention networks 94
8.2.3 Visual networks 96
8.2.4 Motor and somatosensory networks 97
8.2.5 Cerebellar network 97
8.2.6 Temporoparietal network 98
8.2.7 Types of functional connections evidenced by networks 98
8.3 HIV+ vs. uninfected functional connectivity comparisons 98
8.3.1 ICA-revealed within-network differences 98
8.3.2 Functional connectivity with seeds related to neuropsychological domains 99

8.3.3 Functional connectivity with seeds in the structural core 103
8.3.4 Functional connectivity with seeds revealing HIV-related differences at age 7 years 106
8.4 ICA-revealed associations of within-network connectivity with immune measures 107
8.5 Other exploratory analyses 110
8.6 Vulnerability to HIV of functional connectivity in visual regions 111
9 Limitations 112
10 Conclusion 115
Works cited 117
Appendix A: Parameters passed to afni_proc.py 143
Appendix B: Details of preprocessing blocks and supporting theory 144
Appendix C: Cluster-size thresholds employed in independent component analysis 149
Appendix D: Nuisance features observed in group components revealed by group independent component analysis 150
Appendix E: Associations of functional connectivity with immune measures, before controlling for age voxelwise 151

List of Figures

Figure 1: Visualisation of the default mode network (DMN)..... 33

Figure 2: Visualisation of networks involved in cognition and control..... 35

Figure 3: Visualisation of networks involved in low-level sensory and motor processing 38

Figure 4: Pipeline for the preprocessing of all participants' resting state (EPI) data. 44

Figure 5: The in-house algorithm employed to truncate participants' resting state (EPI) runs to the 140-volume interval containing the least in-scanner motion..... 46

Figure 6: The number of subjects that would be excluded under motion criteria, evaluated over a meshgrid of threshold value combinations. 48

Figure 7:Summary of the analyses performed in this study. 50

Figure 8: Group resting state networks identified at ages 7 years. Valid networks were identified from a 20-dimensional decomposition performed using FSL's MELODIC (Beckmann & Smith 2004), and were thresholded at Z > 3 62

Figure 9: Group resting state networks revealed by independent component analysis..... 67

Figure 10: Seeds assocaited with neuropsychological domains showing impairment in HIV+ children at age 5 or 7 years, and used to investigate differences in seed-to-whole-brain connectivity between infected and uninfected children at age 9 years. 71

Figure 11: Each panel shows a region (blue) of significantly increased connectivity to a seed (not shown) in HIV+ compared to uninfected (HIV-) children (perintatally-exposed and unexposed), where seeds correspond with neuropsychological domains showing significant HIV-related impairment at ages 5 or 7 years. 74

Figure 12: Glass-brain renderings of seeds (indicated with black arrow tips) and clusters between which functional connectivity is greater in HIV+ compared to uninfected children, for the results detailed in Table 7 and Figure 11. Seeds are associated with neuropsychological domains showing HIV-related impairment. 75

Figure 13: Seeds placed in the structural core and used to investigate differences in seed-to-whole-brain connectivity between HIV+ and uninfected (perintatally-exposed and unexposed) children.... 77

Figure 14: Each panel shows a cluster (blue) of significantly increased connectivity to a seed (not shown) in HIV+ children compared to uninfected (perintatally-exposed and unexposed) children, where seeds were placed in the structural core (cf. Hagmann et al. 2008). 80

Figure 15: Glass-brain renderings of seeds (indicated with a black arrow tip) and clusters, for the results detailed in Table 9 and Figure 14 (regions revealing significantly increased connectivity to 'structural core' seeds in HIV+ compared to uninfected children)..... 81

Figure 16: Seeds placed, at age 9 years, at the same coordinates as seeds revealing significant differences in seed-to-whole-brain connectivity between HIV+ and uninfected (perintatally-exposed and unexposed) children at age 7 years. 83

Figure 17: Comparison of group resting state networks revealed by independent component analysis (ICA) at ages 7 (left) and 9 (right) years; specifically, those networks where the network peak had functional projections that differed significantly between HIV+ and uninfected children at age 7 years. Seeds were placed at these peaks at age 9 years. 84

Figure 18: Each panel shows a cluster (blue) with significantly greater connectivity to a seed (not shown) in HIV+ compared to uninfected (perinatally-exposed and unexposed) children. Seeds were placed in regions revealing significant between-group differences at age 7 years..... 87

Figure 19: Glass-brain renderings of seeds (indicated by a black arrow tip) and clusters, for the results detailed in Table 11 and Figure 18 (regions revealing significantly increased connectivity to a seed in HIV+ compared to uninfected children, where seeds were placed at coordinates revealing significant between-group differences at age 7 years). 88

Figure 20: (Left) Two nearby clusters (blue) within the cerebellar resting state network (hot colours) where better immune health, both at enrolment and at age 9 years, is associated with increasing within-network connectivity at age 9 years..... 90

Figure 21: (Left) One cluster (shown in blue) within the medial visual network (hot colours) demonstrated lower within-network connectivity in HIV-exposed uninfected (HEU) children compared to unexposed (HU) children..... 92

Figure 22: Separate mean spatial maps for the HIV+ and uninfected groups, obtained by performing one-sample t-tests on subject-specific maps estimated by dual regression, and controlling the family-wise error rate at 5% through correction for multiple voxel comparisons. 105

List of Tables

Table 1: Covariates included in the voxelwise model for each analysis performed in this study. 52

Table 2: Meta-analyses of functional MRI activation studies were carried out using Neurosynth (Yarkoni et al. 2011), to identify brain regions selectively involved in neuropsychological domains where we have previously found impairment in HIV+ children from this cohort (Laughton et al. 2017; Merkle 2015). For each meta-analysis, the query term input to Neurosynth, along with the number of studies contributing to the resultant statistical inference map, is given. 60

Table 3: Sample characteristics of HIV+ and uninfected groups. 65

Table 4: Sample characteristics of the HIV-unexposed uninfected (HU) and HIV-exposed uninfected (HEU) groups. 66

Table 5: Topological descriptions of the 12 resting state networks (RSNs) revealed by group ICA, as visualized in Figure 9. 68

Table 6: Seeds associated with neuropsychological domains showing abnormalities in HIV+ children at age 5 or 7 years, and used to investigate differences in seed-to-whole-brain connectivity between HIV+ and uninfected children (perintatally-exposed and unexposed) at age 9 years using seed-based correlation analysis (SCA). 70

Table 7: Size and peak coordinates of regions showing significantly increased functional connectivity to seeds in HIV+ children compared to uninfected (HIV-) children (perintatally-exposed and unexposed), obtained using seed-based correlation analysis (SCA). Seeds correspond with neuropsychological domains showing significant between-group differences at ages 5 or 7 years (Laughton et al. 2017; Merkle 2015). 73

Table 8: Seeds placed in the structural core and used to investigate differences in seed-to-whole-brain connectivity between HIV+ and uninfected (perinatally-exposed and unexposed) children using seed-based correlation analysis (SCA). 76

Table 9: Size and peak coordinates of regions showing significantly increased connectivity to seeds in HIV+ compared to uninfected (HIV-) children (perintatally-exposed and unexposed), obtained using seed-based correlation analysis (SCA). One seed was placed at the peak of each ICA-generated group resting state network that had its peak situated in the structural core, as defined by Hagmann et al. (2008). 79

Table 10: Seeds placed, at age 9 years, at the same coordinates as seeds revealing significant differences in seed-to-whole-brain connectivity between HIV+ and uninfected (perintatally-exposed and unexposed) children at age 7 years. 82

Table 11: Size and peak coordinates of regions showing significantly greater functional connectivity to seeds in HIV+ children compared to uninfected (HIV-) children (perintatally-exposed and unexposed) at age 9 years, obtained using seed-based correlation analysis (SCA). These seeds were placed at the same coordinates as seeds revealing significant between-group differences at age 7 years (Toich et al. 2017). 86

Table 12: Size and peak coordinates of two nearby regions showing significant association of immune health with functional integration into the cerebellar network (obtained using ICA)..... 89

Table 13: Size and peak coordinates of a region in the medial visual network having significantly lower within-network connectivity (obtained using ICA) in HIV-exposed uninfected (HEU) children compared to HIV-unexposed uninfected (HU) children. 91

List of Abbreviations

2-D	2-dimensional
3-D	3-dimensional
4-D	4-dimensional
AIDS	acquired immunodeficiency syndrome
ART	[highly-active] antiretroviral therapy/treatment
ARV	antiretroviral [drugs]
B_0	main static magnetic field [of MRI scanner]
BBB	blood-brain barrier
BOLD	blood oxygen level-dependent [signal]
BVN	blood vessel network
CBF	cerebral blood flow
CD4%	the percentage of circulating lymphocytes that are $CD4^+$ T lymphocytes
$CD4^+$	absolute count of $CD4^+$ T lymphocytes in a sample of blood plasma
CD4+:CD8+	ratio of the counts of $CD4^+$ T lymphocytes and $CD8^+$ T lymphocytes
CHER	Children with HIV Early Antiretroviral [clinical trial]
CNS	central nervous system
CSF	cerebrospinal fluid
CT	computed tomography
CUBIC	Cape Universities Body Imaging Centre
DMN	default mode network
DNA	deoxyribonucleic acid
DTI	diffusion tensor imaging
EPI	echo planar imaging (the imaging sequence employed to obtain fMRI data)
FC	functional connectivity

FDR	false discovery rate
fMRI	functional magnetic resonance imaging
FoV	field of view
FA	fractional anisotropy (DTI measure)FSL FMRIB Software Library
FWHM	full width at half maximum
GLM	general linear model
H	hydrogen
HbO	oxygenated haemoglobin
HbR	deoxygenated haemoglobin
HEU	HIV-exposed uninfected
HIV	human immunodeficiency virus
HIV+	HIV-infected
HU	HIV-unexposed uninfected
IC	independent component
ICA	independent component analysis
IFOF	inferior fronto-occipital fasciculus
ILF	inferior longitudinal fasciculus
IQR	interquartile range
KABC-II	Kaufman Assessment Battery for Children
M_0	net tissue magnetisation (induced parallel to the main magnetic field, $\boldsymbol{B_0}$)
M_{xy}	transverse component of $\boldsymbol{M_0}$
M_z	longitudinal component of $\boldsymbol{M_0}$
MD	mean diffusivity/diffusion (DTI measure)
MELODIC	Multivariate Exploratory Linear Optimized Decomposition into Independent Components (FSL program for ICA)
MEMPRAGE	Multiecho Magnetization Prepared Rapid Gradient Echo

MRA	magentic resonance angiography
MRI	magnetic resonance imaging
MRS	magnetic resonance spectroscopy
MTCT	mother-to-child transmission
NNRTI	non-nucleoside reverse transcriptase inhibitors
NRTI	nucleoside reverse transcriptase inhibitors
PCR	plasma polymerase chain-reaction [viral load test]
PET	positron emission tomography
PFC	prefrontal cortex
RF	radiofrequency
RNA	ribonucleic acid
ROI	region of interest
rs-fMRI	resting state functional magnetic resonance imaging
RSN	resting state network
SCA	seed-based correlation analysis
SD	standard deviation
SMA	supplementary motor area
SSA	Sub-Saharan Africa
T_1	time constant for 'spin-lattice' relaxation (recovery of longitudinal magnetisation, $\boldsymbol{M_z}$)
T_2	time constant for 'spin-spin' relaxation (decay of transverse magnetisation, $\boldsymbol{M_{xy}}$)
T_2*	T_2 after adjustment for magnetic susceptibility of tissues and inhomogeneities in the main magnetic field
TE	echo time
TF-IDF	term frequency-inverse document frequency

TI	inversion time
TR	repetition time
VL	[HIV plasma] viral load

1 Introduction

Over 2.5 million children live with the human immunodeficiency virus or the associated acquired immune deficiency syndrome (HIV/AIDS) - the majority of whom reside in Sub-Saharan Africa (SSA) (UNAIDS 2015b; UNAIDS 2015a). Infection is largely by mother-to-child transmission (MTCT). The use of highly active antiretroviral therapy[1] (ART) has been shown to reduce mortality, and improve immunological and neurodevelopmental outcomes in HIV-infected (HIV+) children (Lindsey et al. 2007; Chiriboga et al. 2005). Treatment advances have led to the first groups of vertically infected children (that is, children acquiring the virus via MTCT, either in utero or during the perinatal period) now entering into late adolescence (Tassiopoulos et al. 2016).

Treatment coverage in SSA is steadily gaining momentum: between 2009 and 2014, the percentage of children living with HIV who received ART rose from 10% to 31% among the 21 priority countries of SSA (UNAIDS 2015b). It follows that the number of HIV+ children with viral load suppression from a young age has been, and can be expected to continue, rising. Yet we know very little about the long-term neurological development of such children.

Neurodevelopment is of particular relevance, as the virus enters the central nervous system (CNS) soon after infection and here produces a compartmentalised population, causing the CNS to act as a viral reservoir (Van Rie et al. 2007). Although ART is designed to cross the blood-brain barrier (BBB) in order to be active within the CNS (McCoig et al. 2002), the degree to which this is achieved is variable (Letendre et al. 2008) . Furthermore, there is ongoing research into the potential neurotoxic effects of long-term exposure to ART (Shah et al. 2016; Robertson et al. 2012). Early in the HIV epidemic, encephalopathy was the first AIDS-defining event in a significant fraction of children (Vincent et al. 1989; Cooper et al. 1988), and was diagnosed at the highest rate in infancy and early childhood (Tardieu et al. 2000; Lobato et al. 1995; Janssen et al. 1992). It is therefore reasonable to suspect that

[1] ART is generally defined as a combination therapy consisting of at least three different antiretroviral (ARV) drugs from two different classes. We employ the more contemporary shortened abbreviation, rather than HAART or cART.

the developing CNS of children is particularly susceptible to the effects of HIV and ART toxicity. In sum, there is a strong call to further explore the nature and pathophysiology of HIV- and ART-mediated abnormalities in the neurodevelopment of children.

In the absence of early (before indications of immunosuppression) effective treatment, impacts of HIV infection on an immature and developing brain frequently include static or progressive HIV encephalopathy, apparent as missed or lost motor, mental and language developmental milestones, retarded brain growth, and pathological reflexes (Walker et al. 2013; Cooper et al. 1998; Epstein et al. 1986). With the availability of ART, encephalopathy is now rare, being diagnosed in less than 2% of children on standard treatment regimens (Chiriboga et al. 2005). Yet subtle deficits in neurodevelopmental outcomes (such as visual perception and fine motor skills), executive and cognitive function (such as global cognitive functioning, cognitive regulation, attentional flexibility, and visuospatial working memory), as well as processing speed, remain common (Laughton et al. 2017; Nichols et al. 2015; Garvie et al. 2014; Koekkoek et al. 2008; Jeremy et al. 2005).

Neuroimaging, and particularly the set of emerging variants of magnetic resonance imaging (MRI) techniques, is well suited to non-invasively detect subtle changes in brain anatomy, function, metabolite concentrations and connectivity (Thompson & Jahanshad 2015). The sensitivity of neuroimaging enables the identification of early changes missed by neuropsychological testing (Ernst et al. 2002). Yet the existing body of pediatric HIV neuroimaging literature is relatively small, and several limitations in study design make it difficult to draw conclusions on the aetiology, profile, and response to treatment of neurocognitive abnormalities. The majority of studies have a large age range (3 to 12 years) in their cohorts (Iqbal et al. 2016; Donald et al. 2015; Hoare et al. 2015; Sarma et al. 2014; Hoare et al. 2012; Nagarajan et al. 2012; Depas et al. 1995). This precludes conclusions on how neuroimaging-indicated effects of HIV (measured cross-sectionally) are parameterised by stage of neurodevelopment. Characteristics and incidence of HIV-related neurologic and neurocognitive effects vary with age in childhood, likely due to the rapid brain development during this period (Van

Rie et al. 2007). Another limitation is that many pediatric HIV neuroimaging studies do not include an HIV-uninfected group (Hoare et al. 2015; Donald et al. 2015; Andronikou et al. 2014; Van Arnhem et al. 2013; Depas et al. 1995) as comparison. Those that do include uninfected controls often lack a subgroup of children born uninfected to HIV+ mothers (HIV-exposed uninfected, HEU), in addition to children born to uninfected mothers (HIV-unexposed uninfected, HU) (Yadav et al. 2017; Iqbal et al. 2016; Sarma et al. 2014; Hoare et al. 2012; Nagarajan et al. 2012). This makes it difficult to isolate effects of perinatal exposure to HIV/ART from ongoing exposure, and to isolate primary effects of HIV (and ART) toxicity from secondary effects of viremia (detectable levels of HIV in the blood) and compromised immunity.

The observed impairment in neurocognitive development and performance among HIV+ children suggests neural abnormalities in this group. To better understand these abnormalities at the level of large-scale architecture, we use resting state functional MRI (rs-fMRI) to explore functional connectivity (FC): the coactivation of separated brain regions, as revealed by covariation in spontaneous neuronal activity. Using various analysis techniques, FC can be used to map large scale neural networks in the resting state (resting state networks, RSNs), which consist of anatomically separated but functionally integrated regions, and which largely correspond with sets of regions known (from clinicopathological[2] studies or task-based imaging) to coactivate during goal-oriented behaviour (Rosazza & Minati 2011; Laird et al. 2011). Resting state analysis is appropriate to a pediatric study, as only a single MRI scan (of approximately six minutes) is required to examine whole-brain connectivity, as opposed to a set of scans under a variety of stimuli or task conditions. Furthermore, factors such as attention and language comprehension which may confound task-based measurements in a pediatric cohort, are avoided. Critically, there is strong evidence to suggest that

[2] Studying the signs and symptoms associated with the pathology of particular brain regions. This led to the earliest 'mappings' of behaviour to neuroanatomy.

the brain's full repertoire of function is open to investigation when the brain is not engaged in goal-directed behaviour (Smith et al. 2009).

The HIV+ cohort studied here was recruited at birth into the (now-completed) Children with HIV Early Antiretroviral (CHER) clinical trial (Cotton et al. 2013; Violari et al. 2008), along with uninfected controls from an interlinking vaccine trial (Madhi et al. 2010). These children are now in follow-up at the Tygerberg Children's Hospital (Cape Town), with multimodal neuroimaging and neuropsychological testing already performed at ages 5, 7 and 9 years, and testing at age 11 years underway. The analyses performed in the present work, while unimodal and cross-sectional, contribute to this larger multimodal longitudinal study.

Resting state FC differences have been identified in HIV+ adults when compared to uninfected controls (Ann et al. 2016; Ipser et al. 2015; Ortega et al. 2015; Thomas et al. 2015; Thomas et al. 2013; Wang et al. 2011), and associations of FC with disease severity in HIV+ youth (Herting et al. 2015). In the CHER cohort, HIV-related FC differences were observed at age 7 years (Toich et al. 2017). In this work, we will analyse rs-fMRI data acquired at age 9 years to investigate whether alterations observed at age 7 years resolve or become more pronounced as the children grow older.

Rs-fMRI data will be analysed to fulfil the following aims:

i. Assess the impact of HIV infection on FC among children stable on ART at age 9 years, as compared with uninfected controls. This is the primary objective.

ii. Explore, within HIV-uninfected children, the effect of perinatal exposure to HIV/ART on FC.

iii. Explore, within HIV+ children, the effect of the timing of ART initiation on FC.

iv. Explore, within HIV+ children, associations of FC with measures of immune health as recorded in infancy (6–8 weeks of age) and at the time of scan.

After reviewing the HIV neuroimaging literature in Section 2, we present the hypotheses that were tested to meet these aims (Section 3).

2 Prior HIV Neuroimaging Research: Results and Significance

2.1.1 Neuroimaging in vertically infected children and adolescents

Neuroimaging studies conducted among vertically infected children and adolescents have largely used structural MRI, although a number of other imaging modalities are also represented (Musielak & Fine 2015). These include diffusion tensor imaging (DTI) (Jankiewicz et al. 2017; Ackermann et al. 2016; Uban et al. 2015; Hoare et al. 2012), magnetic resonance spectroscopy (MRS) (Mbugua et al. 2016; Nagarajan et al. 2012), magnetic resonance angiography (MRA) (Izbudak et al. 2013), computed tomography (CT) (Donald et al. 2015), cerebral angiography (Izbudak et al. 2013), and positron emission tomography (PET) (Depas et al. 1995). Outside of our own longitudinal study, published functional MRI (fMRI) and resting state fMRI (rs-fMRI) studies, discussed hereafter (Sections 2.1.2, 2.1.3), have only been conducted in adults (with one exception in rs-fMRI: Herting et al. 2015).

The focus of pediatric HIV neuroimaging literature has been primarily on white matter (Musielak & Fine 2015), perhaps as a consequence of the observed association of HIV with subcortical dysfunction in the pre-ART era (Paul et al. 2007). However, in the post-ART era of more recent years, patterns of neurocognitive impairment have shifted to suggest cortical involvement as well (Heaton et al. 2011). White matter focus has, nevertheless, yielded the important observation that white matter abnormalities in vertically infected children are prevalent across nearly all ages (Musielak & Fine 2015). Abnormalities include reduced volume (Donald et al. 2015), decreased integrity (Jankiewicz et al. 2017; Ackermann et al. 2016; Uban et al. 2015; Hoare et al. 2012) and lesions (Ackermann et al. 2014). Lesions are most commonly found in both subcortical and deep white matter of the frontal and parietal lobes (Ackermann et al. 2014). Anatomical insults are, however, not limited to white matter. Among children with HIV encephalopathy, loss of grey matter and calcification of the basal ganglia have been identified by CT and structural MRI studies (Donald et al. 2015).

DTI of the children in our cohort identified disrupted development of white matter microstructure at ages 5 and 7 years, despite early ART and early viral load suppression (Jankiewicz et al. 2017; Ackermann et al. 2016). Disruption of the inferior longitudinal fasciculus (ILF) and inferior fronto-

occipital fasciculus (IFOF) was revealed at both ages. At age 5 years, clusters in these tracts showed significantly higher mean diffusivity (MD) in HIV+ children than controls; at age 7 years, both tracts showed reduced fractional anisotropy (FA), while the IFOF additionally showed increased MD again. The locations of other regions showing microstructure disruption in HIV+ children (increased MD or reduced FA) differed between the two ages. This spatial variation over time may indicate that HIV-mediated developmental delays resolve in some regions, but lead to persisting damage in others. No abnormalities were found in the corpus callosum, which is commonly implicated in adult HIV (Gongvatana et al. 2009; Filippi et al. 2001), perhaps as a positive outcome of early ART.

Another DTI study conducted among vertically infected HIV+ youth also found that the white matter microstructure of the ILF and IFOF is sensitive to HIV infection, with past measures of disease severity being associated with higher fibre bundle counts or lower FA, respectively. Moreover, that the effect of past disease severity on working memory performance was partly mediated by lower FA in the IFOF, gives credence to the expectation that such alterations in brain development contribute to the cognitive deficits observed among HIV+ youth (Uban et al. 2015).

2.1.2 Task-based functional MRI in adults

The limited literature analysing task-based fMRI data examines only adult HIV patients. Task-based fMRI demonstrates that HIV+ adults may exert greater cognitive effort to perform the same working memory task, as compared with uninfected controls (Tucker et al. 2004). In asymptomatic patients showing no cognitive dysfunction, this is observed as greater activation in the lateral prefrontal cortex (Ernst et al. 2002). In cohorts with some cognitive deficits, there is greater activation within the parietal lobe during simpler tasks, and both greater parietal and frontal activation during more complex tasks (Chang et al. 2001). In contrast, among HIV+ patients, those with cognitive deficits have reduced general activation during motor tasks compared to asymptomatic subjects (Tucker et al. 2004).

Combined, these results indicate that HIV-associated cognitive deficits are correlated with alterations in cortical activation. Whether these differences are expressed as greater or reduced activation may

depend on the task or functional brain network in question. Further research is required to elucidate this apparent discrepancy.

2.1.3 Resting state functional MRI in children and adults

The use of rs-fMRI to study HIV first appears in the literature in 2011, with the number of published papers quickly increasing in 2015.

The effect of HIV on adult FC shows some correspondence to neurodegenerative aging: default mode network (DMN), executive control, and salience within-network FC, as well as DMN-salience between-network correlations, are significantly diminished in both (Thomas et al. 2013). However, the application of weighted graph theory has helped to disentangle the pathophysiology of HIV and aging through the interpretation of metrics of graph topology. The association of HIV with a globally lowered closeness centrality metric indicates a loss of functional brain integration; especially inhibited is the passing of information between both the DMN or the frontoparietal network and the rest of the brain (Thomas et al. 2015). On the other hand, aging is associated with a globally increased entropy metric, indicative of reduced differentiation of brain regions (Thomas et al. 2015). While graph theory analyses fall outside the scope of the current project, it would form a valuable extension in future studies.

Sensitivity of resting state FC to HIV pathology is not restricted to the cortex, as corticostriatal[3] RSNs are also affected. Subcortical regions carry the highest HIV viral load in the brain and the literature demonstrates subcortical atrophy (Ortega et al. 2015). HIV+ subjects have reduced FC between the striatum and the ventral attention and DMN networks, with the latter deficit reduced among those on ART (Ortega et al. 2015). Prompted by the consistency of HIV-associated cognitive deficits with injury to *fronto*striatal circuitry, investigations corroborate reduced FC in this particular corticostriatal

[3] The striatum is one of the principle components of the basal ganglia and consists of the caudate, putamen and nucleus accumbens.

network as well (Ipser et al. 2015). These results caution against the restricting of FC analysis to the cortex, as in cortical surface-based analysis (for a description of this technique, see Fischl et al. 1999).

To the authors knowledge, only our longitudinal study has investigated FC in HIV+ children with reference to age-matched controls. At age 7 years, rs-fMRI indicated that lowered immune health in infancy ($CD4^+$ count, CD4%) may have lasting impacts on FC, and that HIV-related abnormalities predominantly involve medial brain regions and between-network connections (Toich et al. 2017). Adults with recent HIV-infection do not seem to show an association between FC and clinical measures, though FC is still impaired (Wang et al. 2011). Taken together, it may be the case that while the early stages of infection impact FC in both children (Toich et al. 2017) and adults (Wang et al. 2011), immunosuppression in infancy is particularly impactful.

The above and similar arguments must, however, be considered with caution. A discrepancy prevalent in the rs-fMRI literature is the lack of consistent correlation of HIV laboratory markers and neuropsychological performance measures with FC measures (Ortega et al. 2015; Ipser et al. 2015; Thomas et al. 2013). However, this observation is not singular to rs-fMRI, but is representative of neuroimaging measures in general (Ortega et al. 2015). Far from motivating for a shying away from investigating such associations, this rather motivates for detailed reporting of methodologies as the HIV neuroimaging literature grows and begins to elucidate discrepancies.

Several explanations are proposed for absent associations with HIV laboratory markers. Plasma markers are used in place of cerebrospinal fluid (CSF) markers and may not accurately reflect changes in the brain under all circumstances – particularly in advanced HIV disease (Edén et al. 2010; Canestri et al. 2010; Ellis et al. 2000). Yet ART typically does effectively suppress viral load and immunoactivation in the brain compartment in parallel with the blood, albeit at a slower rate (Price & Spudich 2008). An alternative explanation is that, in the post-ART era, traditional laboratory markers (plasma viral load, $CD4^+$ T lymphocyte count) may be less accurate in reflecting disease severity measured at the same timepoint. A well-established example is the significant prevalence of

neuropsychological deficit among patients whose plasma viral load has been successfully suppressed (Cysique & Brew 2011). Thus, it appears that the histories of ART regimen, viral load, and inflammation in a patient need to be considered, as they may have complex and persisting effects.

This notwithstanding, interesting correlations have been identified in the rs-fMRI literature. Among older adults (> 60 years), FC deficits in the salience network are associated with current detectability of viral loads, but not with infection status. This suggests that the integrity of FC may be restored with successful viral load suppression under certain conditions (Guha et al. 2016). In a pioneering paper, Herting et al. (2015), while not investigating HIV-related abnormalities with respect to a control group, found associations in HIV+ youth (11.6–20.7 years-old) between clinical measures of disease severity and FC to seeds in the default mode network (DMN). Lower nadir[4] $CD4^+$ and higher peak RNA were associated with characteristics of a 'less mature' DMN: that is, one with weaker within-network FC and stronger integration with task-positive networks (the DMN itself being task-negative in healthy subjects; Section 5.7.1). Among the implicated connections, between-network FC of the medial prefrontal cortex (PFC) and posterior cingulate cortex DMN nodes correlated with processing speed performance. Psychomotor slowing is frequently reported in HIV+ children and adults (Nichols, Chernoff, Malee, Sirois, Woods, et al. 2016; Nichols et al. 2015; Smith et al. 2012; Sacktor et al. 2010; Koekkoek et al. 2008; Martin et al. 2006; Schmahmann 2005).

[4] Lowest recorded.

3 Hypotheses

Based on the findings of the literature (Section 2), we made the following hypotheses, relating to the project aims described in Section 0:

I. HIV-infection will be associated with reduced functional integration (within-network FC) in RSNs commonly implicated in HIV: default mode, ventral cognitive control[5] (salience, central executive), visual, and sensorimotor networks (Sarma et al. 2017; Toich et al. 2017; Thomas et al. 2015; Herting et al. 2015; Ortega et al. 2015; Thomas et al. 2013; Wang et al. 2011).

II. Given the congruence between structural and functional connectivity (Damoiseaux & Greicius 2009; Hagmann et al. 2008), the disruption of both in HIV, and the apparent preference for medial regions in HIV-related FC differences in our cohort at age 7 years, we hypothesise that the FC of brain regions forming hubs of structural connectivity[6] (which are posteromedial; Hagmann et al. 2008) will differ between HIV+ and uninfected children at age 9 years.

III. Given select correlations of processing speed with FC in perinatally HIV+ youth (Herting et al. 2015), and the observation of FC deficits in regions implicated by profiles of cognitive impairment in HIV (Ipser et al. 2015), we hypothesise that FC of brain regions underpinning neuropsychological domains that are impaired in our cohort – visual perception, learning, planning and simultaneous processing (Laughton et al. 2017; Merkle 2015) – will differ between HIV+ and uninfected children.

IV. Given both strong commonalities and differences in the patterns of white matter disruption observed in our cohort at age 5 and 7 years (Jankiewicz et al. 2017; Ackermann et al. 2016), we hypothesise that investigation of seed regions showing HIV-related FC differences at age

[5] These networks tend to be classified in varying ways. This is discussed in Section 5.7.2.

[6] Functional connections of the structural core with any brain region, not necessarily with another region in the structural core. Hypothesis III should be understood similarly.

7 years will reveal HIV-related differences in functional connectivity to both similar and new target brain regions at age 9 years, with some FC abnormalities resolving by age 9 years.

V. Given that our virologically-suppressed HIV+ cohort has revealed, at ages 5 and 7 years, associations of immune health in infancy, but not current immune health, with neuronal integrity and FC (respectively) (Toich et al. 2017; Mbugua et al. 2016), we expect to observe (at age 9 years) neural correlates of immune health in infancy (but not current immune health) in early-maturing RSNs.

VI. Among uninfected children, perinatal exposure to HIV/ART will affect the functional integration (within-network connectivity) of early-developing RSNs.

VII. Given associations of early treatment with higher mental development scores in infancy (Laughton et al. 2012) and reduced morbidity (Cotton et al. 2013), we hypothesise that younger age at ART initiation will predict higher functional integration (within-network connectivity) in RSNs commonly implicated in HIV (see Hypothesis I).

4 Pediatric HIV: Clinical Background

4.1 ART: 20 years of effective treatment

The first attempts to treat HIV with antiretroviral (ARV) drugs, through the late 1980s, were unsuccessful. Monotherapy with nucleoside reverse transcriptase inhibitors (NRTIs) – which block reverse transcription of viral RNA into DNA, required for its integration into the host cell's DNA – had high toxicity and was further unable to support stable immune recovery (Brinkman et al. 1998; Lewis & Dalakas 1995; Volberding et al. 1995; Lundgren et al. 1994). Marginal success with synergistic dual NRTI therapy gave the first indications that combatting drug resistance is key to successful treatment (Kuritzkes et al. 1999). The Vancouver AIDS Conference of 1996 ushered in the era of highly active ART (now simply 'ART'), as a group of observations revealed that the HIV pool in the human body has rapid turnover, and that complete suppression of viral replication in the patient is required to prevent resistance-producing viral mutation (Vella et al. 2012). Around the same time, new classes of drugs were being developed, such as non-nucleoside reverse transcriptase inhibitors (NNRTIs), and protease inhibitors, which prevented the replication of infectious virus particles in different ways. Combination therapy, consisting of a dual NRTI backbone and a third drug of a different class, became the standard recommendation (WHO 2006b; WHO 2006a). In 1998, the success of such therapy in shifting HIV from a fatal to a chronic disease was indicated in probably the most famous study in the history of ART (Palella et al. 1998). The form of ART today remains largely unchanged, with recent innovation largely concerning improving tolerability, adherence and cost (Vella et al. 2012).

4.2 Treatment of vertically infected children

With the availability of effective ART, a major question is when treatment should be initiated. The question is perhaps nowhere more pertinent than in infants infected *in utero*, during perinatal gestation, or around birth. Older guidelines only administered treatment when children had advanced or severe disease, or when $CD4^+$ T cell levels dropped below a threshold (WHO 2006b). Since then, several studies have indicated that earlier treatment in infants or children (including asymptomatic children) is associated with better survival rates (Cotton et al. 2013; Violari et al. 2008), better clinical, virologic, and immunologic outcomes (Chiappini et al. 2009), greater weight and height gain (Diniz et

al. 2011), and improved neurodevelopmental outcomes (Laughton et al. 2012). Among these studies is the CHER trial (Cotton et al. 2013; Violari et al. 2008), from the cohort of which our own HIV+ sample is taken. As a result of these findings, international guidelines now universally recommend immediate ART for all HIV+ children (vertically infected, or otherwise), where the recommendation is strongest for those younger than 1 year of age (Foster et al. 2017; WHO 2016; CHIVA 2017; Panel on Antiretroviral Therapy and Medical Management of HIV-Infected Children n.d.).

Another question is whether treatment should be interrupted when children become virologically and immunologically stable. This strategy has been partially explored, with a view to decreasing toxicity or drug resistance that may result from early and cumulative treatment. Experimentation with structured interruption in adults and children has been largely unsuccessful, since viral rebound quickly necessitates the restarting of treatment (Thompson et al. 2014; SMART Study Group 2006). Current guidelines suggest lifelong ART for all children and adults.

4.3 Mother-to-child transmission

The vast majority of HIV-infected children, both in SSA and globally, acquire the virus by mother-to-child transmission (MTCT) (Eisenhut 2013; WHO 2010; Wiktor et al. 1997). Such 'vertical infection' can occur via the placenta (in utero, or during the perinatal period of gestation), during labour and delivery, or through the gastrointestinal tract in breast feeding, with the latter two avenues having greater rates (Dabis & Ekpini 2002).

Programmes for the prevention of MTCT involve prophylaxis administered to the mother and the infant. Newer regimens administer ARV drugs to pregnant woman as early as possible (since the most effective way to reduce transmission risk is by suppressing maternal viral load), and integrate this with lifelong ART for the mother's health. Neonates are given 6 weeks of dual post-exposure prophylaxis (longer if breast-feeding), consisting of azidothymidine and nevirapine (WHO 2016). Older prophylaxis recommendations, according to which the children in this study were treated in infancy (during the CHER trial), consist of single-dose nevirapine to the mother (during labour) and to the neonate

(Gourlay et al. 2013). The percentage of HIV+ pregnant woman able to access some form of ARV treatment in Southern Africa has risen from around 10% in 2004 (WHO 2010) to almost 90% in 2016 (UNAIDS 2016). As a result, large numbers of children are now born HIV-negative after having been exposed to HIV and ART perinatally.

4.4 HIV pathogenesis in the periphery

The early, acute stage of HIV infection is associated with rapid loss of $CD4^+$ T helper cells. The infection begins in the mucosa, where at least half of the $CD4^+$ cells are located during homeostasis, a large fraction of which are in an activated state (Stebbing et al. 2004). Active $CD4^+$ cells are readily infected, and ensuing viral replication and cytopathy (destruction of the host cell) is efficient (Stevenson 2003). The virus then spreads via the lymphoid tissue and the blood. The chronic stage of HIV infection is characterised by generalised activation of the immune system (Anthony et al. 2003). This chronic inflammation, as opposed to the direct cytopathic effect of the virus, is postulated to mediate continued $CD4^+$ cell pool depletion (Smith 2006). Some other immune cells – largely macrophages and dendritic cells – have transmembrane receptors[7] that also leave them susceptible to HIV-infection. The highly-migratory macrophage cells may play an important role in transmitting the virus into the brain (Koppensteiner & Wu 2012). $CD8^+$ (cytotoxic) T cells, though activated as part of immune inflammation, are not infected by the virus at a high rate (Stebbing et al. 2004).

Even when the plasma viral load (quantity of the virus in the blood) has been suppressed by ART to undetectable levels for many years, it can rebound quickly (in about two weeks) if treatment is stopped (Imamichi et al. 2001; Davey et al. 1999). Covert reservoirs of latent HIV persist even when HIV replication is prevented by treatment (Finzi et al. 1999). At the cellular level, the major reservoir consists of resting memory $CD4^+$ T cells that have been productively infected (integration of viral RNA into cell DNA), but have returned into a metabolically-inactive state before succumbing to the destructive effects of the virus (Stebbing et al. 2004). Because of the biological function of these cells

[7] Namely, CCR5 and CXCR4 chemokine receptors.

– providing lifelong immunity against previously-encountered antigens – they have an extremely long half-life (about four years) and hence provide a stable source for later viral replenishment. When these cells are reactivated by the presentation of an antigen, they will begin to produce viral proteins and replicate the virus. Early ART initiation from infancy, while perhaps slowing the treatment-reactive evolution of the virus in the patient, does not prevent the formation of a stable viral reservoir (Persaud et al. 2000).

4.5 HIV and antiretroviral drugs in the brain

4.5.1 Penetration of the virus

Free virus and infected immune cells cross the blood-brain-barrier (BBB) through complex transport processes (Banks et al. 2006), possibly within two weeks of HIV-infection (Valcour et al. 2012). The BBB is a continuous membrane formed by the modified endothelium of the brain capillary bed, and regulates biological transport into and out of the CNS. Because of the sparsity of T lymphocytes (such as $CD4^+$ cells) in the brain, the entered virus evolves to infect perivascular monocytes, parenchymal microglia and astrocytes (Churchill & Nath 2013) – cells which sense threats, maintain homeostasis, and respond to injury in the CNS. Microglia have an extremely slow turnover (even more so than that of the resting $CD4^+$ T cells of the periphery) and do not quickly succumb to the cytopathic effects of the virus, forming a stable site of replication for HIV in the brain (Churchill & Nath 2013). Astrocytes, the most abundant cell type in the brain, are more susceptible to infection in neonates than adults, and might be involved in major pathways of HIV-mediated neurotoxicity (Tornatore et al. 1994; Blumberg et al. 1994). Viral proteins, proinflammatory cytokines (signalling molecules) and nitric oxide produced by infected CNS cells cause neurotoxic events which can damage brain parenchyma. The dominant hypothesis is that these secondary effects, rather than mass infection of neurons, are responsible for neuronal damage and loss (for a review of this mechanism, see Kaul et al. 2001). Aside from the neurotoxic effect of brain-resident HIV, toxic proteins produced by HIV in the periphery can cross the BBB (Banks et al. 2006). The virus also induces the BBB to produce proinflammatory substances (Didier et al. 2002; Hofman et al. 1999; Zidovetzki et al. 1998).

4.5.2 Penetration of antiretroviral drugs

Different ARV drugs can therapeutically penetrate the CNS to varying degrees, as indirectly inferred from molecular properties, CSF concentrations, and the ability to reduce CSF viral load or improve cognitive outcomes. At least two of the three drugs (zidovudine, ritonavir-boosted lopinavir[8]) forming first-line therapy in our cohort could be considered to have a relatively higher penetration rate (Letendre et al. 2008). But even in the post-ART era, the extent to which therapeutic ARV levels can be maintained in the brain is considered suboptimal (Van Rie et al. 2007): the BBB actively pumps ARV drugs out of the brain compartment (Banks et al. 2006). This raises concerns that the brain forms a compartmentalised viral reservoir partially protected from ART, the viral load kinetics and drug resistance of which become separated from the lymphoid tissue (Van Rie et al. 2007). Such compartmentalisation is likely to occur not only in adults, but also in children (McCoig et al. 2002)

Nevertheless, partial effectiveness of ART in the brain, including the developing brain, is evident. Before the availability of ARVs, progressive encephalopathy[9] was reported at rates as high as 50% of HIV+ children (Epstein et al. 1986). Children would not typically survive longer than 2 years after encephalopathy diagnosis (Lobato et al. 1995). In the era of ART, this rate has been reduced to less than 2%, and diagnosed cases can be halted and potentially reversed with treatment (Chiriboga et al. 2005). Yet even with the availability of effective treatment, residual cognitive deficits do persist, both in asymptomatic children and those with halted encephalopathy (Chiriboga et al. 2005).

4.5.3 Neurotoxicity of antiretroviral drugs

Another concern is that ARV drugs themselves have a neurotoxic effect within the CNS (for a recent review, see Shah et al. 2016). As HIV shifts from a fatal to a chronic condition, and policies suggest earlier ART initiation in children, it is becoming more urgent to understand the long-term effects of cumulative drug exposure. While several adult HIV studies demonstrate better neurocognitive

[8] The third being lamivudine.

[9] Progressive encephalopathy is characterised by: retarded development of brain circumference, or neuroimaging-indicated brain atrophy; missed or lost developmental milestones; corticospinal tract signs, such as pathological reflexes (Janssen et al. 1991).

outcomes for drugs with higher CNS penetration scores (Carvalhal et al. 2016; Eisfeld et al. 2013; Smurzynski et al. 2011), more than one has indicated the inverse (Caniglia et al. 2014; Marra et al. 2009). Several classes of ARVs have been found to produce neuropsychiatric adverse effects, such as depression, hallucination, and psychosis (Shah et al. 2016). Some of these are known to modify the concentration/activity of signalling molecules and enzymes in the CNS in ways that could provide a mechanism for neuropathy (Streck et al. 2008; O'Mahony et al. 2005). Select ARVs have been associated with neuropathy in the peripheral nervous system – through depletion of mitochondrial DNA in nerves (Dalakas et al. 2001), for example – further raising concerns about neuropathy in the CNS as well. In addition, while combination ARV therapy has constituted a major advance in successful management of HIV, it also invites possibilities of complex neurotoxic drug-drug interactions (Shah et al. 2016).

Because animal models allow for invasive testing, they may provide essential insights into the HIV-independent effects of ART on the CNS. At present, such literature is far too sparse to be conclusive. Yet the initial results do warrant further investigation. In a study among adult primates, ART was linked with reduced synaptodendritic integrity, while nevertheless being effective and essential in preventing encephalitis (Akay et al. 2014). Two studies found perinatal/transplacental exposure to ART to be associated with moderate mitochondrial damage in the CNS of primate neonates or primate fetuses, respectively (Divi et al. 2010; Ewings et al. 2000), complementing observations of peripheral mitochondrial damage in ART-treated humans.

4.6 Cognitive and behavioural profile of vertically infected children on ART

Over the last decade, the literature has begun to explore the effects of vertical HIV-infection and HIV/ART exposure on cognitive performance and behaviour in children on ART. Prospective investigations have been conducted as part of two longitudinal studies, the Adolescent Master Protocol (AMP) of the Pediatric HIV/AIDS Cohort Study (PHACS) (Tassiopoulos et al. 2016), and the CHER clinical trial (Cotton et al. 2013; Violari et al. 2008).

Compared to the general population, executive function (Nichols, Chernoff, Malee, Sirois, Woods, et al. 2016; Nichols et al. 2015), learning and memory (Nichols, Chernoff, Malee, Sirois, Williams, et al. 2016; Nichols et al. 2015), adaptive and overall cognitive function (Garvie et al. 2014; Smith et al. 2012), academic achievement (Garvie et al. 2014), and early neurodevelopmental outcomes (Laughton et al. 2012) of both HIV+ and HEU children have been found to be either within the low average range or significantly below age expectations. In addition, the incidence of mental health problems in these two groups is higher than expected from population surveys (Malee et al. 2011). Perinatal exposure to HIV/ART cannot be ruled out as an explanation for the commonality of the deficits between these two groups, since studies generally lack an unexposed (HU) control group. Nevertheless, several authors also speculate a significant contribution of non-clinical environmental factors.

A general pattern emerges that HIV+ children with asymptomatic clinical histories do not perform significantly worse in cognitive or adaptive functioning than HEU children (Nichols, Chernoff, Malee, Sirois, Williams, et al. 2016; Nichols et al. 2015; Garvie et al. 2014; Smith et al. 2012) after controlling for demographic and socioeconomic variables. Visual perception may be an exception (Laughton et al. 2012). On the other hand, HIV+ children with previous CDC[10] Class C events (instances of AIDS-defining illness, including encephalopathy) do differ significantly from asymptomatic HIV+ or HEU children in visual recognition memory (Nichols, Chernoff, Malee, Sirois, Williams, et al. 2016), full-scale intelligence quotient (Smith et al. 2012; Wood et al. 2009), self-endorsed ratings of cognitive regulation (Nichols et al. 2015), and executive functions involving processing speed elements (Nichols, Chernoff, Malee, Sirois, Woods, et al. 2016; Smith et al. 2012). Further, within HIV+ children, histories of CDC Class C events and greater past disease severity (lower nadir $CD4^+$, higher peak viral load) are associated with higher rates of psychiatric impairment and learning disability (Wood et al. 2009), lower intelligence quotients (Smith et al. 2012), and impairment of several cognitive and adaptive functions

[10] Center for Disease Control and Prevention.

(Nichols et al. 2015). Of note, Smith et al. (2012) found that processing speed was significantly impacted by past disease severity even among HIV+ children who had no prior encephalopathy diagnosis, while all other functions were not. Psychomotor slowing might underlie differences in executive performance observed in HIV+ and HEU children. Much literature describes the particular vulnerability of processing speed in pediatric (Herting et al. 2015; Koekkoek et al. 2008; Martin et al. 2006; Schmahmann 2005) and adult (Sacktor et al. 2010) HIV infection. A strong trend in the above results suggests that even short-lived AIDS-related diagnoses can greatly increase the risk of later neurocognitive impairment, reinforcing the importance of early treatment to prevent immunosuppression.

Incidence of behavioural (Nichols et al. 2015) and mental health (Malee et al. 2011) problems may be higher in HEU than HIV+ children, though they are not absent in the latter group (Jeremy et al. 2005). While it has been suggested that cognitive impairment might limit acting-out behaviour, this trend most likely indicates a considerable influence of non-clinical environmental and caregiver factors on neurocognitive and behavioural development.

4.7 Measures of immune health in HIV infection

When not controlled, HIV infection results in a spectrum of diseases, opportunistic infections and viral-induced cancers associated with immune suppression (AIDS). Immune status is therefore an essential marker of the progression of HIV-infection and associated disease. In particular, the level of $CD4^+$ T lymphocytes circulating in the blood, which are the primary targets of HIV, has high prognostic value for predicting risk of AIDS or death in both children and adults. Both baseline (i.e. before the commencement of ART) $CD4^+$ cell levels and those during ART regimens are predictive (Badri et al. 2006; HIV Paediatric Prognostic Markers Collaborative Study Group 2006; HIV Paediatric Prognostic Markers Collaborative Study Group 2003; Egger et al. 2002; Anastos et al. 2002). $CD4^+$ levels may better predict short and long term disease progression than viral load (HIV Pediatric Prognostic Markers Collaborative Study Group 2003; Egger et al. 2002). The latter is nevertheless a more direct measure of the extent to which treatment achieves its aim of inhibiting viral replication and is the

preferred indicator of treatment failure (WHO 2016). $CD4^+$ cell levels are the central measure for ART prioritisation in settings with resource limitations (WHO 2016), and historically the indicator for ART commencement (O'Gorman & Zijenah 2008).

The levels of this T lymphocyte can be quantified in various ways. The absolute count of $CD4^+$ T cells has the strongest biological basis (Taylor et al. 1989), and is the preferred measure for patients older than 5 years (WHO 2016), but is highly variable in younger ages. The percentage of total circulating lymphocytes that are $CD4^+$ T cells is more age invariant, and is the preferred measure for patients younger than 5 years (WHO 2016; O'Gorman & Zijenah 2008). The $CD4^+$:$CD8^+$ ratio, which compares the counts of the two major T lymphocytes, is less commonly used, but might also have some prognostic value. There have been suggestions for using this ratio as a surrogate measure of HIV-infection among infants in resource-poor settings (Zijenah et al. 2005).

5 Principles of Resting State Functional MRI

5.1 A primer on magnetic resonance physics

MRI uses non-ionising electromagnetic radiation to non-invasively image the structure, function or metabolism of the brain. Programming the MRI apparatus to produce different series of radiofrequency pulses and magnetic field gradients – called 'pulse sequences' – enables the experimenter to obtain such differently-weighted images. The MRI scanner consists of a magnet (typically, a superconducting electromagnet), radiofrequency (RF) coils (for transmission and receiving), and gradient coils. The doughnut-shaped magnet produces a large field, $\boldsymbol{B_0}$, known as the main static magnetic field, which is oriented longitudinally through its bore. This field passes inferiorly to superiorly (designated as the 'Z-axis') through a patient positioned supine within the bore.

Atoms with an uneven number of protons or neutrons in their nuclei can interact with an externally applied magnetic field to produce measurable signal in MRI. As the body consists of approximately 60% water, the most abundant such atom in the human body is the hydrogen (H) atom, which contains a single proton in its nucleus. The proton, like all other fundamental particles, spins on its own axis (by way of analogy). Because moving charge produces a magnetic field, each H nucleus has a tiny magnetic dipole moment associated with it, which behaves much like a microscopic bar magnet. In the presence of a magnetic field, these dipole moments tend to align along the direction of the field, similar to the way a compass needle aligns parallel to the earth's field. However, in contrast to an isolated compass needle that will oscillate around north and eventually come to rest pointing north, an individual nucleus in a collection of nuclei never actually comes to rest since it is continuously bumped by neighbouring nuclei due to random thermal motion. In the same way that a compass needle oscillates around north following a disturbance, the 'disturbed' dipole moments precess around the direction of the main magnetic field ($\boldsymbol{B_0}$). Precession can be thought of as a 'wobbling' type motion where the tail of the dipole moment remains fixed and the head traces out a circle. This precession happens at a characteristic frequency, called the Larmor precession frequency, that is proportional to the strength of the main magnetic field and the gyromagnetic ratio of the nucleus (42.6 MHz/T for hydrogen nuclei).

Although individual nuclei are never left alone long enough to reach steady state, the distribution of dipole moments will. The equilibrium distribution of dipole moments is nearly spherical but slightly skewed toward the main magnetic field, resulting in a net tissue magnetisation, $\boldsymbol{M_0}$, parallel to the main magnetic field. This tissue magnetisation is the source of the signal measured in MRI.

MRI measurement begins with the application of an RF pulse to the tissue, in a coil perpendicular to the main magnetic field. If the RF pulse is applied at the resonant frequency of the nuclei, known as the Larmor precession frequency, nuclei will be excited away from their equilibrium state. This RF pulse establishes an oscillating magnetic field perpendicular to the main magnetic field that tips $\boldsymbol{M_0}$ towards the transverse plane – the plane orthogonal to the longitudinal Z-axis. Upon termination of the RF pulse, the dipole moments again precess around $\boldsymbol{B_0}$ and return to their equilibrium distribution with $\boldsymbol{M_0}$ pointing along the main magnetic field. The flux induced in the receiver coils by the transitory transverse component of $\boldsymbol{M_0}$ ($\boldsymbol{M_{xy}}$) is the MRI signal.

The process whereby excited protons return to their equilibrium state is known as 'relaxation.' As a result of this process, $\boldsymbol{M_{xy}}$ decays to $\boldsymbol{0}$ from its peak, and the longitudinal component of $\boldsymbol{M_0}$ ($\boldsymbol{M_z}$) recovers to eventually again be equal to $\boldsymbol{M_0}$. The dynamics of decay and recovery are different for different types of tissue. If we sample the signal induced by $\boldsymbol{M_{xy}}$ at just the right moment, differences in signal between different brain locations will reflect differences in these dynamics, producing image contrast.

It is tempting to think of the decay and recovery processes as happening at the same rate, with both simply reflecting a reduction in the angle of $\boldsymbol{M_0}$ with $\boldsymbol{B_0}$ over time while the magnitude of $\boldsymbol{M_0}$ remains constant**.** In fact, this is not the case. Rather, two independent exponential processes, with different time constants, occur. $\boldsymbol{M_{xy}}$ rapidly decays to $\boldsymbol{0}$ as the H-nucleus dipole moments fan out in the transverse plane, losing their phase coherence though 'spin-spin' relaxation. As the nuclei come near to one another in their random motion, the external magnetic field experienced by each is slightly changed from $\boldsymbol{B_0}$, because the magnetic moment of other nuclei add to or subtract from it. The

precessional frequencies of these nuclei will change relative to one another according to the new field experienced by each nucleus. Since they are no longer precessing at the same frequency, they lose phase coherence, in the same way that two hands on a clock change their relative position if they move at different speeds. Once they move apart, precession returns to the Larmor frequency, but the phase differences acquired are not reversible. The cumulative effect of many interactions is the loss of phase coherence, and hence of net transverse magnetisation, according to:

$$M_{xy}(t) = M_0 e^{\frac{-t}{T_2}} . \tag{1}$$

The time constant T_2 is dependent on tissue properties, and is defined as the time it takes the transverse magnetisation to reduce to about 37% of its initial value. In the same way that nucleus-nucleus interactions modify the experienced magnetic field, causing dephasing, magnetic susceptibility differences of adjacent tissues and inhomogeneities in the main magnetic field will also cause dephasing. When these additional factors are considered, the time constant is referred to as T_2*, which is the source of contrast in the blood oxygen level-dependent (BOLD) signal of fMRI (Section 5.2).

While T_2 relaxation involves no loss of energy, the second, much slower, relaxation process involves excited protons releasing the energy that they previously absorbed (during RF excitation) into the surrounding lattice ('spin-lattice' relaxation). This causes the longitudinal magnetisation to grow back[11] according to:

$$M_z(t) = M_0 \left(1 - e^{\frac{-t}{T_1}}\right) . \tag{2}$$

The time constant T_1 is also dependent on tissue properties, and is defined as the time it takes the longitudinal magnetisation to recovery to about 63% of its equilibrium value.

[11] It would also cause further dephasing in the transverse plane, but the effect of 'spin-spin' relaxation is far greater in that regard.

In practice, the freely decaying signal is not immediately sampled, but is instead caused to 'echo' a second time (through mechanisms not discussed here). The time between the peak of this echo and the main RF excitation pulse is called the 'echo time' (TE). The time between two consecutive excitation pulses (at some point within which the signal is measured) is called the 'repetition time' (TR). Through careful design of pulse sequences, the values of TE and TR can be changed relative to one another, which in turn controls how the resulting image contrasts are weighted by the T_1 and T_2 characteristics of the tissue.

5.2 The BOLD signal and its neurobiological origins

The blood oxygen level-dependent (BOLD) signal captured by fMRI is an indirect measure of neuronal activity. Changes in neuronal activity produce changes in local cerebral blood flow (CBF) and blood oxygenation. This neurogenic departure from homeostasis is known as the haemodynamic response. The haemodynamic response transiently modifies the local transverse relaxation time (T2*) across brain tissue (see Section 5.1 for more details on MRI physics). Modifications to T2* are captured by an echo planar imaging (EPI) sequence to produce maps of functional activity in the human brain. Parts of this process are better understood than others.

The validity of fMRI as a tool for investigating brain function is dependent on there being a proportional relationship between neuronal activity and the BOLD signal measured by the MRI scanner. This relationship is substantiated and widely accepted. Experiments acquiring electrophysiological recordings and fMRI images simultaneously in primates (Logothetis et al. 2001) and in series in humans (Arthurs et al. 2000) indicate that the BOLD signal has a linear relationship with the synaptic activity of neuron populations.

Underpinning this linear relationship is the coupling between neural activity and CBF/blood oxygenation. Animal models indicate that stimulation of local brain activity increases local metabolism (rate of glucose utilisation) and blood flow in cerebral tissue, while reduced activity suppresses it (Nielsen & Lauritzen 2004; Mathiesen et al. 2004; Sokoloff 1981). However, the precise causal

mechanisms by which neural activity acts on the vasculature – known as neurovascular coupling – remains the subject of ongoing research (Hillman 2014; Arthurs & Boniface 2002).

Earlier models proposed that substances produced by neurons (such as glutamate and nitric oxide) act directly on the vasculature (Attwell & Iadecola 2002), while more recent models include other cells of the CNS – astrocytes, pericytes and interneurons – as intermediaries (Peppiatt et al. 2006; Takano et al. 2005; Cauli et al. 2004). In either case, the resulting dilation of vasculature – pial arteries, arterioles penetrating the cerebral parenchyma, and capillaries – facilitates increased CBF. The endothelium of the vasculature might itself be involved, carrying signals upstream from the capillary bed at the site of neuronal activity, to the arteries supplying those beds, causing retrograde dilation along the way (Chen et al. 2014; Chen et al. 2011; Tallini et al. 2007).

Having considered the origin of the haemodynamic response, we consider next how it is translated into the BOLD signal. In brief: the MRI scanner uses haemoglobin as an endogenous contrast agent. The echo planar imaging (EPI) sequence employed in fMRI obtains an image highly weighted by the local transverse relaxation time (T2*) across the brain. This time constant is sensitive to local inhomogeneities in the static magnetic field imposed across brain tissue by the scanner. Metabolism of oxygenated haemoglobin (HbO) carried by red blood cells creates paramagnetic deoxyhaemoglobin (HbR) molecules, which change the magnetic susceptibility of local brain tissue and thereby produce magnetic inhomogeneities. Conversely, increased local blood flow increases the supply of oxygenated HbO, effectively diluting the paramagnetic effect of HbR. It is thus the HbR/HbO ratio that produces image contrast (Logothetis & Wandell 2004). Thus, fMRI relies on the fact that functional (neurally-evoked) increases in CBF are proportional to increased neuronal activity, and that they modify this HbR/HbO ratio.

5.3 Task-based and resting state functional MRI

The BOLD signal can be measured in response to a stimulus or during the performance of a task, together known as task-based fMRI. The signal at each brain voxel[12] is modelled by the expected haemodynamic[13] response to a stimulus, to estimate the extent to which it is activated by the stimulus. The resultant statistical map reflects the level of engagement of each brain region in a task, or the level of modulation by a stimulus.

Conversely, rs-fMRI measures spontaneous fluctuations in the BOLD signal when the subject is at rest. Ideally, the subject is lying still with eyes open (Gusnard et al. 2001), but not engaged in any goal-driven behaviour or primed for a mental task. In this paradigm, the BOLD time course of any one voxel, independent of others, is uninformative. Instead, the extent to which the temporal dynamics of different brain voxels correlate is used to infer the presence of functional communication channels (Van den Heuvel & Hulshoff Pol 2010) or operational interaction between them. This phase locking of the neuronal activity in anatomically separated brain regions is known as 'functional connectivity' (FC). Resting state networks (RSNs) can be estimated from FC in a model-free way by identifying principle modes of temporal variation in the spontaneous BOLD fluctuations, and then identifying regions significantly modulated by that mode (independent component analysis, ICA). Alternatively, the FC of a selected seed region, hypothesised to be key to a given brain function, with every other brain voxel can be used to define an RSN (seed-based analysis, SCA).

There is strong correspondence between RSNs inferred from covarying spontaneous fluctuations and activation networks identified in task-based studies (Smith et al. 2009; Cordes et al. 2000). This pairing gives credibility to rs-fMRI methods and suggests that the brain's full repertoire of function persists in some sense, and is open to investigation, in the resting state. A strength of resting state analysis is, thus, that various functional systems can be investigated from a single MRI acquisition (Biswal et al.

[12] The smallest cubic area of brain tissue that can be digitally isolated given the imaging resolution; the 3-D analogue of a 2-D pixel.

[13] That is, the expected fluctuation in local oxygenated haemoglobin caused by a transient wave of increased local cerebral blood flow, which is in turn expected to be triggered by increased neuronal activity (Section 5.2).

2010). The pairing also provides an avenue for understanding the neuropsychological significance of (task-free) RSNs, since activation networks are produced by tasks that have associated behavioural and cognitive paradigms.

5.4 Artefactual (non-neuronal) contributions to the functional MRI signal

The fMRI signal is noisy. Spontaneous neuronal activity only accounts for about 3% of the signal variance (Bianciardi et al. 2009). Several non-neuronal processes contribute coherent fluctuations, not only affecting task-based estimates of levels of neuronal activation, but also capable of producing spurious patterns of resting state FC. Cardiac and respiratory cycles cause time-varying changes in the magnetic susceptibility of the torso, movement of the brain stem into surrounding tissue and pulsation of blood vessels. In turn, these all produce oscillations of the static magnetic field ($\boldsymbol{M_0}$) in brain tissue as well as complex non-rigid motion artefacts. In addition, changes in the rate of these respiration and heart rhythms, along with other physiological mechanisms, produce fluctuations in $C0_2$ concentration and blood pressure, both of which modify CBF. Modified cerebral flow directly affects the local HbR/HbO measured by the BOLD contrast, confounding the signal (for a review of physiological noise sources, see Murphy et al. 2013). Non-physiological noise sources include bulk motion of the skull (Power et al. 2012), low-frequency drifts in the main magnetic field maintained by the scanner (Bianciardi et al. 2009) and other hardware-related artefacts (Jo et al. 2010).

It is thus essential to preprocess the resting state BOLD time courses to remove signals of non-interest, which greatly increases the specificity of FC analyses (Weissenbacher et al. 2009). Since the BOLD effect operates at low frequencies (0.01 to 0.1 Hz), a key step in isolating neuronal activity involves lowpass filtering. However, due to the low temporal resolution of resting state data, higher-frequency physiological confounds are aliased down into the frequency band of interest (Bhattacharyya & Lowe 2004). Time courses modelling physiological fluctuations must therefore also be regressed from the BOLD time course. In the absence of external readings, physiological fluctuations can be estimated from the data (known as tissue-based regression; see Jo et al. 2013).

5.5 Methods for extracting resting state functional connectivity

The spatial topography and strength of FC between brain regions can be extracted from resting state data using various methods, which can be broadly grouped into model-dependent and data-driven methods. We only discuss approaches that ignore issues of causation. An array of methods attempt also to make inferences about the direction of influence between functionally linked regions (termed 'effective connectivity'), but these are not employed in this study and are not discussed here (for a review, see Rogers et al. 2007).

Data-driven methods attempt to map FC across the whole brain in a manner that is not parameterised by the neuronal activity of any single brain region. Most typical among such methods is group independent component analysis (ICA), a generalisation of principle component analysis (Van De Ven et al. 2004), which has demonstrated good test-retest reliability and inter-session consistency (Zuo et al. 2010; Chen et al. 2008). ICA simultaneously decomposes a matrix of resting state measurements into a set of spatio-temporal sources that linearly mix together to produce the observations. Since fMRI activation maps, after thresholding for noise, are typically clustered and sparse, ICA decomposition is optimised for spatial rather than temporal independence (Beckmann & Smith 2004). A subset of the resulting spatial maps define RSNs, while other components isolate physiological and hardware-related variance (Kelly et al. 2010). Each spatial map has an associated temporal signature, representing how the common activity of the regions associated with that RSN vary over time. For generalisation to multi-subject analysis, the matrix input to ICA consists of a temporal concatenation of data across all subjects (Schmithorst & Holland 2004). Resulting group independent components are then back-reconstructed to find single-subject spatio-temporal variation associated with each RSN. These are input to group-level analyses to test the significance of effects of interest. Single-subject spatial maps are interpreted to indicate the within-network connectivity of each brain region – that is, the extent to which the region is functionally integrated into the associated RSN (Stevens et al. 2009). For a review of different variations and implementations of the ICA algorithm, see Calhoun et al. (2009).

In the model-dependent approach, the average BOLD time course of a selected 'seed' region is correlated with the respective time courses of all other brain voxels. The result is a seed-voxel correlation map describing the strength of all functional connections radiating from the chosen brain region. Instead of a single seed, a set of regions of interest (ROIs) may be chosen *a priori*. The average time course of each is correlated with that of every other, to produce a cross-correlation map, describing the strength of functional connections within the set. The former might be termed a seed-based correlation analysis (SCA) and the latter an ROI-based analysis, although the two names are sometimes used interchangeably. Both necessitate *a priori* knowledge or hypotheses. Single-subject correlation maps are entered into a group-level analysis to test if connections are significantly modulated by effects of interest. Depending on the positions of two functionally connected regions relative to the boundaries of known RSNs, the implicated connection may describe either within- or between-network FC.

5.6 Interpretations of functional connectivity

Resting state FC measures the extent to which neuronal activity in separated brain regions are phase locked. Three related questions are important for the interpretation of rs-fMRI results: 'What is the cognitive and behavioural significance of FC?'; 'What processes give rise to the neuronal coherence observed at rest?'; and 'How does this neuronal coherence contribute to task performance?'

With regard to the first question, positive FC appears to indicate integration of involved brain regions into unified systems that support cognitive performance and behaviour, while negative FC indicates appropriate segregation (Barber et al. 2013). Evidence for the association of FC with cognitive performance comes first from the correspondence between task-based and resting state networks (Section 5.3). Second, several RSNs overlap with collections of regions assigned common functions by classical behavioural neuroanatomy, such as motor, primary visual, and frontoparietal attention systems (Van den Heuvel & Hulshoff Pol 2010). Finally, both local FC and graph-theoretical summary statistics of whole-brain FC have been correlated with inter-individual performance variability across several cognitive domains. These domains include working memory (Sala-Llonch et al. 2012), episodic

memory (La Corte et al. 2016), reading (Koyama et al. 2011), face processing (Zhu et al. 2011), attention and salience processing (La Corte et al. 2016; Poole et al. 2016; Seeley et al. 2007), executive functions (Reineberg et al. 2015; Seeley et al. 2007), and general intellectual performance (Finn et al. 2015; Van den Heuvel et al. 2009). While the behavioural significance of functional networks is well-evidenced, the complex interactions between networks that gives rise to behavioural performance needs to be further explored. In the same way that discoveries of functional and structural networks have cautioned against the localising of cognitive function to isolated brain regions (as in early clinicopathological mappings), simplistic mapping of function to individual networks should likewise be cautioned against (Sheffield & Barch 2016).

To address the second question: there are two non-exclusive theories for the existence of neuronal coherence at rest – that is, of FC (for a review, see Corbetta 2012). Briefly, FC may be a physiological marker of structural connectivity (white matter tracts), or of histories of task-driven coactivation. Both hypotheses suggest a persisting arrangement that exists independently of immediate cognition. Independence of FC from immediate mental activity is evidenced by the fact that resting state FC has been observed in a state of deep anaesthesia in the macaque monkey (Vincent et al. 2007). FC does at least partly arise from structural connectivity, since studies combining rs-fMRI and DTI (which maps white matter pathways through the directional diffusion of water) consistently report the convergence of these two measures (Damoiseaux & Greicius 2009). However, strong FC is also observed between regions that are only indirectly connected by anatomy, suggesting that other variables interact with the matrix of available structural connections to produce functional characteristics (Damoiseaux & Greicius 2009). The second hypothesis – that regions frequently coactivated during task performance have stronger coherence of activity at rest, as a result of mechanisms of synaptic plasticity – is supported by the appearance of new patterns of FC following the learning of a new skill (Lewis et al. 2009).

As to the question of how neuronal synchrony may contribute to task performance, it has been postulated that this coherence provides a framework for information exchange during task behaviour (Fries 2005). Indeed, the dominant interpretation of FC is the presence of channels for efficient information transfer between two regions (Van den Heuvel, Mandl, et al. 2009). Low frequency oscillations measured by the BOLD signal are correlated with slow cortical potentials measured by electroencephalography (He et al. 2008). These oscillating potentials, in turn, persist during task engagement and modulate the amplitude of higher frequency neuronal activity (Monto 2008). FC may thus serve to synchronise the excitability of related regions of the cortex, allowing two or more regions to simultaneously increase sensitivity to dendritic input as well as increase likelihood of action potential output, thereby opening a channel of communication. Communication may be necessary for ongoing recruitment during task engagement. Another hypothesis, though without experimental support, is that neuronal coherence indicates similarity between content or features that are coded ('stored') in different collections of neurons (Corbetta 2012).

5.7 Common resting state networks and their behavioural correlates

Several RSNs have been consistently observed in adults, including default mode, attention, dorsal frontoparietal, salience, visual, and sensorimotor networks. The spatial profile and functional relevance of canonical RSNs are discussed first (Sections 5.7.1 through 5.7.3). Thereafter, we discuss the degree to which these networks are present in children and how they change with age (Section 5.7.4).

5.7.1 The default mode network

The default mode network (DMN) is the only task-negative network. Working from the observation that several brain regions – particularly the posterior cingulate/precuneus and medial prefrontal cortex (PFC) – consistently exhibit reduced activation (as measured by positron emission tomography) over a range of cognitive tasks (Shulman et al. 1997), Raichle et al. (2001) set out to discover if these deactivations were merely artefactual. Task-based imaging is differential, subtracting a signal acquired at rest (in the control state) from that acquired during the performance of a task. It had previously

been suggested that the observed regional deactivations may not in fact be reductions from a baseline, but rather indicate unsuspected transient activation during the control state; arising, for example, from visual fixation. In a famously informative null result, the team found that none of the implicated regions had increased local activity, compared to a global mean, in the resting state (eyes closed or open). The implication was not only that activity in these regions is anticorrelated with goal-directed behaviour, but – critically – also that the activity forms part of the metabolic baseline state itself. Unlike regions that are transiently active under the performance of tasks, these regions are tonically active, analogous to muscles being kept in a state of baseline tension. This discovery of the DMN reignited interest in the intrinsic activity of the brain in the resting state (Raichle 2015), which lead to the discovery of many functional networks.

A large body of rs-fMRI literature has revealed that the set of rest-preferential regions flagged in task-based studies are in fact integrated into a cohesive functional network (e.g. Andrews-Hanna et al. 2010; Greicius et al. 2003). The key nodes of this DMN are the posterior cingulate cortex/precuneus, the ventromedial PFC, and the dorsomedial PFC (Raichle 2015), but additional regions such as the angular gyrus, and the medial (hippocampal formation) and lateral (temporal parietal junction, lateral temporal cortex, and the temporal pole) temporal areas may also be integrated into this system (Andrews-Hanna, Reidler, Sepulcre, et al. 2010) (Figure 1).

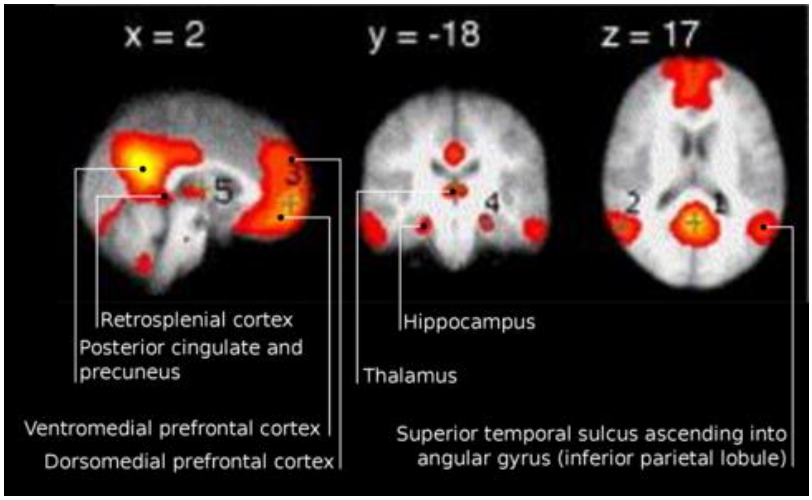

Figure 1: Visualisation of the default mode network (DMN). Figure adapted[14] from De Luca et al. 2006.

Classical behavioural neuroanatomy associated with the key nodes, along with insights from neuroimaging under well-designed tasks, has led to several speculations about what functions this network may subserve. These include: the retrieval of episodic memories and semantic knowledge (Kim et al. 2010; Greicius et al. 2003), perhaps especially to construct simulations of future events for planning purposes (Andrews-Hanna, Reidler, Huang, et al. 2010); attention-free gathering and evaluation (including emotional) of information from the internal and external environment (Raichle et al. 2001); a combination of the above, for rapid "autopilot" application of learned behavioural responses to environmental demands (Vatansever et al. 2017); autonomic processing, or the continuous biasing of such processing (Raichle et al. 2001); affective (emotional and feeling-related) processing, and interplays with self-knowledge and prediction of others' mental states (Andrews-Hanna, Reidler, Huang, et al. 2010); and integration of cognitive and emotional states (Greicius et al. 2003). Overall, the network tends to show a bias for self-referential processing.

Finally, it likely has an essential role in balancing cognitive and goal-directed processing (for a review, see Raichle 2015). Analysis of resting state spontaneous activity shows that the DMN is anticorrelated with RSNs supporting attention and executive functions (Fox et al. 2005; Popa et al. 2009). This

[14] In this and all subsequent cases, permission was obtained from one of the co-authors and, where required, from the publisher, for the use and adaption of the figure.

negative relationship may, for example, constrain preplanned behaviour by taking into account social and environmental variables, preventing impulsivity (Shannon et al. 2011).

5.7.2 The cognitive control group

In contrast to the DMN, several RSNs involve regions flagged as highly active during externally-oriented, goal-directed cognition and behaviour. It is perhaps worth emphasising that the level of activity of regions observed under task conditions, while informing the function of RSNs in which they are included, is separate from the intrinsic connectivity that defines those RSNs. While early ROI-based FC studies conflated commonly activated regions into a single 'task-positive' system (Fransson et al. 2007; Fox et al. 2005) that is anticorrelated with the DMN, ICA indicates that several distinct subnetworks should be recognised. The number and spatial topologies of these networks, and whether they have a hierarchical or centralised organisation, is the subject of ongoing research. ICA methods typically reveal a set of RSNs that together form a 'cognitive control' group, supporting higher level cognition (Allen et al. 2014).

This group includes an executive control network – consisting of extensive medial-frontal areas (anterior-/mid-cingulate and paracingulate) together with the insulae, opercula, and select subcortical and inferior parietal regions (Figure 2a) – and two lateralised and symmetrical frontoparietal networks (Figure 2b,c) consisting of dorsal frontal and parietal neocortices (Zuo et al. 2010; Smith et al. 2009). A dorsal attention network is sometimes observed separately (Zuo et al. 2010; Biswal et al. 2010), with extensive bilateral coactivation in the intraparietal sulci and frontal eye fields (meeting of the precentral and superior frontal sulci) (Figure 2d).

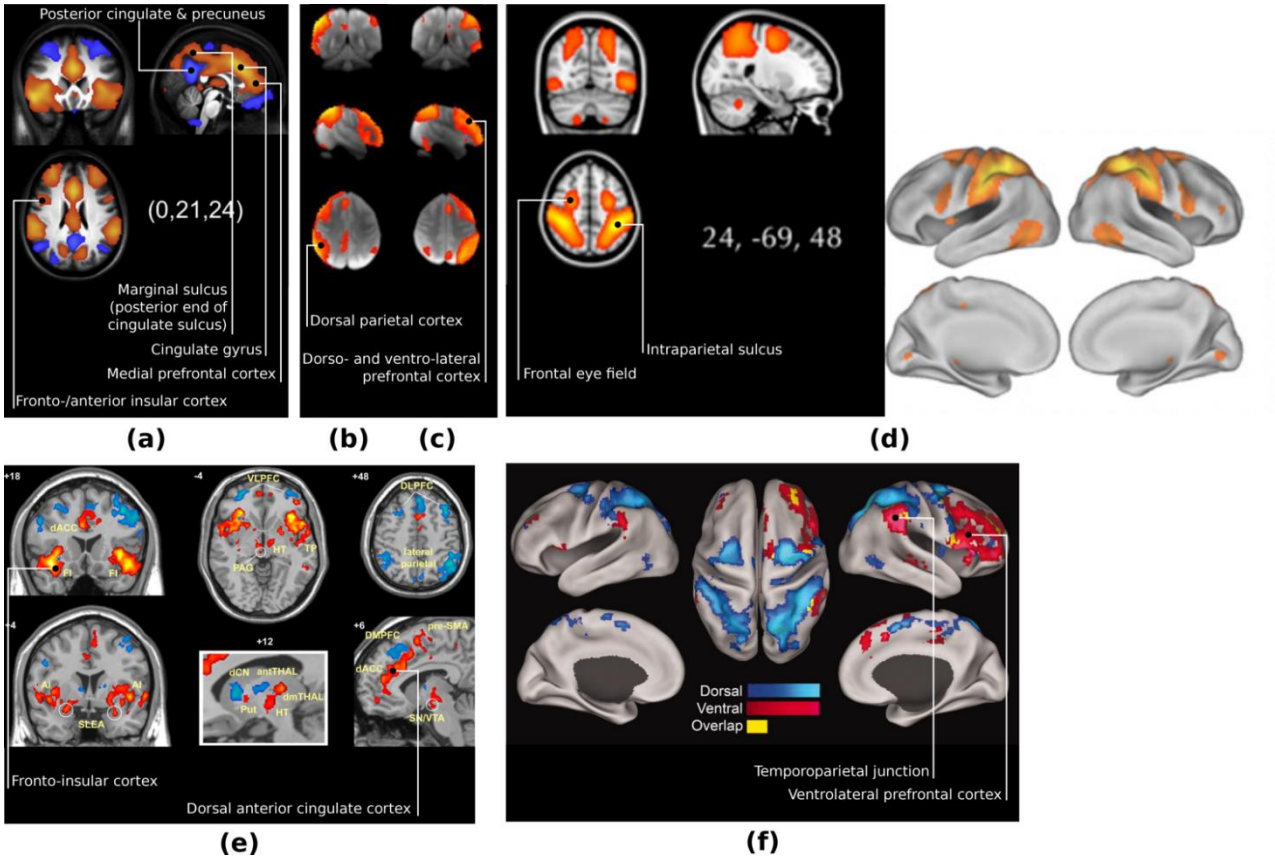

Figure 2: Visualisation of networks involved in cognition and control: (a) executive control network; hot colours represent regions forming part of the network, while cold colours indicate regions anticorrelated with it; notice the anticorrelation with the posterior cingulate node of the task-negative DMN; radiological convention, with left=right (figure adapted from Zuo et al 2010); (b) and (c) right and left frontoparietal networks, respectively; radiological convention (adapted from Smith et al. 2009); (d) dorsal attention network; radiological convention (adapted from Biswal et al. 2010); (e) hot colours indicate the domain of the salience network, as originally defined by seed-based methods; neurological convention, with left=left (Seeley et al. 2007); (f) hot colours indicate the domain of the ventral attention network (adapted from Fox et al. 2006).

The executive control network has a uniquely transitional behavioural profile, being associated with both emotion-related/interoceptive (including pain) processes and executive function processes (Smith et al. 2009). Its executive function is biased towards action and inhibition, as opposed to working memory and reasoning, though both are apparent (Laird et al. 2011; Smith et al. 2009). Hierarchical clustering of RSNs indicates that this network uniquely has positive correlations with modules of both the systems for intrinsic processing and extrinsic processing, facilitating information exchange between the two (Doucet et al. 2011). Its spatial profile is largely made up of the salience network (Figure 2e), as identified by Seeley et al. (2007) using seed-based techniques. It also overlaps strongly with the cingulo-opercular network identified by Dosenbach et al. (2007) using ROI-based methods, though the latter differs by the inclusion of extensive ventrolateral PFC. The salience

network includes the dorsal anterior cingulate and fronto-insulae, known to be responsive to salient stimuli such as unexpected (highly informative) error feedback or threats to homeostasis (Ham et al. 2013; Seeley et al. 2007; Holroyd et al. 2004). Investigating onset latencies of activation responses, together with Granger causality estimates, reveals that especially the right fronto-insular node of the salience network has high causal outflow to key nodes of the frontoparietal network and the DMN, activating the former and deactivating the latter for task focus (Sridharan et al. 2008). Taken together, it emerges that the executive control network plays a topologically central role, detecting salient stimuli and initiating cognitive control signals (Menon & Uddin 2010). These signals facilitate dynamic switching between networks to engage executive function (such as working memory) and to disengage task-irrelevant processes. Signals are not only transient cues for task initiation, but also longer-acting signals for stable control of task mode and strategy (Dosenbach et al. 2007).

The lateralised frontoparietal networks are associated with a broad range of cognitive and language paradigms (Laird et al. 2011; Smith et al. 2009). In contrast with the executive control network, the executive function supported by these networks is more biased towards working memory, reasoning and language than attention and inhibition (Laird et al. 2011). Speech and language processing is largely only associated with the left network, consistent with known lateralisation of language function, while perception of integrated body sensation is largely right literalised (Smith et al. 2009). Non-lingual cognition is associated with both (Smith et al. 2009). Hierarchical clustering of RSNs suggests that the two lateralised networks together support information storage and manipulation (Doucet et al. 2011). Indeed, within-network FC of the networks' lateral parietal nodes is correlated with working memory performance (Seeley et al. 2007). It can cause some confusion that this set of networks, like the cingulate/insulae/parietal network, is sometimes referred to as 'executive control' or 'central executive,' consistent with its essential role in executive function. The author prefers to assign this label to the cingulate/insulae/parietal network, given its topologically central role.

The dorsal attention network (Figure 2d) is thought to be associated with top-down focusing of attention (Fox et al. 2006). This mechanism is often described in terms of the biased-competition model of attention (Desimone & Duncan 1995): as there is limited capacity for processing sensory information, top-down signals bias the competition between sensory inputs so that only the most goal-relevant ones are perceived and enter working memory (Corbetta et al. 2008). The biasing mechanism is evidenced by preparatory activation of the dorsal system under expectation of observing a stimulus at a particular location (Corbetta et al. 2000) or by recall of a visual scene from short-term memory (Astafiev et al. 2003). The dorsal attention system is often contrasted with a right-lateralised ventral attention system, the key nodes of which are the temporoparietal junction and ventrolateral frontal cortex (Fox et al. 2006) (Figure 2f). The ventral attention system facilitates reorienting of attention to salient and behaviourally-relevant stimuli, especially when unexpected or unattended (Corbetta et al. 2008; Fox et al. 2006), and thus has functional overlap with the previously-described executive control network. The literature has not yet converged on a single model for the dynamic interaction between the two attention networks, nor between the attention networks and the signalling hubs in the executive control network (Menon & Uddin 2010; Corbetta et al. 2008; Dosenbach et al. 2007).

5.7.3 Sensory and motor networks

In contrast to the anatomically-distributed RSNs supporting cognition and attention, several anatomically-local RSNs support low level sensory processing and motor function. Visual RSNs are robust and frequently explain the largest variance in ICA decompositions (Biswal et al. 2010; Smith et al. 2009; De Luca et al. 2006). The medial visual network (Figure 3a), consisting of the cuneus, has the highest test-retest reliability (Zuo et al. 2010), but occipital pole (Figure 3b) and lateral occipital cortex (Figure 3c) visual networks are often also observed (Biswal et al. 2010; Smith et al. 2009). These networks are associated with behavioural paradigms involving visual perception, cognition related to space, and processing of written words (Smith et al. 2009).

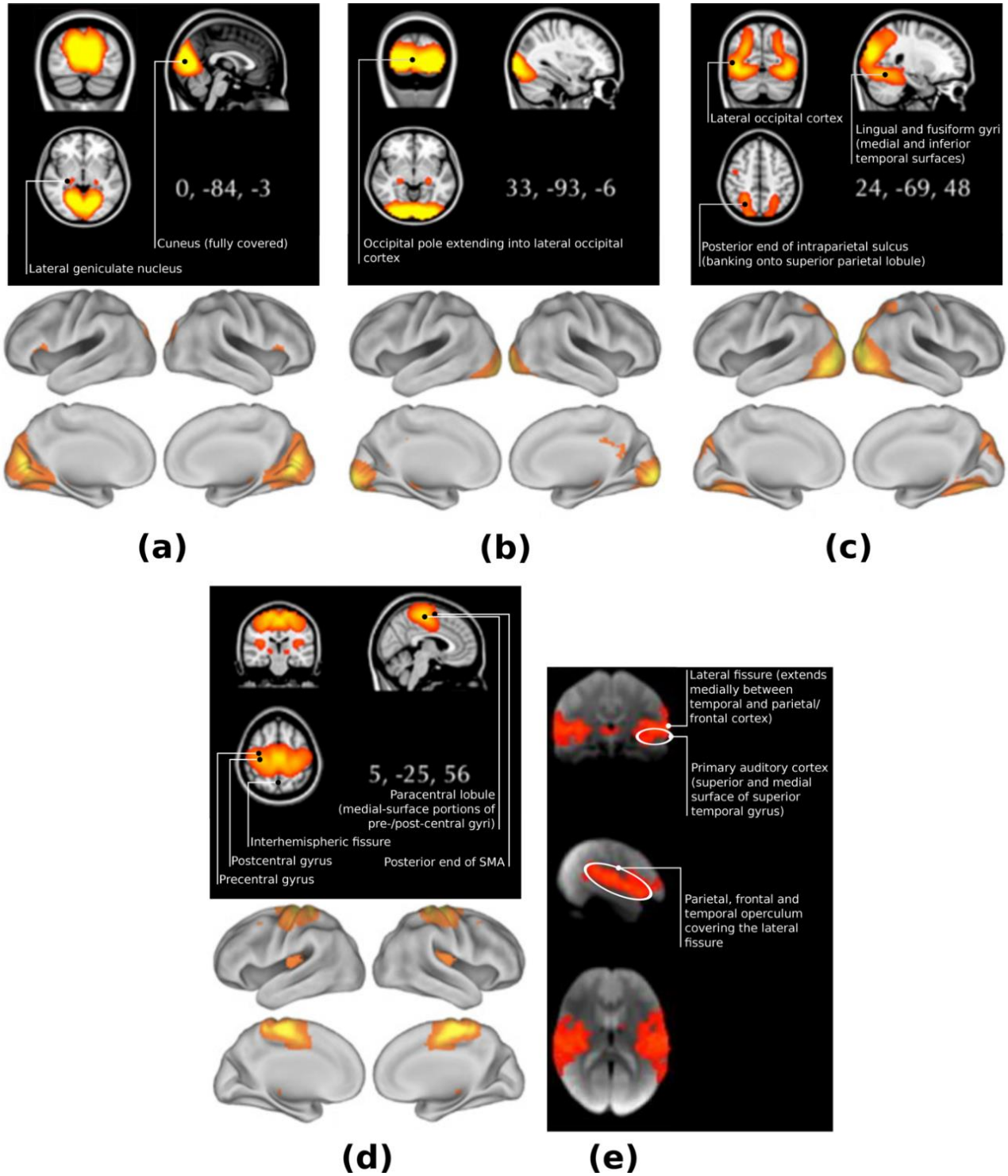

Figure 3: Visualisation of networks involved in low-level sensory and motor processing : (a), (b) and (c) medial, occipital pole, and lateral occipital cortex visual networks; the lateral occipital cortex visual network may also be integrated with the occipital pole visual network or else be absent, in which cases the occipital pole network is referred to as the 'lateral visual' network, as in Beckmann et al. 2005; radiological convention (figures adapted from Biswal et al. 2010); (d) sensorimotor network; radiological convention (adapted from Biswal et al. 2010) (e) auditory network; radiological convention (adapted from Smith et al. 2009).

The sensorimotor network (Figure 3d) consists of the pre- and postcentral gyri (extending from the lateral fissure to the interhemispheric fissure) and the supplementary motor area (SMA)[15] (Beckmann et al. 2005; Biswal et al. 1995). It corresponds to activation observed in bimanual motor tasks (Biswal et al. 1995), and is associated with the perception of touch and movement-related senses, as well as the execution of action (Smith et al. 2009). The sensorimotor network might be referred to as the 'somatosensory' network in cases where secondary motor areas (SMA and pre-SMA on the medial surface of the frontal lobe, and premotor cortex[16] on the dorsal surface) are excluded.

An auditory RSN (Figure 3e) consisting of the superior temporal cortex may be revealed as a separate component by ICA methods (Smith et al. 2009; Mantini et al. 2007), and corresponds to audio tasks such as text-listening (Cordes et al. 2000). Primary and secondary auditory cortex may alternatively be seen integrated into other RSNs (Zuo et al. 2010).

5.7.4 Resting state networks in children, and age-related changes

The earliest developing RSNs, including medial visual, somatosensory, and auditory networks, are already well-formed in infancy (Fransson et al. 2007). By age 7 years, all major canonical networks described in adults are noted (Thornburgh et al. 2017). While sensory and motor networks display robust functional organisation at this age, higher cognitive networks might still be incomplete or fragmented (Thornburgh et al. 2017; De Bie et al. 2012).

The literature has reported several trends in the maturing of RSNs through childhood and adolescence. The spatial profile of RSNs become less diffuse and more focal towards adulthood (Littow 2010). The strength of short-range functional connections decrease, while the strength of long range connections between regions that are functionally-related in adults simultaneously increase (Uddin et al. 2010; Power et al. 2010; Fair et al. 2009; Supekar et al. 2009). Finally, the integration of brain regions into

[15] A region on the medial surface of the cerebrum, anterior to the paracentral lobule.
[16] Anterior to the precentral gyrus.

their associated RSNs (within-network FC) increases towards adulthood, while between-network FC decreases (Fair et al. 2009; Stevens et al. 2009).

6 Methodology

6.1 Study cohort

Infants born to HIV+ mothers were identified from the public prevention of mother-to-child transmission programme in the Western Cape. Mothers and neonates received a single dose of nevirapine. In addition, zidovudine was given to mothers from 34 weeks' gestation and to neonates for 7 days. Infection-status in infants was established by plasma polymerase chain-reaction (PCR RNA) viral load tests at 4 weeks or later (Cotton et al. 2013). Because of the timing of the tests, the timing of vertical infection – in utero or during the perinatal period – is unknown (Violari et al. 2008).

As part of the CHER study, vertically-infected HIV+ infants with CD4% of at least 25% were randomised into one of three treatment arms at 6 to 12 weeks of age: immediate ART for 40 weeks (with subsequent interruption); immediate ART for 96 weeks (ditto); or deferred continuous ART. Criteria for treatment initiation (in the deferred treatment arm) or re-initiation (in the immediate treatment arms) were any of: CD4% less than 25% in infancy (< 12 months of age), or less than 20% thereafter; severe CDC[17] stage B or C diseases; failure to thrive (see Cotton et al. 2013 Appendix for a more exhaustive description). In some of our other cross-sectional studies, we have retrospectively reclassified children as having started treatment either before or after 12 weeks of age, because of cases of failed adherence or of poor clinical outcomes necessitating early treatment (Jankiewicz et al. 2017; Toich et al. 2017; Mbugua et al. 2016). In this study, which primarily examines differences in FC outcomes between HIV+ and uninfected children, rather than between treatment strategies, we have instead preserved the recorded age at ART initiation as a continuous variable. First-line ART was a combination of zidovudine, lamivudine and lopinavir-ritonavir (Cotton et al. 2013). All children scanned at age 9 years were still on first-line treatment.

We imaged 59 vertically-infected children (mean(SD) age: 9.25(0.19) years; 27 males) from the CHER trial (Section 1; Cotton et al. 2013; Violari et al. 2008) in follow-up at the Children's Infectious Diseases

[17] Center for disease control and prevention.

Clinical Research Unit, Tygerberg Children's Hospital, Cape Town, South Africa. We also imaged 32 age- and socioeconomic-matched uninfected controls (9.48(0.19) years; 15 males) – of which 17 were perinatally exposed (HEU; 9 males) to HIV/ART and 15 unexposed (HU; 6 males) – from an interlinking vaccine trial (Madhi et al. 2010). Both groups were recruited from the same Western Cape community. Subsequent to the completion of the aforementioned trials, the children are being followed as part of the current longitudinal study, with neurocognitive testing and neuroimaging performed every two years.

6.2 MRI acquisition

All neuroimaging was performed on a Siemens Skyra 3T (Erlangen, Germany) MRI scanner situated at the Cape Universities Body Imaging Center (CUBIC) in Groote Schuur Hospital, Cape Town, South Africa. Protocols were approved by the Faculty of Health Science Human Research Ethics Committees of both the Universities of Stellenbosch and Cape Town.

The children were transported to the imaging center approximately one hour before the scheduled scan, having previously been familiarised with the scanning routine at a mock scanner about two weeks prior. The scan is completed in under 40 minutes, including both structural MRI and rs-fMRI acquisitions (analysed here), together with DTI and spectroscopy acquisitions (not analysed here). The children watched a movie during all scans except during the acquisition of the rs-fMRI data, during which the movie was switched off and the children were asked to relax with their eyes open.

The T1-weighted structural volumes were acquired in sagittal slices using a multi-echo magnetization-prepared rapid gradient echo (MEMPRAGE) iPAT (x3)[18] sequence (Van der Kouwe et al. 2008): TR/TE = 2530/1.69 ms; inversion time (TI) = 1100 ms; flip angle = 7 degrees; 224 x 224 acquisition matrix; 1 mm^3 isotropic voxels. The rs-fMRI data were acquired using a 2-D echo planar imaging (EPI) sequence: TR/TE = 2000/30 ms; flip angle = 90 degrees; FoV = 250 x 250 mm^2; 2.98 x 2.98 mm^2 voxels; slice thickness = 4 mm; 33 interleaved slices; 180 volumes. The EPI scanning sequence measures the

[18] Siemens' parallel imaging implementation, with an acceleration factor of 3.

BOLD signal (Section 5.2) at each voxel (the smallest cubic area of brain tissue that can be digitally isolated given the imaging resolution; the 3-D analogue of a 2-D pixel) 180 times, at two second intervals. Every brain location thus has an associated BOLD 'time course', with limited temporal resolution. The time courses of all voxels are synchronised through preprocessing, so that each time point has an associated whole-brain volume.

6.3 Preprocessing

The desired outcome of preprocessing is the rs-fMRI volumetric time course aligned and spatially normalised to a standard brain space, with motion confounds and signals of no-interest removed. An overview of the preprocessing pipeline is given in Section 6.3.1. To combat residual motion artefacts not removed by typical preprocessing, we truncated every time course to an interval of lower-motion volumes, using an in-house method described in Section 6.3.2.

6.3.1 Pipeline overview

Preprocessing was largely carried out in AFNI (Cox 1996) using the afni_proc.py tool (see Appendix A for a list of parameters). The pipeline (Figure 4) generally followed a standard form (Gotts et al. 2012; Shulman et al. 2010) and included: removing the first 4 volumes; despiking; slice timing correction; within-subject volume registration; warping to the Haskins Pediatric Brain template (Molfese et al. 2015), via the native T1-weighted volume; 6 mm spatial smoothing; tissue-based regression (locally averaged white matter) and regression of motion realignment parameters; detrending; bandpass filtering (0.01–0.2 Hz); and truncation of the EPI series to the run of 140 successive volumes which contains the least in-scanner motion. Details of the final step are discussed in Section 6.3.2. Further details of each of the other preprocessing blocks, together with supporting theory, are discussed in Appendix B.

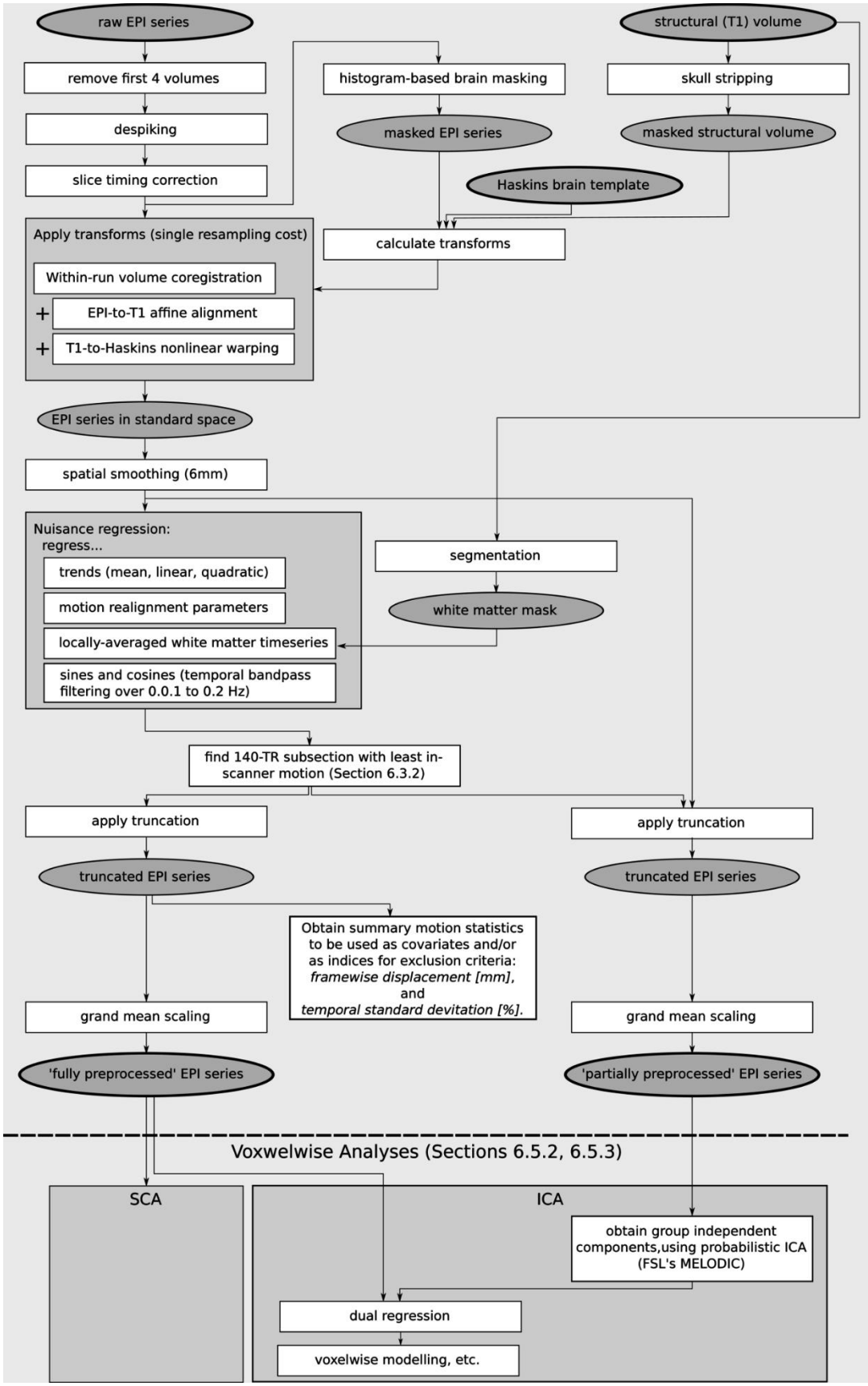

*Figure 4: Pipeline for the preprocessing of all participants' resting state (EPI) data. **EPI**, [2-D] echo planar imaging: the sequence employed to acquire resting state fMRI data; **TR**, repetition time; **SCA**, seed-based correlation analysis; **ICA**, independent component analysis.*

Following the approach of the Functional Connectomes Project (Biswal et al. 2010), two different preprocessing outputs are obtained: a 'partially-preprocessed' EPI dataset, which has been spatially normalised to the Haskins template and Gaussian-smoothed, but has not undergone nuisance regression and bandpass filtering; and a 'fully-preprocessed' dataset, which has additionally undergone these final steps. The former preserves more signal variance, and is used purely for estimating group resting state networks using probabilistic ICA (Section 6.5.2), while the latter is employed for all statistical analyses. After obtaining summary measures of subject motion (Section 6.4.1), every 4-dimensional dataset of each type was grand-mean intensity normalised using a single multiplicative factor, as is common (Sato et al. 2015; Smith et al. 2014; Starck et al. 2013).

6.3.2 EPI run truncation

To identify the optimal truncation, a sliding window isolates and quantifies the motion of every possible subset in the EPI series (Figure 5). Subject motion was quantified using a combination of two summary statistics corresponding with those employed in other studies (Guha et al. 2016; Thomas et al. 2013): the root mean square framewise displacement of the brain; and the voxel-wise temporal standard deviation of the rs-fMRI signal (measured after nuisance regression), averaged spatially over the whole brain. The former is a standard measure of rigid-body motion, while the latter offers sensitivity to large framewise amplitude changes (Power et al. 2014; Satterthwaite et al. 2013) or large fractions of outlying voxels in a volume (Ipser et al. 2015).

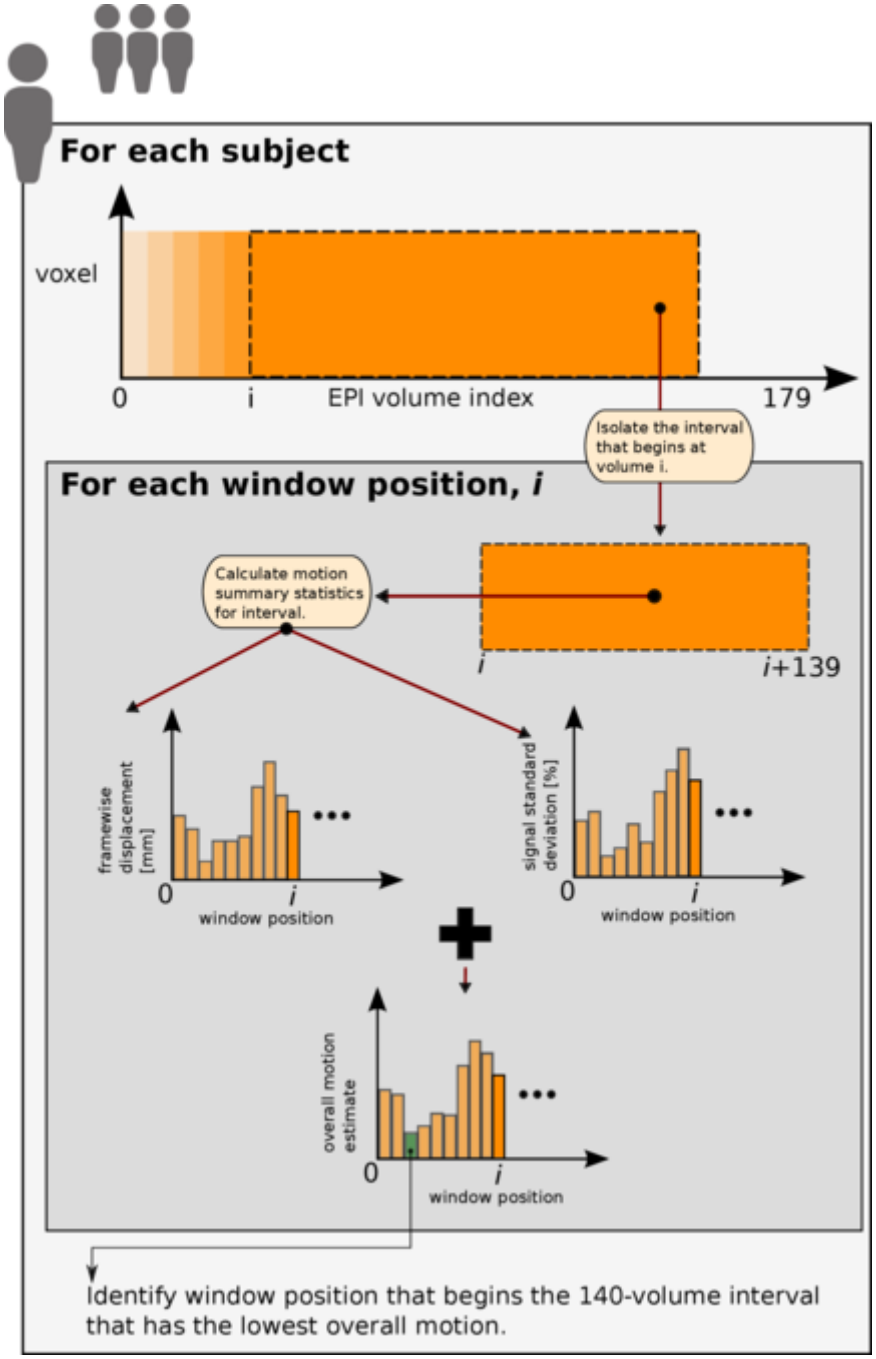

Figure 5: The in-house algorithm employed to truncate participants' resting state (EPI) runs to the 140-volume interval containing the least in-scanner motion. Two summary statistics of motion are used: mean framewise displacement; and temporal standard deviation of the resting state signal, averaged over the brain. ***EPI****, echo planar imaging.*

Framewise displacement was based on the Euclidian norm of the first time difference of rigid-body motion estimates (Jo et al. 2013):

$$\sqrt{(x_i - x_{i-1})^2 + (y_i - y_{i-1})^2 + \cdots} \ . \tag{3}$$

This index, calculated automatically by the AFNI preprocessing stream (afni_proc.py), is averaged over the EPI series to obtain framewise displacement. The rigid-body motion estimates employed in this index consist of three translational and three rotational elements, and are obtained during the alignment of the EPI volumes to a base volume (within-run coregistration; Figure 4). Temporal standard deviation, the second index employed, was normalised by each subject's modal value of brain voxel intensity (Power et al. 2012). The optimal interval of EPI volumes is considered that with the lowest sum of the two motion indices, where each index is first converted into a percentile rank (the relative standing of the value in the distribution over all possible window positions).

6.4 Exclusion criteria

6.4.1 Within-scanner motion criteria

Subjects were excluded if their 140-volume truncated EPI series included excessive motion – that is, if either of the two motion indices (defined in Section 6.3.2), as calculated over the truncated series, exceeded an associated threshold. Subjects with less than 140 volumes[19] in their time course were automatically excluded. To select a pair of thresholds that best compromised between data quality and residual sample size, the number of excluded subjects was evaluated over a meshgrid of threshold value combinations, as illustrated in Figure 6.

[19] More accurately, 140 volumes after preprocessing. The first four volumes are removed during preprocessing, such that at least 144 volumes had to have been acquired to avoid exclusion.

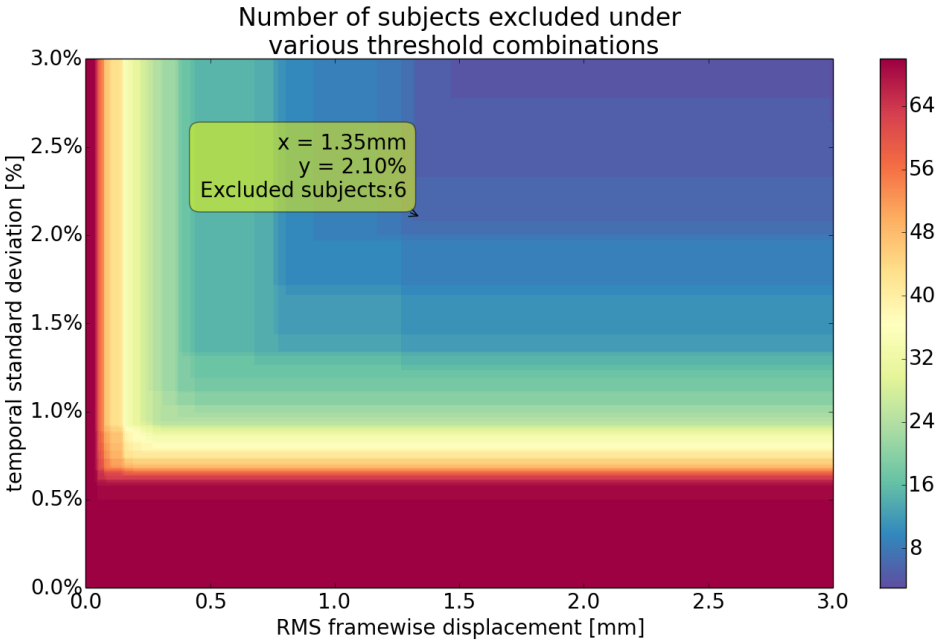

Figure 6: The number of subjects that would be excluded under motion criteria, evaluated over a meshgrid of threshold value combinations. Subjects were excluded if either the mean framewise displacement, or the temporal standard deviation of the resting state signal, exceeded the chosen thresholds. ***RMS****, root mean square.*

Limits of 1.35 mm and 2.1% were selected for mean framewise displacement and temporal standard deviation of the resting state signal, respectively. These values satisfy standards previously employed in the literature (Guha et al. 2016; Ortega et al. 2015; Thomas et al. 2015; Wang et al. 2012).

In summary, subject-level motion correction was performed through: i) rigid-body motion correction during preprocessing, in the alignment of EPI volumes to a base volume (Section 6.3.1); ii) trimming of the EPI series to the 140-volume interval containing the least motion (Section 6.3.2); and iii) exclusion of participants whose trimmed series contained excessive motion. Nevertheless, subject-level correction typically does not bypass the need for group-level correction (Yan et al. 2013). The more standard of the two motion indices, framewise displacement, was modelled as a covariate in all group-level analyses (Section 6.5.1). A disadvantage of this approach is that it decreases the ability to detect the effect of interest to the extent that it covaries with motion (Power et al. 2014; Satterthwaite et al. 2012). However, prior HIV rs-fMRI studies do not show significant covariation of motion with HIV infection status (Guha et al. 2016; Ipser et al. 2015). Group level regression can also only control for linear effects of motion; but nonlinear effects seem to be insignificant for some resting state networks (Satterthwaite et al. 2012).

6.4.2 Other criteria

Subjects with resting state and anatomical datasets that had severe imaging artefacts, such as incorrect field of view or field bias, were excluded. Subjects were also excluded for failed alignment of datasets to the template in standard space. For every subject, the alignment of the EPI base volume (that to which other EPI volumes in the series are registered during preprocessing) to the native structural volume, the alignment of the native structural volume to the Haskins template, and the resultant alignment of the EPI volume to the template, were all visually inspected as a quality control measure.

6.5 Statistical analysis

The primary aim of this study was to compare FC between HIV+ and HIV-uninfected children at age 9 years. This contrast was explored using two different methods: independent component analysis (ICA) and seed-based correlation analysis (SCA). ICA facilitates exploratory investigation of FC, but enables inferences about within-network connectivity only. SCA facilitates testing of particular hypotheses, and allows inferences about both within- and between-network connectivity. These two pipelines use *Z*-score maps of within-network and seed-to-whole-brain connectivity, respectively, as their dependent variables. The set of analyses performed in this study is summarised in Figure 7.

Additional investigations were carried out within ICA-defined RSNs, which lend themselves particularly well to exploratory analyses, not requiring *a priori* selection of anatomical regions of interest (Beckmann et al. 2005). Within the uninfected children, the effect of perinatal exposure to HIV and ART was investigated. Amongst HIV+ children, we explored the effects of age at ART initiation, as well as immune health both at enrolment to the CHER trial (age 6–8 weeks) and at the time of scanning (9 years). Markers of immune health included $CD4^+$ count, CD4% and the $CD4^+$:$CD8^+$ ratio. However, $CD8^+$ measures at age 9 years were unavailable for a significant number of participants and the $CD4^+$:$CD8^+$ ratio was therefore only included in the investigation of immune health at enrolment.

For clarification, we highlight that no comparison was performed between the HIV-infected and the HEU groups, or between the HIV-infected and the HU groups. Together, these two comparisons would

yield similar insight as a comparison between the HIV-infected and HIV-uninfected groups combined with a comparison between the HEU and HU groups. The latter approach, which is employed in this study, is (i) more aligned with the separation between the research aims (see Section 1); and (ii) affords more statistical power to the primary study objective, namely to assess the impact of HIV-infection in children stable on ART.

The pipelines for ICA and SCA are described in Sections 6.5.2 and 6.5.3, respectively. Both approaches model FC on a voxelwise basis. The design of these models is discussed in Section 6.5.1.

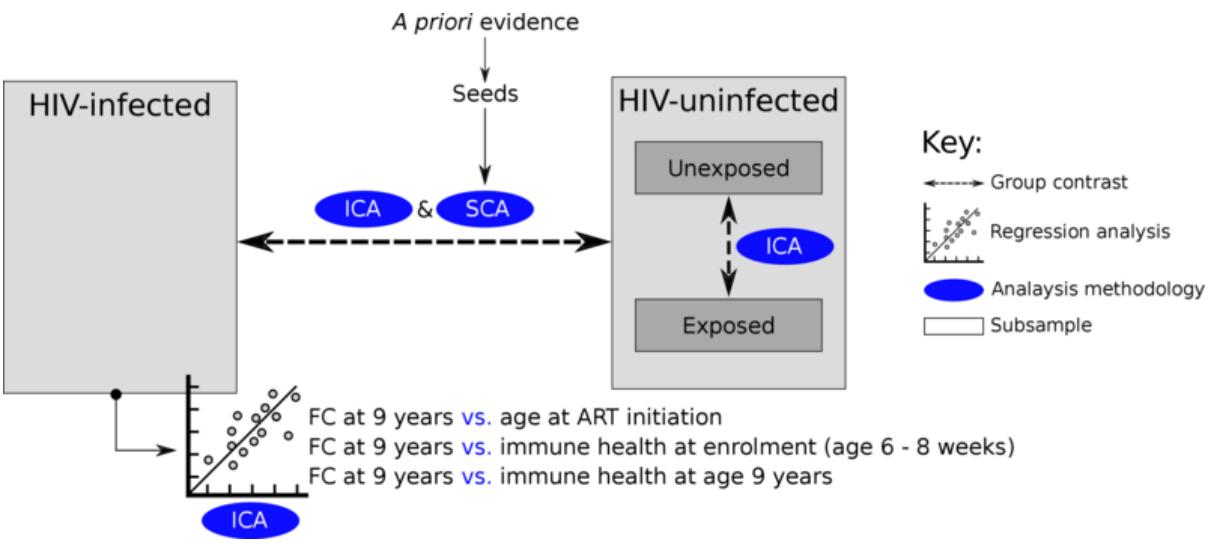

Figure 7:Summary of the analyses performed in this study. Comparison of resting state functional connectivity (FC) between the HIV+ and HIV-uninfected groups was the primary focus of this study, and was performed using both independent component analysis (ICA) and seed-based correlation analysis (SCA) methods. Additional exploratory analyses were performed within these two groups, though within the ICA-generated resting state networks only, to better understand the factors contributing to the results of the primary analysis.

6.5.1 Model design

All statistical analyses were performed in a unified multiple linear regression framework, which models the FC in each voxel as a linear function of explanatory variables. The portion of between-subject variance explained by each explanatory variable, as given by the associated regression coefficient, is an indication of the magnitude of its partial effect on FC. First, we discuss the approach employed to select variables for inclusion in voxelwise models, then which variables were in fact included, and finally how these variables were coded in the design matrices.

Approach to covariate selection

Since our hypotheses investigated causal effects, our variable selection approach chiefly aimed to prevent bias resulting from the omission of confounders. Such bias negatively or positively distorts the estimate of the causal effect of interest through the contribution of a non-causal component.

However, identification of confounders is complex. An atypical approach is to bypass selection by including all measured variables in the model. Ordinarily, this will result in sparse data bias, which is essentially overfitting of the regression model to peculiarities of the sample data (Austin & Steyerberg 2015). With too great a number of predictor variables, the data cannot support accurate parameter estimation, because of limited sample size and uneven distribution of covariate values across the sample (Greenland et al. 2016). Modern fitting techniques address this problem through 'shrinkage' – pulling estimated regression coefficients toward zero in proportion to their instability (Greenland 2008). Yet other problems remain, such as the introduction of measurement noise associated with each explanatory variable, linearly modelling nonlinear effects, and the difficulty of parameter interpretation in complex models. Variable selection methods typically penalise model complexity to some extent.

Potential confounders were identified using classical tests (Kamangar 2012; McNamee 2003), which require that the following criteria be met:

i. *The variable is causally associated with FC (or is a surrogate measure of such a cause)*.

   Both the causality and existence (or lack thereof) of the association was established on *a priori* evidence. The mass-univariate nature of FC made statistical tests for the association impractical.

ii. *The variable is associated with the effect of interest*.

   Where the effect of interest is a grouping variable (such as HIV-infection status), this simply amounts to there being a between-group difference in the covariate. Preference was given to

a priori evidence, as we did not wish to assume that there was sufficient statistical power to establish the association.

iii. *The variable is not on the causal pathway from the effect of interest to the FC outcome.*

Further, any variable with a sample variance considered too small to produce measurable variance in FC was not included, even if it satisfied the above criteria (Greenland 2008). It is important to note that the 'measured' FC, in this sense, is the FC captured by the EPI protocol and which has survived (and been revealed through) preprocessing.

Selected covariates

Table 1 presents a summary of the covariates included in the various analyses.

Table 1: Covariates included in the voxelwise model for each analysis performed in this study.

Effect of interest	Covariates included in voxelwise model
HIV-infection	Sex; framewise displacement.
Perinatal exposure to HIV and ART	Sex; framewise displacement.
Treatment timing (age at ART initiation)	Framewise displacement; duration of ART interruption.
Immune health in infancy ($CD4^+$ count; CD4%, $CD4^+$:$CD8^+$ ratio)	Sex; framewise displacement.
Current immune health ($CD4^+$ count, CD4%)	Sex; framewise displacement.

Although our HIV+ and uninfected groups differed in age, and various cortico-cortical and cortico-subcortical RSNs demonstrate evidence of increasing intrinsic connectivity through adolescence (Sole-Padulles et al. 2016), the fairly small sample variance of age-at-scanning in our cohort (roughly 5 months on average; Table 3) is unlikely to produce measurable variance in FC. To the author's knowledge, there is no literature demonstrating effects of age on FC over a comparably small age range (IQR: 9.1–9.3 years; full range: 9.0–10.4 years). We did, however, perform *post hoc* tests for associations of connectivity scores with age in significant clusters revealed by voxelwise analyses to confirm that observed differences are not attributable to age.

Sole-Padulles et al. (2016) detected no effects of sex on voxelwise FC among adolescents. Conversely, the global and regional topological organisation of RSNs – particularly of the default mode, language, and visual networks – appears to differ between boys and girls (Wu et al. 2013). There is also evidence of sex-related differences in frontal grey and white matter volumes in childhood; but the limited number of longitudinal studies in the literature leaves the matter unsure (Blakemore & Choudhury 2006). Overall, there is some reason to expect an effect of sex on intrinsic connectivity. Further, it has been shown that girls may be more susceptible to vertical transmission of HIV than boys (Gabiano et al. 1992; Taha et al. 2005). Therefore, there is *a priori* evidence for an association of sex with HIV-infection status in the population, in addition to an association with FC measures. Thus, we controlled for sex in comparing FC between the HIV+ and uninfected groups. Since the association of sex with infection status may more generally indicate that the virus affects boys and girls differently, both perinatally as well as later in development, we also controlled for this covariate in the HU vs. HEU analysis.

Treatment timing was randomised in HIV+ subjects, and there is thus no expectation of an association of sex with age at ART initiation; *post hoc* testing confirms this (female(F) : male(M) = 17.7 : 17.8 weeks, $p = 0.98$). To the author's knowledge, no study has reported baseline immunologic measures as differing between genders in HIV+ infants. Nevertheless, gender differences in CD4% and $CD4^+$:$CD8^+$ ratio at enrolment were observed in our sample (CD4%: F : M = 37.0 : 33.5, $p = 0.19$; $CD4^+$:$CD8^+$: F : M = 1.6 : 1.1, $p = 0.03$), though interestingly not in $CD4^+$ count at enrolment (F : M = 1893 : 2018 cells per µl, $p = 0.62$). Similarly, gender differences in current CD4% (F : M = 35.1 : 38.8, $p = 0.17$), but not current $CD4^+$ count (F : M = 1322 : 1317 cells per µl, $p = 0.94$), were observed, even though the literature suggests no gender differences in immunologic or virologic outcomes during long-term ART (Nicastri et al. 2005; Moore et al. 2003). Given the *post hoc* evidence, sex was controlled for in all investigations of relations with immune health measures.

While abnormal muscle tone, developmental delays in gross motor skills, and deficits in fine motor control are reported in pediatric HIV-1 infection (Van Arnhem et al. 2013; Koekkoek et al. 2008; Van Rie et al. 2007), hyperkinesia is not. We therefore do not expect in-scanner motion to correlate with infection status nor with any other effect under investigation. *Post hoc* testing revealed no associations of effects of interest with motion in our sample ($p > 0.3$ across all cases). Here, framewise displacement (Section 6.4.1) was employed as the measure of motion. Though not a confounder, framewise displacement was nevertheless included in all models to increase statistical power through minimising error variance (Tabachnick & Fidell 2014), as it is well recognised that in-scanner motion significantly affects the BOLD signal and FC measures (Yan et al. 2013; Van Dijk et al. 2012; Satterthwaite et al. 2012).

Treatment was interrupted in some HIV+ children commencing ART before 12 weeks of age, according to the treatment arm into which they were randomised (Section 6.1). In the CHER sample (Sections 0, 6.1), there is evidence that interruption may be harmful to white matter development, and thus may diminish the potential benefits of earlier ART (Ackermann et al. 2016). We therefore controlled for duration of treatment interruption when investigating the effect of treatment timing on FC at age 9 years, as it may have a suppression effect.

With one exception, the skewness (Joanes & Gill 1998) of all predictor variables (effects of interest and covariates; Table 1) was less than 2, satisfying classical thresholds for medium sample size (Kim 2013) and suggesting normal distribution. No predictor variables were mathematically transformed. When coding interrupt duration with 0 for HIV+ subjects whose ART treatment was not interrupted, this covariate had moderate skewness of 2.6; but among interrupted subjects only, the covariate had skewness less than 2. To guard against false inference resulting from violated assumptions of multivariate normality, we investigated the effect of age at ART initiation in three different ways: i) among uninterrupted subjects only ($N = 20$); ii) among interrupted subjects only ($N = 20$), controlling

for duration of interruption; iii) among all HIV+ subjects (N = 40), controlling for interrupt duration, coding non-interruption with a value of 0.

Construction of the design matrix

The design matrix was generated using a custom python script. All continuous predictors were mean-centered, and categorical predictors were represented using unweighted factor effects coding. An 'intercept'/grand-mean parameter was included in the model.

6.5.2 Independent component analysis

FSL's MELODIC, an implementation of probabilistic ICA (Beckmann & Smith 2004)[20], was used to estimate 20 group spatio-temporal processes, or 'independent components' (ICs). The *a priori* assumption of 20 sources is typical for rs-fMRI studies with samples of similar size and was adopted also by the Functional Connectomes Project (Biswal et al. 2010). Partially-preprocessed EPI datasets (see Section 6.3) are mapped into a 20-dimensional subspace using principal component analysis. The resultant reduced datasets – that of both HIV+ and uninfected subjects – are temporally concatenated to form a single matrix of observations (time × voxels). The matrix is decomposed into the desired sources using a model similar to the general linear model, but where the mixing matrix is unknown and estimated from the data (Beckmann et al. 2005). Each IC consists of a single time course, and a spatial map. The latter indicates the extent to which each brain voxel's BOLD signal is modulated by the IC – that is, by its temporal characteristic. The spatial maps are converted into so-called 'Z-statistic' maps by normalising by the residual noise[21] left unexplained by the entire decomposition.

Probabilistic ICA employs a simplistic noise model, with the result that variance attributable to more complex nuisance signals – such as cardiac and respiratory cycles, blood vessel networks, template alignment errors, and motion – tends to be isolated as separate ICs (Beckmann et al. 2005).

[20] Beckmann and colleagues give a mathematical and probabilistic formulation of the ICA algorithm employed in this study.

[21] More correctly, dividing voxelwise the raw IC estimate by the square root of the noise variance. The data has been pre-whitened, so that this is equivalent to normalising by the standard error of the IC estimate (Beckmann et al. 2005).

Interestingly, Beckmann et al. (2005) illustrated that even when physiological signals are temporally aliased into the BOLD spectrum during EPI acquisition, probabilistic ICA can separate their spatial maps from those representing spontaneous brain activity. Proceeding on this assumption, the spatial ICs were classified as signals-of-interest (neural-modulated BOLD signal) or non-interest by visual inspection of the spatial maps, loosely applying the criteria of Kelly et al. (2010). For this purpose of visual inspection, thresholded versions of the ICs were created by alternative hypothesis testing at $p > 0.95$ (Kelly et al. 2010).

Components classified as artefacts were not used in later statistical analyses. The remainder were assumed to be RSNs, reflecting large scale patterns of FC. To obtain a sense of the reliability and reproducibility of these maps, they were visually compared to a similar decomposition performed on 1000 adult subjects in the Functional Connectomes Project (Biswal et al. 2010). The RSNs were assigned standard names by comparison with visual maps and anatomical descriptions in the literature (Section 7.2).

To obtain subject-specific spatial maps associated with each group-level IC, the dual regression approach of Beckmann et al. (2009) was used (see also Filippini et al. 2009). The mechanisms of dual regression are somewhat complex, and do not need to be fully unpacked to appreciate the significance of its output (for a technical review, see Erhardt et al. 2011). But briefly: two regressions were performed against every subject's fMRI dataset. The full set of group-level spatial maps was fit against each subject's fully-preprocessed EPI dataset (see Section 6.3) separately, producing a matrix describing that subject's temporal dynamics associated with each IC (the 'spatial regression' step). All 20 group-level maps (nuisance or otherwise) were included in this regression, so that variance associated with artefactual components would not be distributed into subject-specific time courses of valid RSNs. In the second 'temporal regression' step, the previously-acquired matrix of time courses is fitted against the associated subject's same EPI dataset to estimate the subject-specific spatial maps associated with each IC. Voxel magnitudes in the single-subject map are hence the normalised betas

from the second regression. They represent the temporal variance explained in that subject by the corresponding IC at a particular brain location[22]. In the case that the IC is a valid RSN, the parameter estimate is interpreted to be the level of local connectivity, or functional integration, of the region into the associated network (Filippini et al. 2009). Cross-subject voxelwise analyses were performed on these single-subject FC maps.

Between-subject variance in FC associated with a particular RSN was investigated only within the spatial extent of that RSN. This restriction, though common (Rytty et al. 2013), has non-trivial implications: it excludes, for example, detection of large group differences in the connectivity of brain regions that are only marginally associated with the RSN. But given the non-stationarity of fMRI noise smoothness (Cox et al. 2017), constraining the bounds of analyses in this way is essential when using cluster-size correction to adjust for multiple voxelwise comparisons. The extent of each RSN was defined by thresholding the group-level statistic map at $Z > 3$ and binarizing the result to form a template (Poppe et al. 2013). Implicit in this simple non-probabilistic threshold is the exclusion of brain regions that are 'negatively' coactivated by the functional network – that is, where the BOLD signal synchronously decreases as opposed to increases.

For each analysis, the single-subject FC maps (3-D) of the sample of interest were masked with the associated RSN template and then combined into a single 4-D dataset (with the final dimension being variation across subjects). The 4-D dataset was input along with a design matrix, a contrast file, and an *F*-test file to FSL-randomize, which uses non-parametric permutation inference to identify voxels where an effect of interest (such as HIV-infection) is significantly non-zero (Winkler et al. 2014). The default number of permutations (5000) were performed for each analysis. The so-called *F*-test file configures FSL-randomise for two-sided testing, performing simultaneous inference on two one-sided

[22] Or equivalently, the coherence of the local timecourse with the temporal characteristic of the associated single-subject IC.

contrasts, while controlling the family-wise error rate. The construction of the design matrix was discussed in Section 6.5.1.

The mass-univariate (voxelwise multiple regression) approach is standard in neuroimaging, because high spatial resolution prohibits multivariate modelling, assuming reasonable sample sizes. Voxelwise FC measures that are significant at the group level have been shown to be reliable across time (Shehzad et al. 2009). The approach does however present the difficulty of multiple comparison correction, to control the false discovery rate (FDR). Typical adjustments, such as Bonferroni correction, are too harsh and are not appropriate, because hypotheses about FC are made at the scale of brain regions and not at that of discrete voxels. Put differently, we need to control the false positive rate of topological features – spatially contiguous clusters of FC – not of voxels (Chumbley & Friston 2009). Thus, Gaussian random field theory, which correctly considers the underlying connectivity to be continuous (Chumbley & Friston 2009), is used in the rs-fMRI literature (Farrant & Uddin 2015). This involves estimation of the topological features of fMRI noise in different brain regions.

The inherent spatial smoothness of noise in respective RSN masks was estimated over each subject's fully-preprocessed EPI dataset using the 3dFWHM function of AFNI 17.0.09, with the new 'mixed autocorrelation function' methodology (Cox et al. 2017), and then group-averaged. For the spatial domain associated with each RSN mask, the estimated noise smoothness was input to AFNI's 3dClustSim to calculate[23] the cluster size that would be produced at frequency α by thresholded random noise alone – where α is the desired cluster-level FDR. Cluster-forming (voxelwise) thresholds were applied to the probability maps output by FSL-randomise for each test. Due to lack of consensus in the literature, two different thresholds were applied: $p < 0.001$ (Melrose et al. 2008; Chang et al. 2004) and $p < 0.005$ (Liu et al. 2013). Cluster-size thresholds associated with a corrected, two-sided

[23] Using 5000 Monte Carlo simulations. The simulations constructed clusters using a combination of face and edge (but not vertex) connections ($NN = 2$).

cluster significance of α = 5% were enforced. These sizes, one for each RSN and for each cluster-forming threshold, are given in Appendix C.

6.5.3 Seed-based correlation analysis

Seed locations were selected based on three domains of *a priori* evidence: structural connectivity, neuropsychological testing, and FC. The functional radiations of these seeds were analysed to investigate Hypotheses II, III, and IV, respectively (Section 3). Spherical seeds of radius 6 mm were placed at the chosen coordinates in Haskins Pediatric space, using a transform from standard MNI space that is supplied with the Haskins atlas. Each seed was masked to include only regions lying within the brain, and outside of ventricles.

Seeds selected from neuropsychological results

The first set of seed coordinates were informed by neurodevelopmental testing performed at age 5 years, and neurocognitive testing at age 7 years, within a larger cohort of HIV+ and uninfected children from which this study's sample is drawn (Section 6.1). At age 5 years, the Beery-Buktenica Developmental Tests of Visual-Motor Integration (Beery-VMI) revealed significantly reduced visual perception in HIV+ children compared to uninfected controls (Laughton et al. 2017). Neurodevelopmental differences, as measured by the Griffiths mental development scales (Luiz et al. 2006), were observed in infancy between uninfected and HIV+ children, and between treatment arms (Laughton et al. 2012). However, these had apparently resolved by age 5 years (Laughton et al. 2017). At age 7 years, HIV+ children performed significantly worse on the learning, planning, and simultaneous processing subscales of the Kaufman assessment battery for children (KABC-II) (Kaufman & Kaufman 2004) compared to HU[24] subjects (Merkle 2015).

For each of the above-mentioned neuropsychological domains showing impairment in HIV+ subjects, we aimed to identify brain regions selectively involved in that domain. Neurosynth (Yarkoni et al. 2011) was used to perform reverse-inference meta-analyses of fMRI peak activations described in the

[24] But not when compared to HIV-exposed uninfected (HEU) subjects.

literature. The Python-based interface was used in conjunction with database version 0.6, which contains activation coordinates, key study metadata, and term-based features. Table 2 gives the query terms used to generate separate statistical brainmaps for the associated domains. Only studies employing the query term with sufficient frequency were included in each meta-analysis: the term frequency-inverse document frequency (TF-IDF) threshold was set to 0.05. The *Z*-score at each voxel in the resultant FDR-corrected ($p < 0.01$) maps indicates the relative selectivity with which that region activates for the given query term. A seed was placed at the *Z*-score peak, and a second at the second largest *Z*-score that is separated from the first by at least the seed radius (to prevent overlapping). Thus, 8 seed regions associated with neuropsychological testing were defined.

Table 2: Meta-analyses of functional MRI activation studies were carried out using Neurosynth (Yarkoni et al. 2011)*, to identify brain regions selectively involved in neuropsychological domains where we have previously found impairment in HIV+ children from this cohort (Laughton et al. 2017; Merkle 2015). For each meta-analysis, the query term input to Neurosynth, along with the number of studies contributing to the resultant statistical inference map, is given. An asterisk in the query term will include in the meta-analysis not only studies that contain that exact term (with sufficient frequency), but also those which contain a longer phrase beginning with that term, so long as that phrase is registered in the Neurosynth lexicon.*

Neuropsychological domain	**Query term**	**Number of studies matching the query, and satisfying the minimum frequency criterion**[a]
Visual perception	'visual perception*'	69
Learning	'learning*'	755
Planning	'planning'	206
Simultaneous processing	'(simultaneous | simultaneously) &~ simultaneous eeg'[b]	391

[a] Term frequency-inverse document frequency (TF-IDF) of at least 0.05.
[b] That is, studies whose abstracts include the term 'simultaneous' or the term 'simultaneously', but do not include the term 'simultaneous eeg'.

Seeds placed in the structural core

The second set of seeds were placed at the coordinates of the peak *Z*-scores[25] of those ICA-generated group RSNs for which the peak was located in the structural core. In a landmark paper, Hagmann et al. (2008) identified this 'structural core' through the investigation of cortico-cortical tracts in the human brain. Diffusion spectrum imaging followed by computational tractography was used to

[25] Precedent for placing seeds at peak coordinates of group RSN maps can be seen in (La Corte et al. 2016).

construct a cortical connection matrix, which was interrogated with various network analysis methods. The core has various characteristics indicative of stability and topological centrality within the massive graph of cortical connections. Its components are likely to provide the shortest path between any two regions, constitute connector hubs which have a high propensity to form connections with nodes in other structural modules, and are densely connected among themselves. The core is located in the posteromedial and parietal cortex, its sub-regions being: the posterior cingulate cortex, isthmus of cingulate, precuneus, cuneus, paracentral lobule, banks of the superior temporal sulcus, and the inferior and superior parietal cortex (all bilateral). All connections showing reduced FC at age 7 years in HIV+ children from the same cohort studied here, compared to uninfected children, involve a region in the structural core, suggesting that this backbone may be especially susceptible to HIV-infection or ART neurotoxicity (Toich et al. 2017).

The structural core resembles the spatial profile of the posterior portion of the well-known DMN resting state network. More generally, Hagmann et al. (2008) observed a strong correspondence between structural connectivity and resting state FC measured in the same sample, indicating that the core may comprise hubs not only of structural connectivity, but also of FC. If this is so, FC radiations seeded in the core are likely to be robust under measurement and testing, in addition to their being potentially vulnerable to HIV effects.

Seeds placed at coordinates revealing significant HIV-related differences in FC at age 7 years

Finally, to investigate whether FC abnormalities observed in our cohort at age 7 years resolve or become more pronounced as the children grow older, we retested[26] the 7 seeds which revealed differences in connectivity between HIV+ and uninfected children at that age (Toich et al. 2017). The seeds were originally centerd on one or more of the peak *Z*-scores of each RSN group map generated by ICA. The full set of group RSNs observed at age 7 years is given in Figure 8.

[26] One difference is that the seed radius employed in this study is 6 mm, while at age 7 years a radius of 5mm was used.

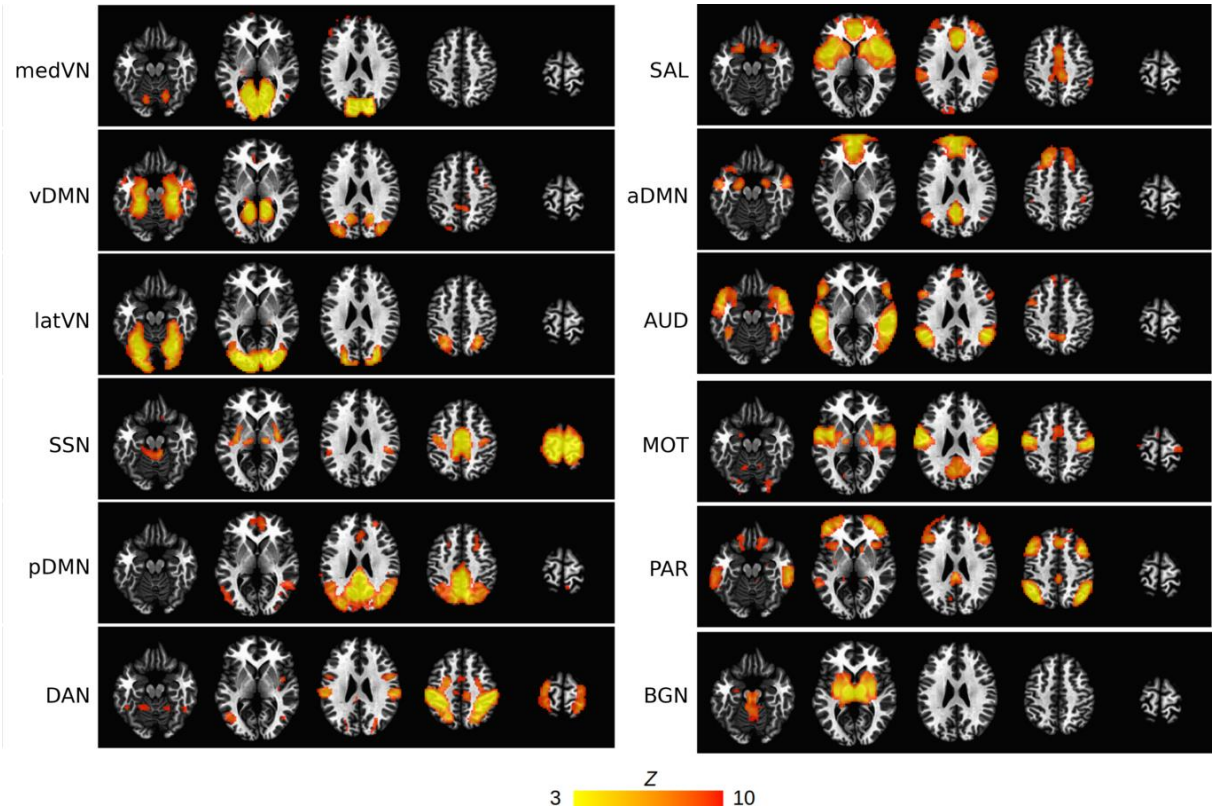

Figure 8: Group resting state networks identified at ages 7 years. Valid networks were identified from a 20-dimensional decomposition performed using FSL's MELODIC (Beckmann & Smith 2004), and were thresholded at Z > 3 : medVN = medial visual [network], vDMN = ventral DMN, latVN = lateral visual, SSN = somatosensory, pDMN = posterior DMN, DAN = dorsal attention, SAL = salience, aDMN = anterior DMN, AUD = auditory, MOT = motor, PAR = frontoparietal, BGN = basal ganglia. The networks are ordered – top to bottom in the first column, and continuing into the second column – according to the amount of signal variance each explains in the decomposition. This figure is taken from Toich et al. (2017). With the author's permission, labels have been changed to facilitate more intuitive comparison with networks observed here at age 9 years (*Figure 9*).

For each of the seeds in these three sets, a subject-specific reference time course was obtained by averaging the BOLD time courses of all voxels in the seed region. The seed reference was correlated with the time courses of all brain voxels to generate a seed-to-whole-brain FC map. The subject-specific maps were Fisher *Z*-transformed to improve normality of the Pearson correlation coefficients ahead of significance testing (for precedent, see Herting et al. 2015). For a given seed, the maps of all subjects were combined into a single 4-D dataset. As in the ICA pipeline (Section 6.5.2), this was input along with a design matrix, a contrast file, and an *F*-test file to FSL-randomize to perform voxelwise non-parametric permutation inference (Winkler et al. 2014).

Thresholding proceeded exactly as in ICA (Section 6.5.2), except that the minimum cluster volume required for significance was based on the average noise smoothness over the entire brain, as opposed to over an ICA-generated RSN mask. Cluster-forming thresholds of $p < 0.001$ and $p < 0.005$ were combined with associated cluster-extent thresholds of 378 mm^3 and 918 mm^3 (calculated using AFNI's 3dClustSim), to yield a two-sided cluster-level FDR of 5%. As is typical in the literature, no separate adjustment was performed to account for testing of multiple seeds (e.g. Herting et al. 2015, Wang et al. 2006). To do so would require impractically severe cluster-forming and cluster-extent thresholds. This is an inherent limitation of voxelwise analysis (mass univariate testing). Significant clusters are not constrained to lie within the same RSN as the seed, and so may represent either regions of affected within-network or between-network FC, depending on the anatomical location of the cluster relative to the seed.

7 Results

7.1 Sample characteristics

Of the 59 HIV+ and 32 uninfected (17 exposed, HEU) Xhosa children scanned at age 9 years, 19 HIV+ and 8 uninfected children were excluded on the following grounds: severe field bias in the structural MRI volume (2 HIV+); incomplete or missing resting state data (11 HIV+; 2 HU; 3 HEU); incorrect field of view in the resting state data (1 HIV+); failed alignment of the resting state volumes to the Haskins pediatric template (1 HIV+, due to severe ventricular enlargement; 1 HEU, due to an EPI signal void in the dorsal brain); and not meeting motion criteria, as described in Section 6.4.1 (4 HIV+; 1 HU; 1 HEU)[27]. We therefore present analyses and results for 40 HIV+ and 24 uninfected (12 exposed) children.

Demographics, treatment details and clinical data for the HIV+ and uninfected groups are given in Table 3. Although groups did not differ on sex or in-scanner motion, as measured by framewise displacement, uninfected children were about 5 months older. All HIV+ children for whom data are presented had initiated ART by 65 weeks (less than 18 months), and all were still on first line ART at the time of scanning. Half had a period of treatment interruption between these two time points. By age one year, first viral load suppression had been achieved in 72,5% of HIV+ children, in 90% by 2 years, and in 100% by just over 3 years (160 weeks).

[27] All but one of the 6 excluded subjects exceeded the thresholds associated with both indices employed to quantify motion, demonstrating congruence of the two indices, and to some extent validating their reliability against each other.

Table 3: Sample characteristics of HIV+ and uninfected groups.

	HIV Uninfected	HIV Infected	| *t* | / $\chi 2$	*p*
Demographics				
N	24	40		
Sex: M	12 (50%)	16 (40%)	0.27	0.60
Age at scan (years)	9.6 ± 0.52	9.2 ± 0.20	2.78	0.01
In-scanner motion (mm) [a]	0.3 ± 0.4	0.2 ± 0.3	0.88	0.38
Perinatally unexposed	12 (50%)	NA		
Treatment-related measures				
Age at ART initiation (weeks)	NA	10 (8–23)		
Age at first viral load suppression (weeks)	NA	46 (33–62)		
ART interrupted	NA	20 (50%)		
Duration of ART interruption (weeks)[b]	NA	41 (29–64)[c]		
Clinical data at enrolment				
$CD4^+$ cell count (cells/µl)	NA	1920 ± 722		
CD4%	NA	36 ± 8		
$CD4^+/CD8^+$ [d]	NA	1.4 ± 0.7		
Viral load (RNA copies/ml)				
High (>750,000)	NA	18 (45%)		
Low (400–750,000)	NA	22 (55%)		
Suppressed (<400)	NA	0 (0%)		
Clinical data at scan (age 9 years)				
$CD4^+$ cell count (cells/µl)[e]	NA	1327 ± 661		
CD4%[e]	NA	37 ± 8		
Viral load (RNA copies/ml)				
High (>750,000)	NA	0 (0%)		
Low (400–750,000)	NA	1 (2.5%)		
Suppressed (<400)[f]	NA	39 (97.5%)		

Values are **mean ± SD**, **median (interquartile range)**, or **N (% of total)**.
ART, antiretroviral therapy; **M**, male.
[a] On the measurement of in-scanner motion, see Sections 6.3.2 and 6.4.1.
[b] All interrupted subjects had restarted treatment at the time of scanning.
[c] Calculated over interrupted subjects only.
[d] $CD4^+/CD8^+$ at enrolment missing for two children. These two subjects are excluded from all subsequent analyses concerning immune measures at enrolment.
[e] $CD4^+$ cell count (and CD4%) at scan missing for two children. These two subjects are excluded from all subsequent analyses concerning immune measures at scan.
[f] Assays employed to measure viral loads at age 9 years could detect values less than 400 RNA copies/ml (depending on blood sample volume), which was the sensitivity limit of the assays used at enrolment. However, we keep the upper threshold of the 'suppressed' category at 400 copies to aid comparison with enrolment measures. This threshold nevertheless meets the criteria suggested by the World Health Organisation for evidence of virologic suppression in low- and middle-income countries: <1,000 RNA copies/ml (Bennett et al. 2006).

Outliers were defined as values more than 3 SDs beyond the sample mean. To preserve the number of subjects in analyses, winsorization was performed on the following measures with outliers: interrupt duration (2 HIV+), ART initiation age (1 HIV+) and $CD4^+$ count at scan (1 HIV+).

The HIV-uninfected group consists of subjects perinatally-exposed and perinatally-unexposed to HIV and ART. The demographics of these two subgroups is presented in Table 4. There were no significant differences in sex, age at scan, or in-scanner motion (framewise displacement) between these two subgroups.

Table 4: Sample characteristics of the HIV-unexposed uninfected (HU) and HIV-exposed uninfected (HEU) groups.

	Unexposed uninfected (HU)	**Exposed uninfected (HEU)**	$\lvert t \rvert / \chi 2$	p
Demographics				
N	12	12		
Sex: M	5 (42%)	7 (58%)	0.04	0.84
Age at scan (years)	9.4 ± 0.44	9.7 ± 0.55	1.71	0.10
In-scanner motion (mm)	0.3 ± 0.3	0.4 ± 0.5	0.72	0.48

Values are mean ± SD or N (%). **M**, male.

7.2 Resting state networks revealed by group independent component analysis

Eight of the 20 components were classified as artefacts. Appendix D illustrates some typical nuisance features observed in these components.

The remaining 12 ICs, shown in Figure 9, were identified to be RSNs – that is, reflecting large scale patterns of FC. Full RSN names associated with the abbreviations employed in Figure 9 are given in Table 5, along with topological descriptions of the spatial maps, and references to literature identifying RSNs of similar spatial profile.

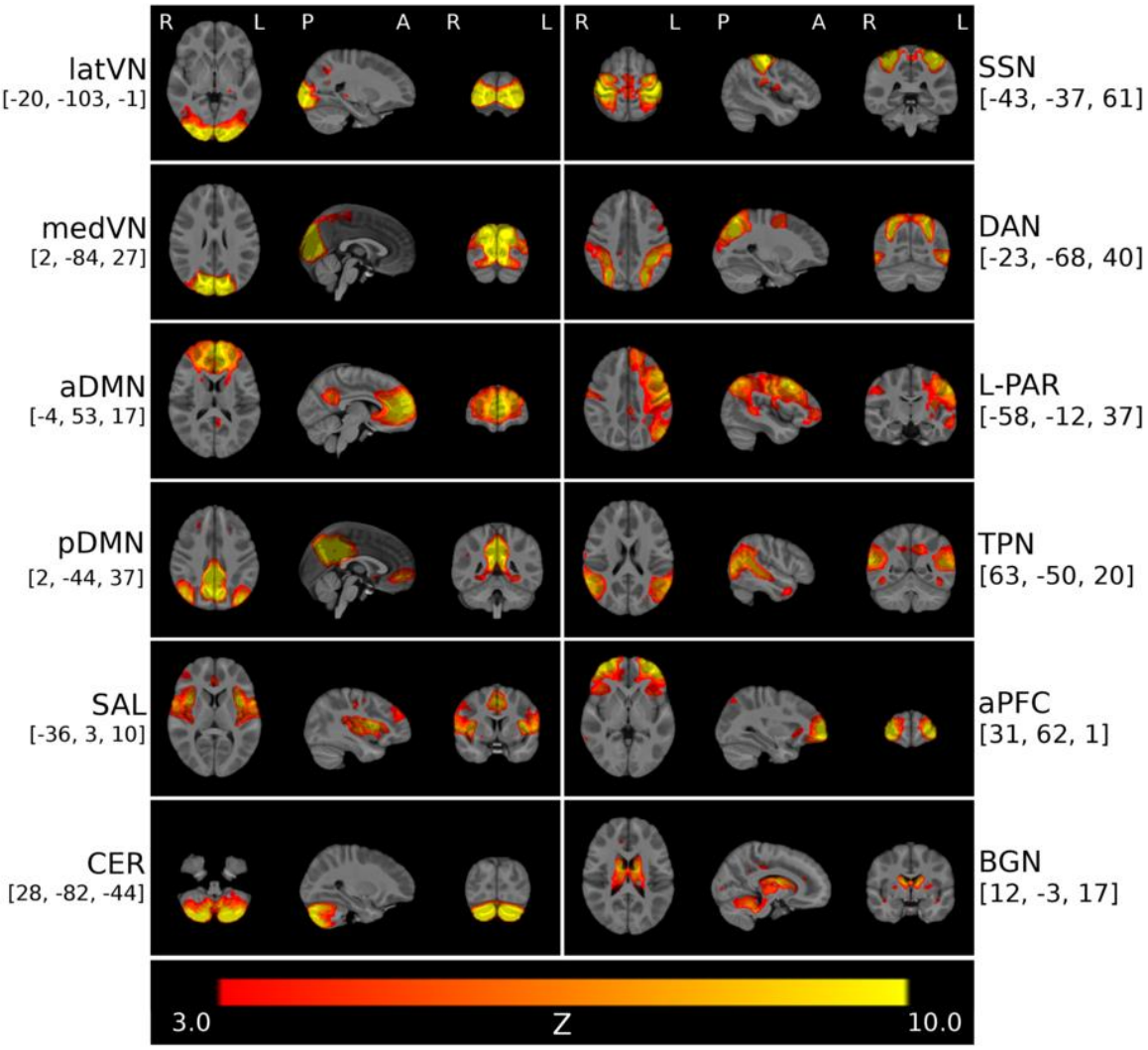

*Figure 9: Group resting state networks revealed by independent component analysis. The networks are ordered – top to bottom in the first column, and continuing into the second column – according to the amount of signal variance each explains in the decomposition. The spatial maps are here shown thresholded at $Z > 3$: latVN = lateral visual [**n**etwork], medVN = medial visual, aDMN = anterior DMN, pDMN = posterior DMN, SAL = salience, CER = cerebellar, SSN = somatosensory, DAN = dorsal attention, L-PAR = left frontoparietal, TPN = temporoparietal, aPFC = anterior prefrontal cortex, BGN = basal ganglia.*

Table 5: Topological descriptions of the 12 resting state networks (RSNs) revealed by group ICA, as visualized in Figure 9. A canonical name for each RSN is selected from among literature identifying a network with a similar spatial profile. Such literature is cited in the last column. Listed grey matter regions are bilateral, unless otherwise indicated; these regions are roughly listed in posterior to anterior order. Coordinates are given in left-posterior-inferior (LPI) convention. ***L****, left;* ***R****, right.*

Abbreviated RSN name	Canonical RSN name	Grey matter structures overlaid, or partly overlaid	Peak coactivation (*Z*), in MNI-152 space	Literature identifying an RSN of similar topography
latVN	Visual network, lateral	Occipital pole (primary visual cortex), extending laterally and widely into the visual association cortex of the occipital lobe. Lingual and fusiform gyri. Posterior intraparietal sulcus. Inferior temporal gyrus (posterior). Lateral geniculate body.	-20, -103, -1 L occipital pole	Yeo et al. 2011 De Luca et al. 2006 Beckmann et al. 2005
medVN	Visual network, medial	Whole medial surface of occipital lobe (cuneus). Parts of the inferior (lingual gyrus) and lateral surfaces of the occipital lobe. Precuneus, extending into the superior parietal lobule. Inferior parietal lobule. Central sulcus. Lateral geniculate body.	2, -84, 27 R visual association cortex (in cuneus)	
aDMN	Anterior default mode network	Precuneus. Cingulate (posterior, anterior). L angular gyrus (inferior parietal lobule). Caudate and putamen. Ventromedial (extending down to rostral gyrus) and dorsomedial prefrontal cortex. Frontopolar prefrontal cortex.	-4, 53, 17 L dorsomedial prefrontal cortex	Andrews-Hanna et al. 2010 Greicius et al. 2003
pDMN	Posterior default mode network	Precuneus. Cingulate (posterior, anterior). Inferior parietal lobule. Posterior hippocampal and parahippocampal gyri. R anterior superior temporal sulcus. Ventromedial prefrontal cortex.	2, -44, 37 R precuneus	
SAL	Salience network	Supramarginal gyrus (superior parietal lobule). Insulae, transverse temporal gyri, and opercula (including superior temporal gyrus). Posterior and mid cingulate gyrus and sulcus, extending into the marginal sulcus and anterior-most precuneus. Ventrolateral postcentral and precentral gyri. Supplementary motor area (medial frontal). Putamen. Dorsolateral prefrontal cortex. Inferior frontal gyrus (opercular and triangular parts).	-36, 3, 10 L frontal operculum	Seeley et al. 2007
CER	Cerebellar network	Cerebellum. Posterior middle and inferior temporal gyri.	28, -82, -44 R posterior cerebellar cortex	Zuo et al. 2010 Smith et al. 2009
SSN	Somatosensory[a] network	R inferior temporal gyrus (posterior, visual processing area). Superior parietal lobule and anterior intraparietal sulcus. Postcentral gyrus, and dorsal precentral gyrus. Paracentral lobule (secondary motor area). Posterior superior temporal gyrus and operculum. Thalamus. Transverse temporal gyri and posterior insula. Medial orbitofrontal cortex.	-43, -37, 61 L postcentral gyrus	Yeo et al. 2011 Beckmann et al. 2005
DAN	Dorsal attention[b] network	Dorsolateral occipital cortex. Intraparietal sulcus. Supramarginal gyrus (inferior parietal lobule). Posterior cingulate (below marginal sulcus). Posterior portions of the inferior temporal and middle temporal gyri (visual processing area). Frontal eye field (premotor cortex). Ventrolateral precentral gyrus. Dorsolateral prefrontal cortex (L hemisphere has greater coactivation). Anterior insular cortex.	-23, -68, 40 Left intraparietal sulcus, posterior part	Yeo et al. 2011 Zuo et al. 2010 Fox et al. 2006

L-PAR	Left-lateralised frontoparietal[c] network	Primary visual cortex (cuneus). L inferior parietal lobule. L intraparietal sulcus. L posterior temporal lobe (visual processing region). Insular cortex (L hemisphere has greater coactivation). L postcentral and precentral gyri. L putamen and caudate. L dorsolateral and ventrolateral prefrontal cortex.	-58, -12, 37 L postcentral gyrus	Shirer et al. 2015 Smith et al. 2009 Calhoun et al. 2008
TPN	Temporoparietal[d] network	Precuneus. Middle and ascending superior temporal sulcus. Temporooccipital transition zone. Temporoparietal junction. Angular gyrus.	63, -50, 20 R angular gyrus	Allen et al. 2011 Smith et al. 2009 Calhoun et al. 2008 Damoiseaux et al. 2006
aPFC	Anterior prefrontal cortex	Inferior parietal lobule. Paracentral lobule, extending into dorsal-most sensorimotor area. Orbitofrontal cortex. Frontal pole extending widely into the ventrolateral prefrontal cortex (and parts of the dorsolateral prefrontal cortex).	31, 62, 1 R frontopolar prefrontal cortex	de Bie et al. 2012 Dosenbach et al. 2007
BGN	Basal ganglia network	Superior cerebellum (lobules 1 to 5). Hippocampus and amygdala. Pontine nuclei (brainstem). Caudate (very extensive) and putamen. Thalamus. Anterior and middle cingulate. Middle temporal gyrus.	12, -3, 17 R ventral caudate	Allen et al. 2011

[a] In adults, this network includes more extensive coactivation in motor regions, and is then referred to as the 'sensorimotor' network (Beckmann et al. 2005).
[b] Synonymous with 'dorsal visual attention stream,' as in (Zuo et al. 2010).
[c] Sometimes called 'executive control' network, as in (Shirer et al. 2015). However, the author prefers to avoid that label, to prevent confusion with the cingulate/insulae/parietal component that has a central role in control signalling, and which is largely constituted by the salience network (for a more detailed discussion, see Section 5.7.2).
[d] Although 'temporoparietal' is sometimes used (Thornburgh et al. 2017), the corresponding adult network is more commonly labelled 'auditory'. Here, however, the primary auditory cortex is not included.

7.3 HIV+ vs. uninfected functional connectivity comparisons

We present differences in FC between HIV+ and uninfected (perinatally-exposed and unexposed combined) children revealed by ICA (Section 7.3.1) and SCA (Sections 7.3.2, 7.3.3, 7.3.4) pipelines.

7.3.1 ICA-revealed within-network differences

We detected no regions within ICA-generated RSNs showing effects of infection status (HIV+ vs. uninfected) at age 9 years.

7.3.2 Functional connectivity with seeds related to neuropsychological domains

Two seeds were selected for each neuropsychological domain showing abnormalities in the HIV+ group at age 5 or 7 years (Table 6) (Laughton et al. 2017; Merkle 2015). In Figure 10a, the seeds are shown overlain on the reverse inference maps from which their locations were selected. The maps were generated by meta-analyses performed in Neurosynth, and highlight regions selectively involved in a particular neuropsychological domain. Figure 10b visualises all the seeds in a glass-brain. Four seeds are located in the left cerebral cortex, one in the right cerebral cortex, two in the striatum of

the right basal ganglia, and one in the left cerebellar cortex. For the learning, planning and simultaneous processing domains, the pairs of seeds were ipsilateral, while the visual perception pair was contralateral, as dictated by the position of *Z*-score peaks in the associated meta-analysis maps.

The reverse inference map for the 'simultaneous processing' meta-analysis is particularly sparse. The forward inference map (indicating regions consistently, rather than specifically, activated in studies associated with the search term) on the other hand, is not: it includes extensive activation in the medial frontal, fronto-insular and thalamic regions, for example (not shown). The sparsity of the reverse inference map may thus indicate that, although various anatomy is consistently involved in supporting cognition that requires the simultaneous holding of multiple pieces of information in working memory, none or little of this anatomy is statically and exclusively dedicated to that function.

Table 6: Seeds associated with neuropsychological domains showing abnormalities in HIV+ children at age 5 or 7 years, and used to investigate differences in seed-to-whole-brain connectivity between HIV+ and uninfected children (perintatally-exposed and unexposed) at age 9 years using seed-based correlation analysis (SCA). Anatomical locations and seed volumes are given. Seeds are initially spherical with a radius of 6 mm, but are masked to remove non-brain tissue. The seeds are visualised in Figure 10.

Seed label	**Neuropsychological domain**	**Anatomical location**	**Coordinates at seed center[a] (MNI, LPI)**			**Seed volume, after masking[b] (mm^3)**
			x	**y**	**z**	
Learn1	Learning	R ventral striatum	25	10	-10	891
Learn2	Learning	R caudate	12	4	13	783
Plan1	Planning	L precentral gyrus (functional area: movement of the trunk)	-26	-14	58	891
Plan2	Planning	L precentral gyrus (functional area: movement of the upper limb)	-54	2	34	864
Sim1	Simultaneous processing	L parahippocampal gyrus, on the medial surface of the temporal lobe	-11	-3	-42	405
Sim2	Simultaneous processing	L cerebellar tonsil / biventral lobule	-14	-57	-42	891
Vis1	Visual perception	R occipital lobe, lateral surface (visual association cortex)	46	-73	-6	891
Vis2	Visual perception	L superior parietal lobule (anterior part)	-16	-60	67	702

[a] The center of the spherical seed, before any non-brain tissue in the seed was masked out.
[b] Voxels lying outside of the brain or within ventricles were excluded from the seed. The residual seed region was used for subsequent seed-based correlation analysis (SCA).

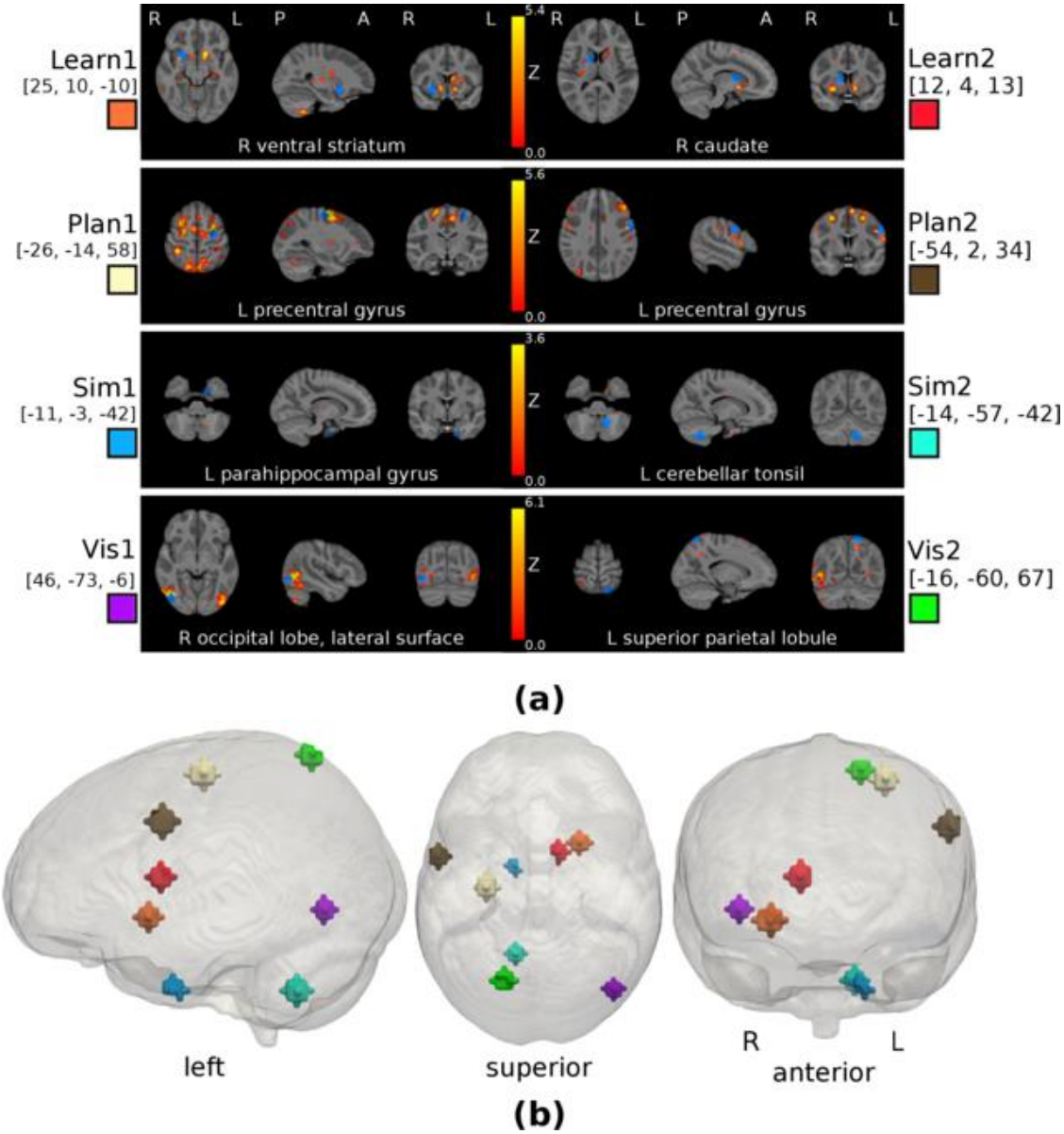

Figure 10: Seeds assocaited with neuropsychological domains showing impairment in HIV+ children at age 5 or 7 years, and used to investigate differences in seed-to-whole-brain connectivity between infected and uninfected children at age 9 years. ***(a)*** *Each seed is shown overlain on the reverse inference map (hot colours) produced by the meta-analysis performed in Neurosynth* (Yarkoni et al. 2011) *for that domain. This map is thresholded at an FDR of $p < 0.01$. Where the map is sparse, the seed may visually occlude the map in the slices shown. The saturation levels for the map's colour-bar are the 2nd and 98th percentiles of non-zero values. Seed labels in the margins reference seed details given in Table 6. Coordinates under the seed label are those of the seed center, in MNI standard space, using left-posterior-inferior (LPI) convention. Each seed is assigned a colour-code, which is used to identify that seed in (b), and to index regions showing HIV-related differences in connectivity with that seed in Figure 11 and Figure 12.* ***(b)*** *All the seeds in (a) are rendered together in a glass-brain.*

Three of the eight seeds revealed significant between-group differences. Four regions showed significantly differing FC to the first planning seed (left precentral gyrus) in HIV+ compared to uninfected (HU and HEU combined) children: bilateral precuneus, right paracentral lobule, left putamen, and bilateral ventromedial prefrontal cortex (PFC). The right angular gyrus showed

significantly differing FC to the first visual perception seed, and the left occipital pole to the second visual perception seed. In all instances, the HIV+ positive group demonstrated greater positive BOLD correlations compared to uninfected children. For the planning seed, the effect of infection on FC only with the precuneus is observed at both the $p < 0.005$ and $p < 0.001$ cluster-forming thresholds. All of the clusters associated with the visual perception seed disappear at the stricter threshold.

Table 7 presents locations and volumes for the clusters showing group differences in FC to seeds, together with group means of the cluster-averaged FC *Z*-scores. Being Fisher *Z*-transformed correlation coefficients rather than normalised parameter estimates, connectivity scores tabulated for SCA clusters differ from those recorded for ICA by about an order of magnitude (compare Table 13, Section 7.4). *Post hoc* testing revealed no significant association of scan age with cluster-averaged FC ($p > 0.2$).

Table 7: Size and peak coordinates of regions showing significantly increased functional connectivity to seeds in HIV+ children compared to uninfected (HIV-) children (perintatally-exposed and unexposed), obtained using seed-based correlation analysis (SCA). Seeds correspond with neuropsychological domains showing significant between-group differences at ages 5 or 7 years (Laughton et al. 2017; Merkle 2015). Clusters are grouped by the cluster-forming threshold (p < 0.005 or p < 0.001). Also given are group means of the cluster-averaged connectivity scores. Alphabetic cluster labels (A – F) correspond with those in Figure 11.

Seed information				**Clusters of FC difference (uninfected < HIV+)**								
						Cluster peak coordinates (MNI, LPI)				**Group means (SD) of average FC *Z*-scores over cluster region**		
Seed label	**NP domain**	**Seed location**	**RSNs (identified at age 9 years) which contain the seed**[a]	**Cluster location**[b]	**RSNs which contain the cluster**[a]	*x*	*y*	*z*	**Cluster volume (mm³)**	HIV-	HIV+	**Cluster label**
Cluster-forming threshold: *p* < 0.005												
Plan1	Planning	L precentral gyrus	Somatosensory (SSN)	Precuneus (bilateral)	Posterior DMN (pDMN); salience (SAL)	**-7**	**-47**	**44**	2484	0.0611 (0.158)	0.198 (0.131)	A
.	.	.	.	R paracentral lobule; SMA	Salience (SAL)	8	-6	61	1620	0.150 (0.117)	0.291 (0.122)	B
.	.	.	.	L putamen; L transverse temporal gyrus; L insula	Left frontoparietal (L-PAR); basal ganglia (BGN)	-30	-19	0	1161	0.0834 (0.0775)	0.205 (0.112)	C
.	.	.	.	Ventromedial PFC (bilateral)	Anterior and posterior DMN (aDMN and pDMN)	2	49	0	918	0.0293 (0.130)	0.154 (0.149)	D
Vis1	Visual perception	R lateral occipital lobe	Lateral visual (latVN); temporoparietal (TPN)	R inferior parietal lobule (angular gyrus)	Posterior DMN (pDMN); temporoparietal (TPN)	53	-59	27	972	0.00338 (0.109)	0.144 (0.0978)	E
Vis2	Visual perception	L superior parietal lobule	Dorsal attention (DAN)	L occipital pole, extending laterally	Lateral visual (latVN)	-14	-103	-4	1782	-0.0353 (0.103)	0.118 (0.135)	F
Cluster-forming threshold: *p* < 0.001												
Plan1	Planning	L precentral gyrus	Somatosensory (SSN)	Precuneus (bilateral)	Posterior DMN (pDMN); salience (SAL)	**-7**	**-47**	**44**	837	0.0662 (0.145)	0.217 (0.162)	A*

NP, neuropsychological; **RSN**, resting state network; **MNI**, Montreal Neurological Institute 152 atlas; **LPI**, left-posterior-inferior; **FC**, [resting state] function connectivity.
HIV-, HIV-uninfected; **HIV+**, HIV-infected.
L, left; **R**: right; **SMA**, supplementary motor area; **PFC**, prefrontal cortex.
[a] An RSN is listed if the majority of the cluster's extent is contained within its spatial domain (RSNs identified at age 9 years are visualised in Figure 9).
[b] Based on cluster overlap in Haskins pediatric atlas.
* Cluster has center coordinates corresponding with that of the similarly labelled cluster at $p < 0.005$, indicating that the effect persists in the same region at the stricter threshold of $p < 0.001$.

Figure 11 shows each cluster overlain on the forward inference map produced by the associated Neurosynth meta-analysis. The forward inference (as opposed to the reverse inference) map describes the consistency, and not the relative selectively, with which brain regions activate in fMRI tasks related to the neuropsychological domain of interest. Five of the six recorded clusters overlap barely or not

at all with the corresponding forward inference map. Figure 11 also presents boxplots of cluster-averaged FC scores for the HIV+ and uninfected groups. Figure 12 visualises all the seeds and clusters together in a glass brain. Clusters are predominantly medial or posterior.

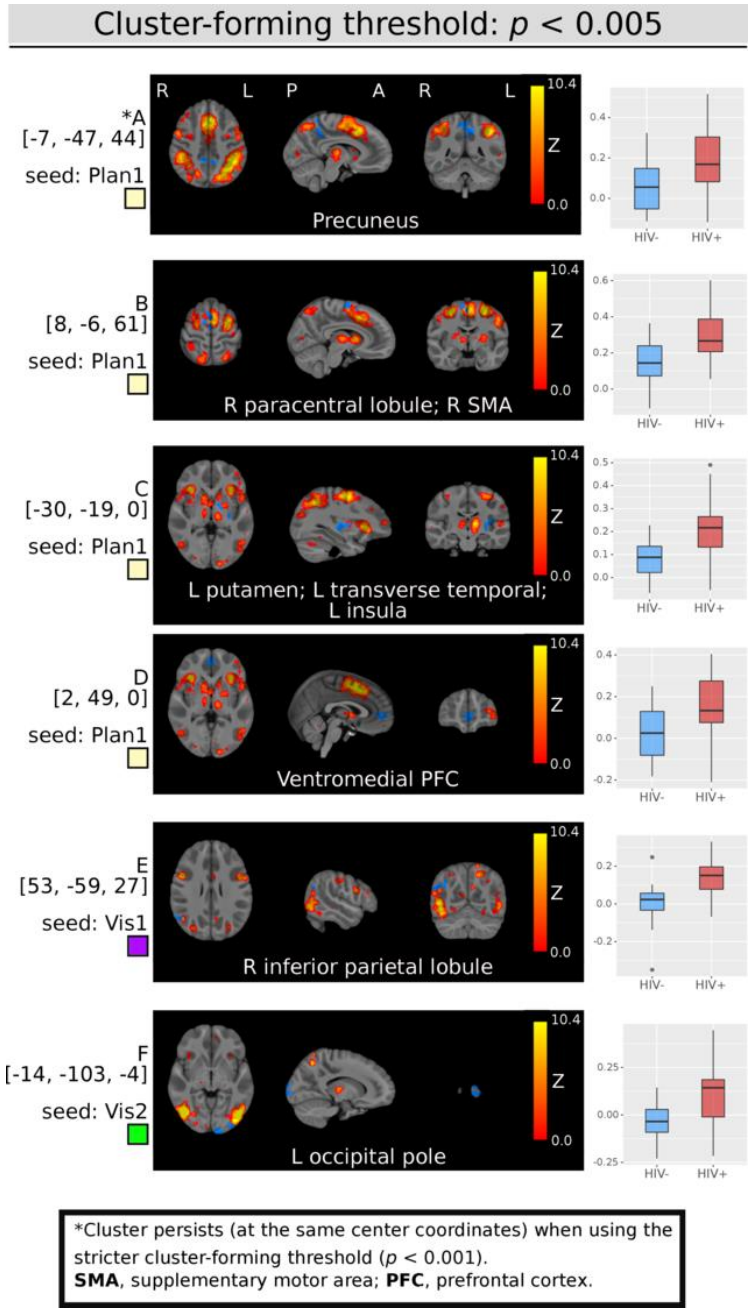

Figure 11: Each panel shows a region (blue) of significantly increased connectivity to a seed (not shown) in HIV+ compared to uninfected (HIV-) children (perintatally-exposed and unexposed), where seeds correspond with neuropsychological domains showing significant HIV-related impairment at ages 5 or 7 years. The cluster is shown overlain on the forward inference map (hot colours) produced by the meta-analysis performed in Neurosynth (Yarkoni et al. 2011) *for that domain. Cluster-forming thresholds of p < 0.001 and p < 0.005 were combined with cluster-size thresholds to yield a corrected cluster significance of p < 0.05 (two-sided) in all cases. To the right of each panel, boxplots visualise the distributions of connectivity Z-scores, averaged over the cluster region, for the two groups. The alphabetic cluster labels in the left margin (A – F) reference the tabulated details in Table 7. Coordinates under the seed label are those of the peak between-group difference, in MNI standard space, using left-posterior-inferior (LPI) convention. Each cluster is assigned a coloured square, which indexes the associated seed in Figure 10 and the associated seed-cluster set in Figure 12.*

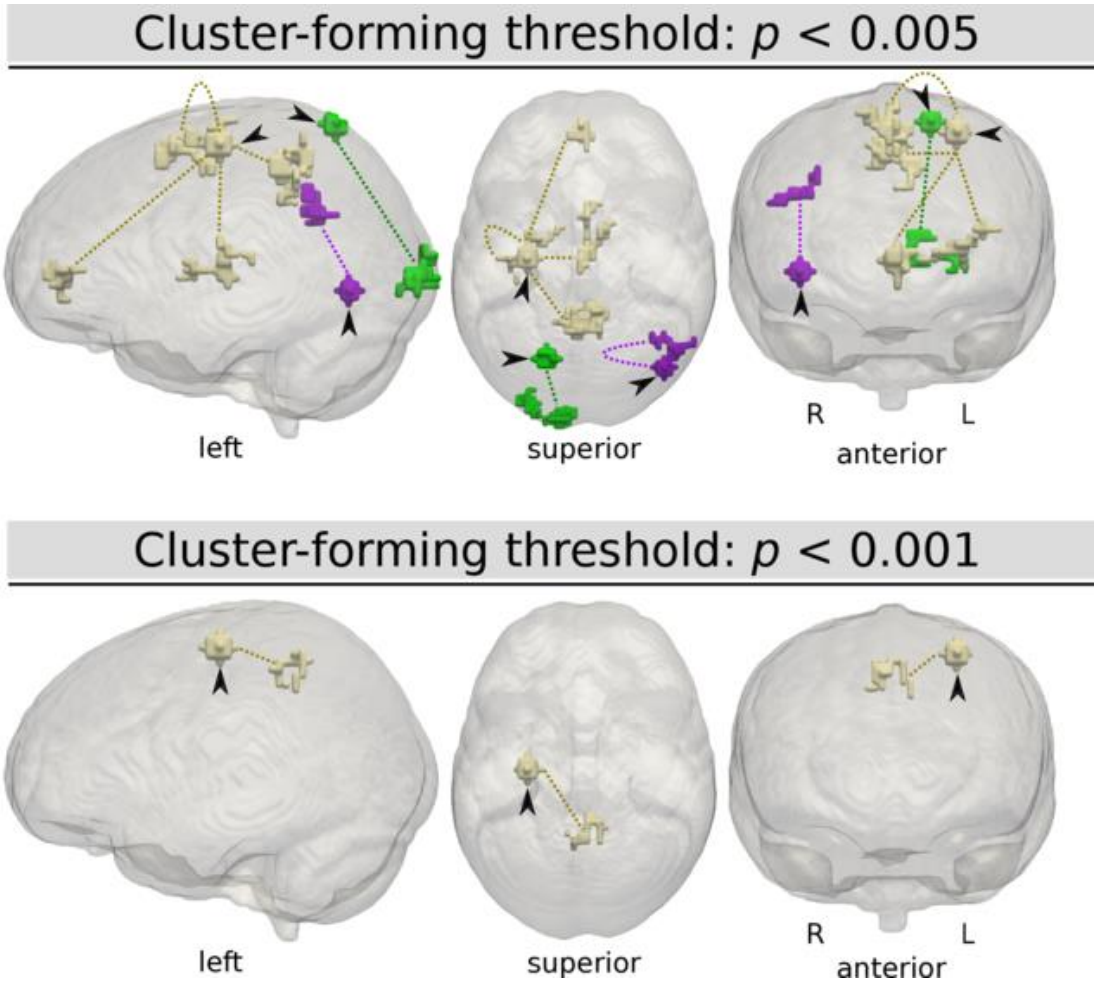

Figure 12: Glass-brain renderings of seeds (indicated with black arrow tips) and clusters between which functional connectivity is greater in HIV+ compared to uninfected children, for the results detailed in Table 7 and Figure 11. Seeds are associated with neuropsychological domains showing HIV-related impairment. All clusters revealed by the same seed, along with the seed itself, are filled with the same colour, which indexes the seed in Figure 10: cream = 'planning' domain, L precentral gyrus seed; purple = 'visual perception' domain, R occipital pole; green = 'visual perception' domain, L superior parietal lobule. Dotted lines indicate seed-cluster connections, but in no way represent the anatomical path of the connection.

7.3.3 Functional connectivity with seeds in the structural core

Four seeds were placed in the structural core – one for each ICA-generated group RSN where the global *Z*-score peak of the ICA-generated group map lies in the structural core (Table 8). In Figure 13a, the seeds are shown overlain on the group RSN from which they were taken, respectively. Two of the seeds lie in the medial surface of the cerebral cortex, while the remaining two lie in the left and right posterior cerebral cortex (Figure 13b).

Table 8: Seeds placed in the structural core and used to investigate differences in seed-to-whole-brain connectivity between HIV+ and uninfected (perinatally-exposed and unexposed) children using seed-based correlation analysis (SCA). Anatomical locations and seed volumes are given. Seeds are initially spherical with a radius of 6 mm, but are masked to remove non-brain tissue. The seeds are visualised in Figure 13.

Seed label	RSN in which the seed is located[a]	Anatomical location of seed center	Coordinates at seed center[b] (MNI, LPI)			Seed volume, after masking[c] (mm^3)
			x	y	z	
medVN	Medial visual network	R extrastriate visual cortex (in cuneus)	2	-84	27	891
pDMN	Posterior default mode network	R precuneus	-2	44	37	891
DAN	Dorsal attention network	Left intraparietal sulcus, posterior part	-23	-68	40	891
TPN	Temporoparietal network	R angular gyrus	63	-50	20	567

RSN, resing-state network; **MNI**, Montreal Neurological Institute 152 atlas; **LPI**, left-posterior-inferior.
L, left; **R**, right.
[a] Seeds are placed at the global *Z*-score peak of the ICA-generated group map.
[b] The center of the spherical seed before any non-brain tissue voxels in the seed were masked out.
[c] Voxels lying outside of the brain or within ventricles were excluded from the seed. The residual seed region was used for subsequent seed-based correlation analysis (SCA).

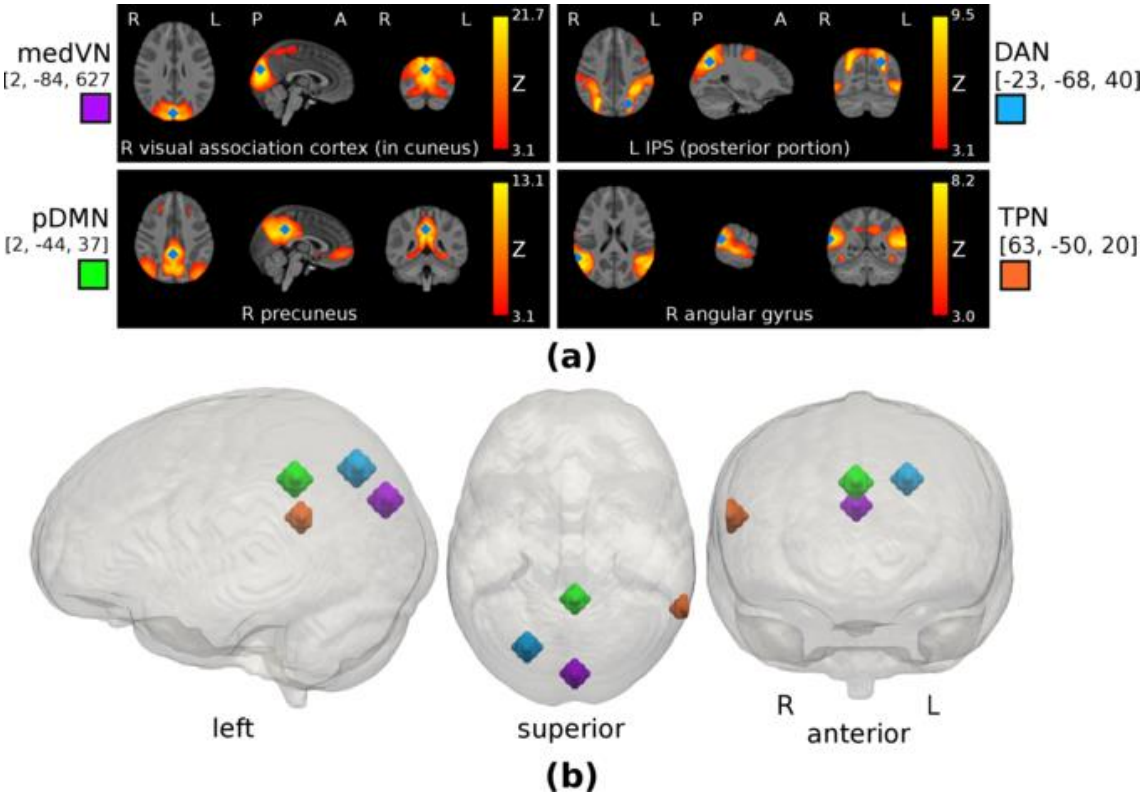

Figure 13: Seeds placed in the structural core and used to investigate differences in seed-to-whole-brain connectivity between HIV+ and uninfected (perintatally-exposed and unexposed) children. ***(a)*** *Each seed (blue) is shown overlain on the group map of the resting state network (hot colours) from which the seed was taken. This map is thresholded at Z > 3. The saturation levels for the network's heatmap are the 2nd and 98th percentiles of non-zero values. Seed labels in the margins reference seed details given in Table 8. Coordinates under the seed label are those of the seed center, in MNI standard space, using left-posterior-inferior (LPI) convention. Each seed is assigned a colour-code, which is used to identify that seed in (b), and to index regions showing HIV-related differences in connectivity with that seed in Figure 14 and Figure 15.* ***(b)*** *All the seeds in (a) are rendered together in a glass-brain.*

At a cluster-forming threshold of $p < 0.005$, five regions showed significantly differing FC to the temporoparietal network seed (right angular gyrus) in HIV+ compared to uninfected (HU and HEU combined) children: left inferior frontal gyrus, left precentral gyrus, left intraparietal sulcus, bilateral extrastriate[28] cuneus, left premotor/pre-SMA. Three of these clusters persist at the stricter cluster-forming threshold of $p < 0.001$ (left inferior frontal gyrus, left precentral gyrus, and left intraparietal sulcus). In addition, the left premotor cortex shows significantly differing FC to the medial visual network seed (right extrastriate cuneus) only at the less severe cluster-forming threshold. In all cases, the BOLD correlations were greater positive in HIV+ compared to uninfected children. The posterior

[28] Visual areas outside of the primary visual cortex, which in turn is considered to be in and immediately around the calcarine fissure.

DMN seed (right precuneus) and dorsal attention network seed (left intraparietal sulcus) revealed no connections with significant between-group differences. *Post hoc* testing revealed no significant association of scan age with cluster-averaged FC ($p > 0.1$).

Figure 14 shows clusters demonstrating greater FC in HIV+ children compared to uninfected children to a seed in the structural core, overlain on the RSN group-map from which the associated seed was taken. In every case, the cluster lies well outside of the bounds of the RSN associated with the seed, indicating between-network connections. Except for a result in the bilateral cuneus, clusters are left-lateralised for both seeds, and all lie in the cerebral cortex (Figure 15).

Table 9: Size and peak coordinates of regions showing significantly increased connectivity to seeds in HIV+ compared to uninfected (HIV-) children (perintatally-exposed and unexposed), obtained using seed-based correlation analysis (SCA). One seed was placed at the peak of each ICA-generated group resting state network that had its peak situated in the structural core, as defined by Hagmann et al. (2008)*. Clusters are grouped by the cluster-forming threshold. Also given are group means of the cluster-averaged connectivity scores. Alphabetic cluster labels (A – F) correspond with those in Figure 14.*

Seed information			**Clusters of FC difference (uninfected < HIV+)**								
					Cluster peak coordinates (MNI, LPI)				**Group means[b] (SD) of average FC *Z*-scores over cluster region**		
Seed label	**Seed network**	**Seed location**	**Cluster location[a]**	**RSNs (identified at age 9 years) which contain the seed[b]**	*x*	*y*	*z*	**Cluster volume (mm³)**	HIV-	HIV+	**Cluster label**
Cluster-forming threshold: *p* < 0.005											
medVN	Medial visual network	R extrastriate visual cortex (in cuneus)	L premotor cortex	Left frontoparietal (L-PAR)	-30	13	61	918	-0.03 (0.10)	0.07 (0.11)	A
TPN	Temporo parietal network	R angular gyrus	L inferior frontal gyrus, orbital part (in ventrolateral PFC)	Left frontoparietal (L-PAR); anterior prefrontal cortex (aPFC)	**-46**	**43**	**-3**	2376	0.01 (0.09)	0.16 (0.13)	B
.	.		L precentral gyrus	Left frontoparietal (L-PAR)	**-36**	**-9**	**51**	2268	0.05 (0.11)	0.20 (0.16)	C
.	.		L intraparietal sulcus	Somatosensory (SSN); dorsal attention (DAN); left frontoparietal (L-PAR)	**-46**	**-37**	**54**	1863	0.03 (0.15)	0.19 (0.17)	D
.	.		Visual association cortex in cuneus, bilateral	Medial visual (medVN)	2	-81	20	1323	0.08 (0.12)	0.24 (0.18)	E
.	.		L premotor cortex; L pre-SMA	Left frontoparietal / dorsal attention + salience (L-PAR/DAN + SAL)[c]	-17	0	51	1188	0.02 (0.11)	0.15 (0.14)	F
Cluster-forming threshold: *p* < 0.001											
TPN	Temporo parietal network	R angular gyrus	L inferior frontal gyrus, orbital part (in ventrolateral PFC)	Left frontoparietal (L-PAR); anterior prefrontal cortex (aPFC)	**-46**	**43**	**-3**	918	0.01 (0.10)	0.17 (0.14)	B*
.	.		L precentral gyrus	Left frontoparietal (L-PAR)	**-36**	**-9**	**51**	567	0.05 (0.10)	0.22 (0.16)	C*
.	.		L intraparietal sulcus	Somatosensory (SSN); dorsal attention (DAN); left frontoparietal (L-PAR)	**-46**	**-37**	**54**	486	0.02 (0.16)	0.18 (0.17)	D*

RSN, resting state network; **MNI**, Montreal Neurological Institute 152 atlas; **LPI**, left-posterior-inferior; **FC**, [resting state] function connectivity.
HIV-, HIV-uninfected; **HIV+**, HIV-infected.
L, left; **R**, right; **PFC**, prefrontal cortex; **SMA**, supplementary motor area.
[a] Based on cluster overlap in Haskins pediatric atlas.
[b] An RSN is listed if the majority of the cluster's extent is contained within its spatial domain (RSNs identified at age 9 years are visualised in Figure 9).
[c] No single RSN contains the majority of this cluster's extent. The premotor portion (in the superior frontal gyrus) is partially contained in the spatial profiles of both the left frontoparietal and dorsal attention networks; the medial pre-SMA portion is fully contained in the salience network.
* Cluster has center coordinates corresponding with that of the similarly labelled cluster at $p < 0.005$, indicating that the effect persists in the same region at the stricter threshold of $p < 0.001$.

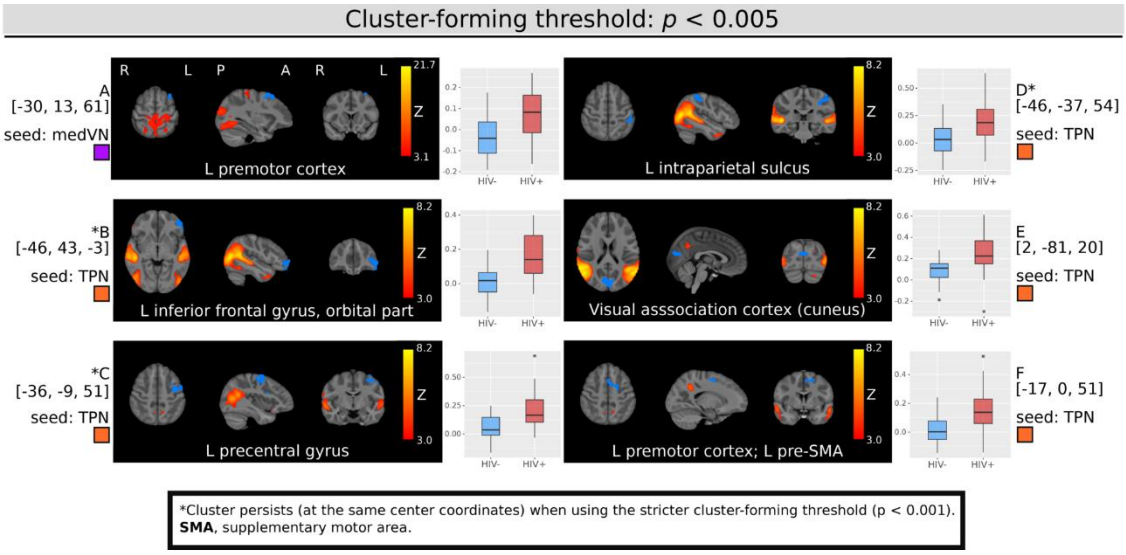

Figure 14: Each panel shows a cluster (blue) of significantly increased connectivity to a seed (not shown) in HIV+ children compared to uninfected (perintatally-exposed and unexposed) children, where seeds were placed in the structural core (cf. Hagmann et al. 2008). The cluster is shown overlain on the resting state network at the peak of which the seed was placed. Cluster-forming thresholds of p < 0.001 and p < 0.005 were combined with cluster-size thresholds to yield a corrected cluster significance of p < 0.05 (two-sided) in all cases. Each network's group map is thresholded at Z > 3. The saturation levels for each network's heatmap are the 2nd and 98th percentiles of non-zero Z-score values. Alongside each panel are boxplots visualising distributions of connectivity Z-scores, averaged over the cluster region, for the two groups. The alphabetic cluster labels in the margins (A – F) reference the tabulated details in Table 9. Each cluster is assigned a coloured square, which indexes the associated seed in Figure 13 and the associated seed-cluster set in Figure 15.

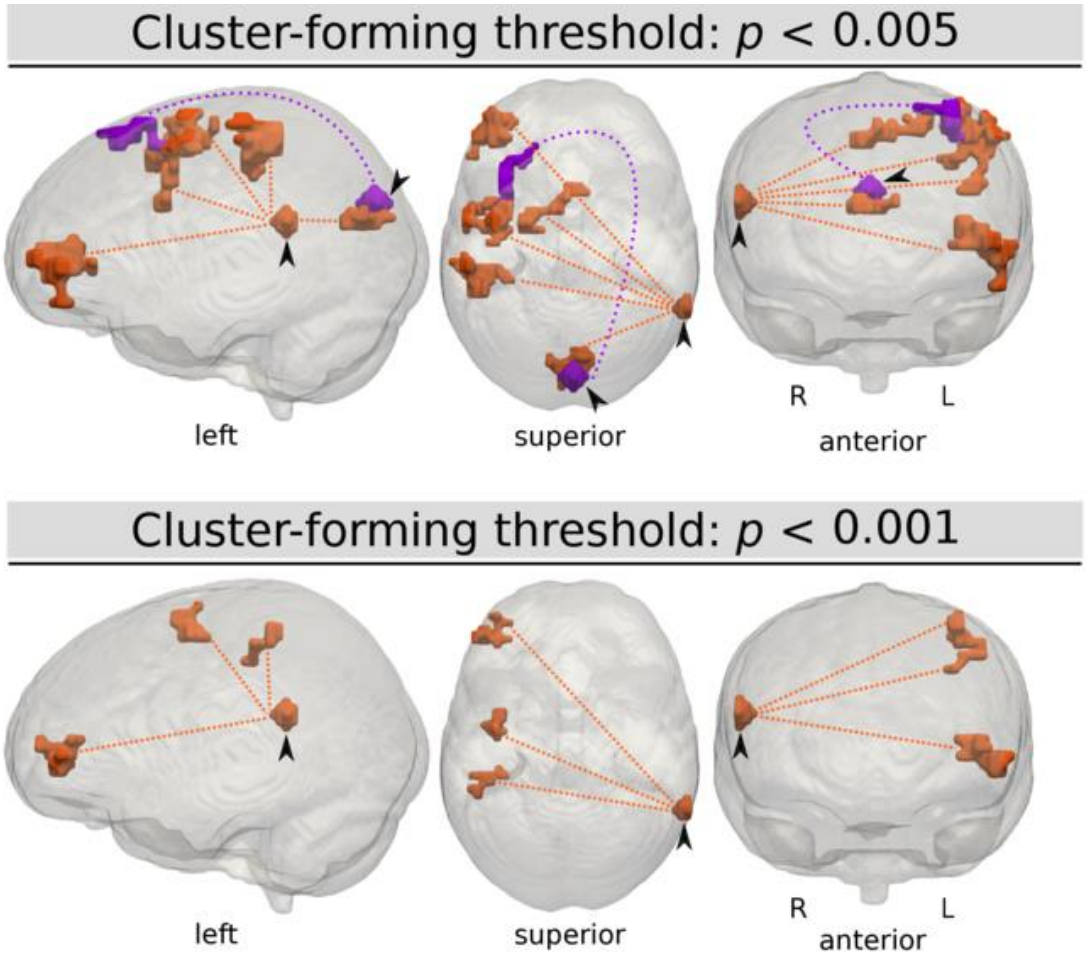

Figure 15: Glass-brain renderings of seeds (indicated with a black arrow tip) and clusters, for the results detailed in Table 9 and Figure 14 (regions revealing significantly increased connectivity to 'structural core' seeds in HIV+ compared to uninfected children). All clusters of between-group differences in connectivity to the same seed, along with the seed itself, are filled with the same colour, which indexes the seed in Figure 13: purple = R cuneus in medial visual network, orange = R angular gyrus in temporoparietal network. Dotted lines indicate seed-cluster connections, but in no way represent the anatomical path of the connection.

7.3.4 Functional connectivity with seeds revealing HIV-related differences at age 7 years

We retested six seeds (Table 10) which revealed differences in FC between HIV+ and uninfected children at age 7 years. In Figure 16a, the seeds are shown overlain on the 9-year RSN that best corresponds to the 7-year RSN from which they were originally taken. The full set of networks identified at ages 7 and 9 years are shown in Figure 8 (Section 6.5.3) and Figure 9 (Section 7.2), respectively.

Table 10: Seeds placed, at age 9 years, at the same coordinates as seeds revealing significant differences in seed-to-whole-brain connectivity between HIV+ and uninfected (perintatally-exposed and unexposed) children at age 7 years. The seeds are used to investigate between-group differences in connectivity at age 9 years using seed-based correlation analysis (SCA). Anatomical locations and seed volumes are given. Seeds are spherical with a radius of 6 mm. The seeds are visualised in Figure 16.

Seed label	RSN at age 7 years from which the seed was taken	Anatomical location	RSN assignment at age 9 years	Coordinates at seed center (MNI, LPI)			Seed volume, after masking[a] (mm^3)
				x	y	z	
SSN_{7years}	Somatosensory[Gl]	L paracentral lobule	Somatosensory (SSN)	-2	-32	60	891
$pDMN_{7years}$	Posterior default mode[Gl]	R precuneus	Posterior default mode (pDMN)	5	-71	32	891
SAL_{7years}	Salience[Loc]	R anterior cingulate	Salience (SAL)	2	35	18	891
$aDMN_{7years}$	Anterior default mode[Loc]	L posterior cingulate	Anterior default mode (aDMN)	-2	-49	29	891
MOT_{7years}	Motor[Gl]	R postcentral gyrus (ventrolateral portion, near lateral fissure)	Somatosensory (SSN)	56	-12	18	891
PAR_{7years}	(non-lateralised) Frontoparietal[Loc]	R dorsolateral PFC (R middle frontal gyrus)	Anterior prefrontal (aPFC)[b]	41	15	43	891

RSN, resting state network; **MNI**, Montreal Neurological Institute 152 atlas; **LPI**, left-posterior-inferior.
L, left; **R**, right; **PFC**, prefrontal cortex.
[Gl] In the study at age 7 years, this seed corresponded to the **gl**obal *Z*-score peak of the ICA-generated group map.
[Loc] In the study at age 7 years, this seed corresponded to a **loc**al maximum in the ICA-generated group map, separated by some distance along the anterior-posterior axis from the global peak. In that study, networks with large anterior-posterior spread were explored with a seed placed at a distant local maximum in addition to a seed at the global maximum. We here investigate only those seeds that produced significant group differences at age 7 years; the seed placed at the global maximum did not.
[a] Voxels lying outside of the brain or within ventricles were excluded from the seed. The residual seed region was used for subsequent seed-based correlation analysis. In this analysis, no such voxels were lost.
[b] The dorsal frontoparietal network changes considerably from age 7 years, becoming left-lateralised at age 9 years (see in-text discussion that follows, as well as Section 8.2.2). As a result, the seed selected from the global *Z*-score peak of this network at age 7 years no longer lies within the spatial extent of the associated network at age 9 years. No ICA-generated network identified at age 9 years seems to contain the majority of this seed's extent; the anterior prefrontal cortex (aPFC) network contains a small portion of the seed's volume.

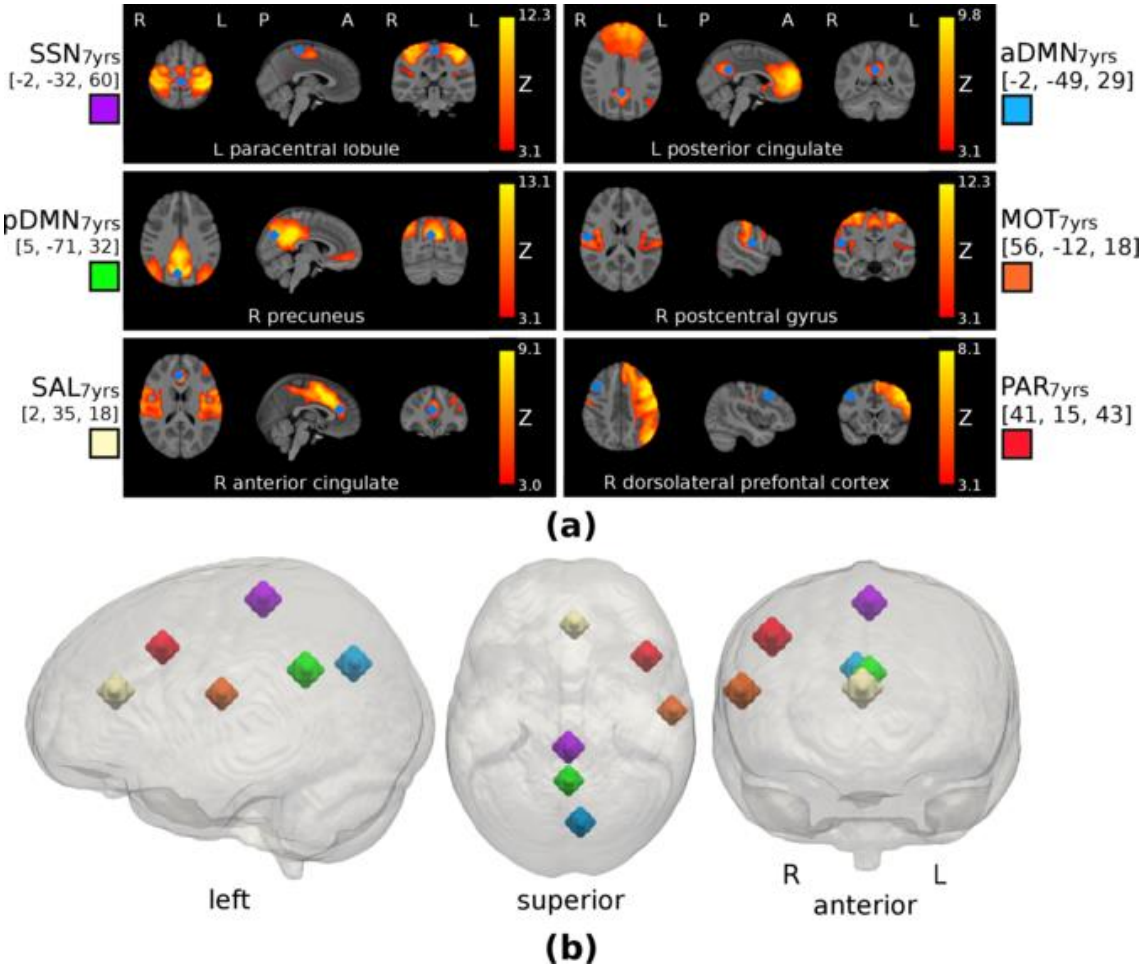

Figure 16: Seeds placed, at age 9 years, at the same coordinates as seeds revealing significant differences in seed-to-whole-brain connectivity between HIV+ and uninfected (perintatally-exposed and unexposed) children at age 7 years. ***(a)*** *Each seed is shown overlain on the group map of the resting state network at age 9 years best corresponding with the seed-containing network at age 7 years. This map is thresholded at Z > 3. The saturation levels for the network's heatmap are the 2nd and 98th percentiles of non-zero values. Seed labels in the margins reference seed details given in Table 10. Coordinates under the seed label are those of the seed center, in MNI standard space, using left-posterior-inferior (LPI) convention. Each seed is assigned a colour-code, which is used to identify that seed in (b), and to index regions showing HIV-related differences in connectivity with that seed in Figure 18 and Figure 19.* ***(b)*** *All the seeds in (a) are rendered together in a glass-brain.*

Network assignments of these seeds at age 9 years were mostly similar to those at age 7 years, with a few exceptions (Figure 17). Separate somatosensory and motor networks are present at age 7 years, while only the somatosensory network is present at age 9 years, which nevertheless contains dorsal (but lacks ventrolateral) primary motor areas (Figure 17: SSN, MOT). The somatosensory network at age 9 years is thus used as the corresponding RSN for the seeds associated with both the motor and

somatosensory networks at age 7 years. Finally, the dorsal frontoparietal network[29] is symmetric and bilateral at age 7 years, but is left-lateralised at age 9 years (Figure 17: PAR, L-PAR).

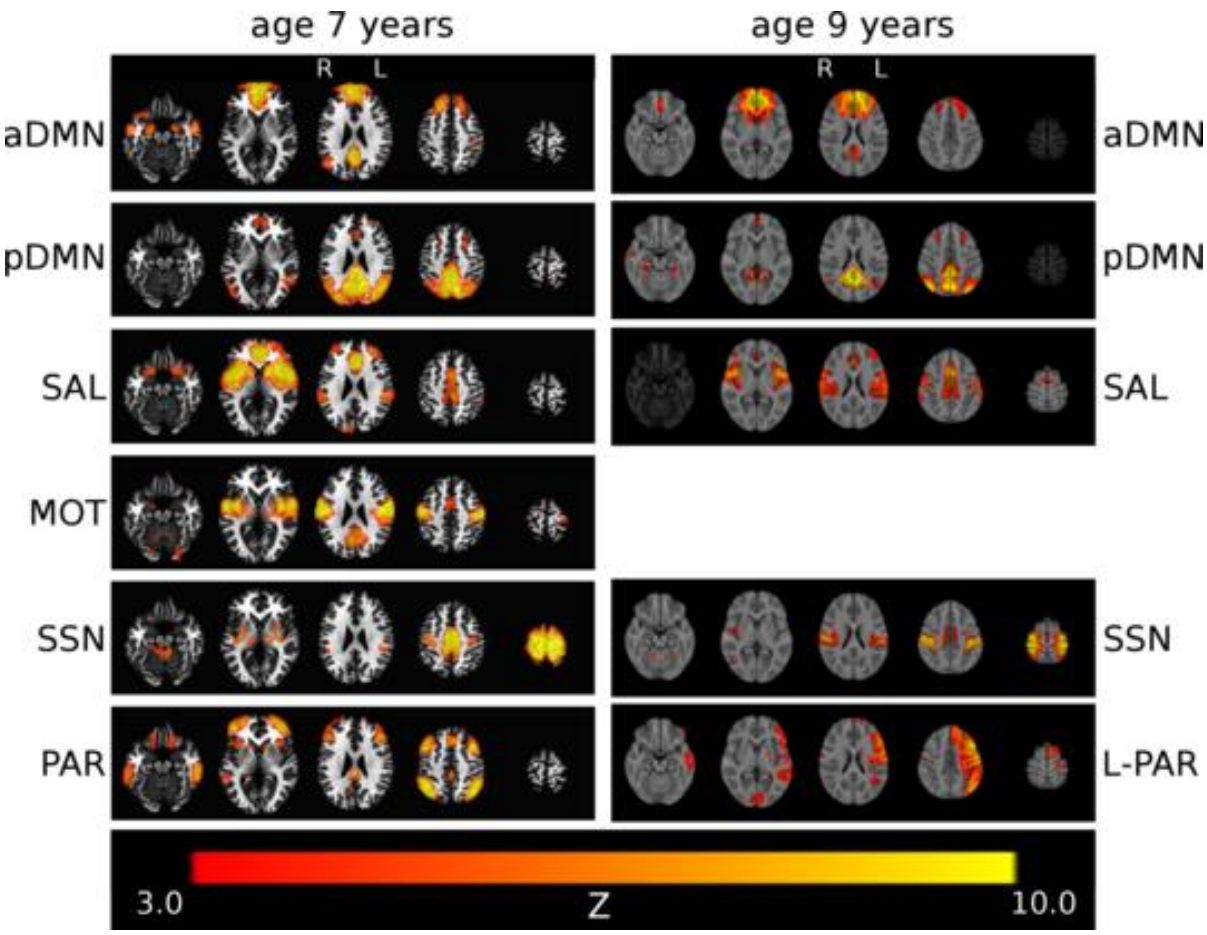

*Figure 17: Comparison of group resting state networks revealed by independent component analysis (ICA) at **ages 7 (left)** and **9 (right)** years; specifically, those networks where the network peak had functional connections that differed significantly between HIV+ and uninfected children at age 7 years. Seeds were placed at these peaks at age 9 years. Obtaining correspondence between networks at age 7 and 9 years allows us to explore: i) whether the seed is still located in the same network at age 9 years; and ii) whether connections showing significant HIV-related differences at age 9 years are within- or between-network connections, according to the positioning of the target region relative to the network containing the seed. aDMN = anterior DMN, pDMN = posterior DMN, SAL = salience, SSN = somatosensory, MOT = motor, PAR = frontoparietal, L-PAR = left-lateralised frontoparietal.*

The somatosensory, salience, and anterior DMN seeds are well located within the bounds of their associated 9-year RSN; the posterior DMN and motor seeds lie on the edge of their associated RSN; and the frontoparietal seed, being in the right hemisphere, lies outside the 9-year RSN (Figure 16).

[29] In the manuscript reporting HIV-related FC differences at age 7 years (Toich et al. 2017), this network was referred to as 'executive control.' In this manuscript, we avoid this label to prevent confusion with the cingulate/insulae/parietal network (largely composed of the salience network) which has a central role in control signalling, and which does not become lateralised in adulthood (for a more detailed discussion, see Section 5.7.2).

Four of the seeds lie in the medial surface of the cerebral cortex, while the remaining two lie in the right mid-to-anterior cerebral cortex (Figure 16b).

Three regions demonstrate increased FC with the somatosensory network seed (left paracentral lobule) in HIV+ children compared to uninfected children: bilateral intraparietal sulcus, and left frontopolar PFC. A further two regions demonstrate increased FC with the posterior DMN seed (right precuneus) in HIV+ children: right occipital pole and left middle temporal gyrus. The clusters were present at a cluster-forming threshold of $p < 0.005$, but not at $p < 0.001$ (Table 11). *Post hoc* testing revealed no significant association of scan age with cluster-averaged FC ($p > 0.1$). None of the seeds revealed clusters of lower FC in HIV+ children compared to controls. The seeds in the salience network, anterior DMN, motor network and dorsal frontoparietal network revealed no clusters of significant between-group differences at age 9 years.

Table 11: Size and peak coordinates of regions showing significantly greater functional connectivity to seeds in HIV+ children compared to uninfected (HIV-) children (perintatally-exposed and unexposed) at age 9 years, obtained using seed-based correlation analysis (SCA). These seeds were placed at the same coordinates as seeds revealing significant between-group differences at age 7 years (Toich et al. 2017). *Also given are group means of the cluster-averaged connectivity scores. Cluster labels (A – E) correspond with those in Figure 18.*

Seed information			**Clusters of FC difference (uninfected < HIV+)**								
					Cluster peak coordinates (MNI, LPI)				**Group means (SD) of average FC *Z*-scores over cluster region**		
Seed label	**Seed network**	**Seed location (abbreviated)**	**Cluster location**[a]	**RSNs (identified at age 9 years) which contain**[b] **the seed**	*x*	*y*	*z*	**Cluster volume (mm^3)**	HIV-	HIV+	**Cluster label**
Cluster-forming threshold: *p* < 0.005											
SSN_{7years}	Somatosensory network	L paracentral lobule	R intraparietal sulcus	Dorsal attention (DAN); posterior DMN (pDMN)	34	-50	37	1323	0.01 (0.16)	0.16 (0.15)	A
.	.	.	L frontopolar PFC	Anterior prefrontal cortex (aPFC); anterior DMN (aDMN); dorsal attention (DAN)	-39	43	17	1134	0.00 (0.13)	0.14 (0.13)	B
.	.	.	L intraparietal sulcus (deep)	Dorsal attention (DAN)	-27	-59	37	999	0.00 (0.14)	0.14 (0.15)	C
$pDMN_{7years}$	Posterior default mode network	R precuneus	R occipital pole, extending laterally	Lateral visual (latVN)	21	-100	-7	1647	-0.05 (0.16)	0.12 (0.17)	D
.	.	.	L middle temporal gyrus	Left frontoparietal (L-PAR)	-61	-13	-20	1296	0.11 (0.11)	0.24 (0.12)	E

MNI, Montreal Neurological Institute 152 atlas; **LPI**, left-posterior-inferior; **FC**, [resting state] function connectivity.
HIV-, HIV-uninfected; **HIV+**, HIV-infected.
L: left; **R**: right; **PFC**, prefrontal cortex.
[a] Based on cluster overlap in Haskins pediatric atlas.
[b] An RSN is listed if the majority of the cluster's extent is contained within its spatial domain (RSNs identified at age 9 years are visualised in Figure 9).

Figure 18 shows each cluster demonstrating significantly greater FC to a seed in HIV+ compared to uninfected children. The cluster is overlain on the RSN group-map at age 9 years best associated with the seed-containing network at age 7 years (as in Figure 16a). Two of the clusters showing between-group differences in FC to the somatosensory seed lie adjacent to the bounds of the ICA-revealed somatosensory group map (Figure 18A, C), while the remaining cluster (Figure 18B) lies well outside of the map's boundaries. Clusters showing between-group differences in FC to the posterior DMN seed also lie well outside the bounds of the posterior DMN group map (Figure 18D, E). All clusters lie

in the cerebral cortex (Figure 19). All are fairly lateral, with the exception of the cluster in the right occipital pole (Figure 18D), produced by the posterior DMN seed.

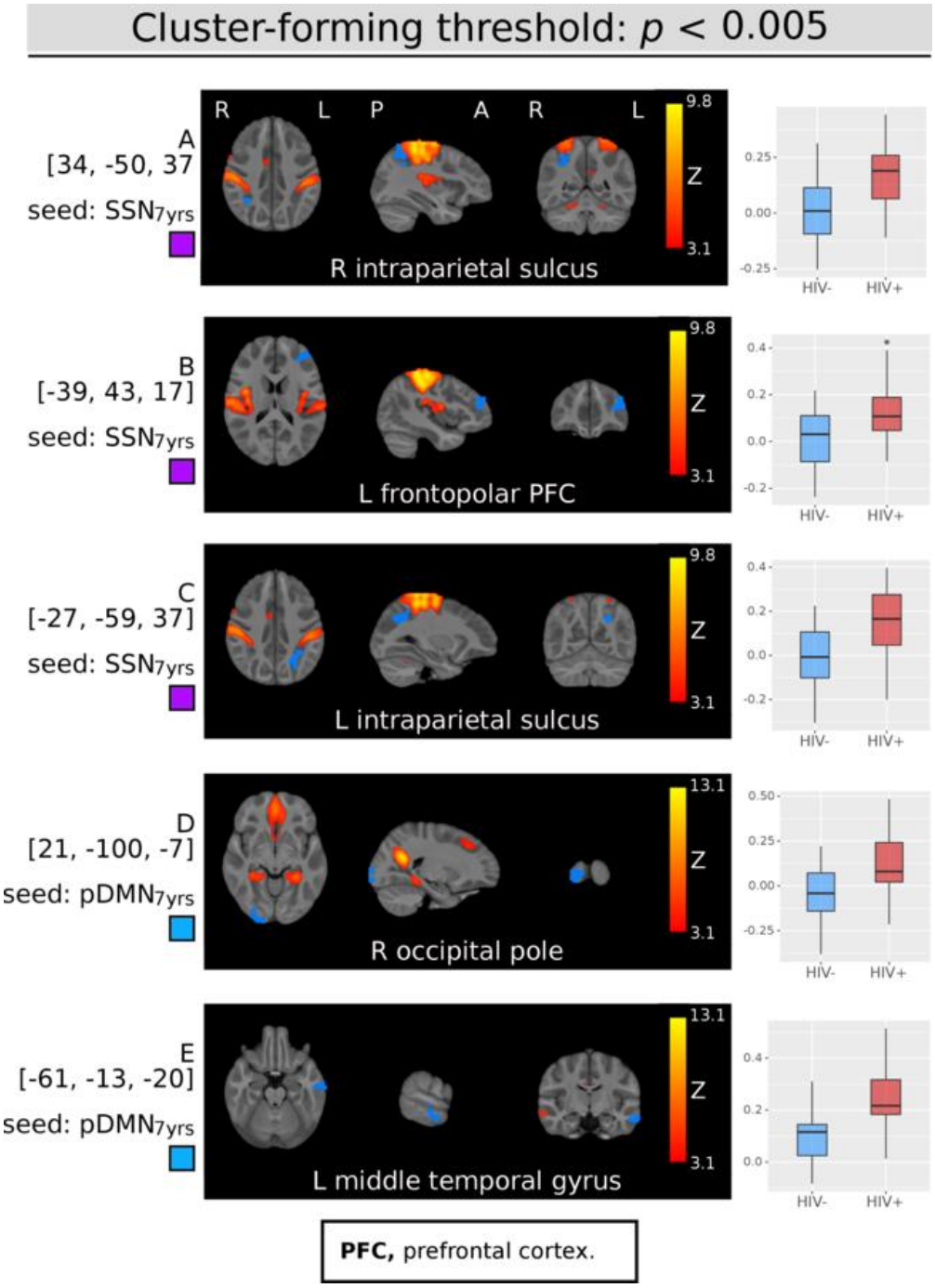

Figure 18: Each panel shows a cluster (blue) with significantly greater connectivity to a seed (not shown) in HIV+ compared to uninfected (perinatally-exposed and unexposed) children. Seeds were placed in regions revealing significant between-group differences at age 7 years. The cluster is shown overlain on the group map of the resting state network at age 9 years that best corresponds with the seed-containing network at age 7 years. Cluster-forming thresholds of $p < 0.001$ and $p < 0.005$ were combined with cluster-size thresholds to yield a corrected cluster significance of $p < 0.05$ (two-sided) in all cases. Each network's group map is thresholded at $Z > 3$. The saturation levels for each network's heatmap are the 2nd and 98th percentiles of non-zero Z-score values. Alongside each panel are boxplots visualising distributions of connectivity Z-scores, averaged over the cluster region, for the two groups. The alphabetic cluster labels in the left margins (A – E) reference the cluster details in Table 11. Each cluster is assigned a coloured square, which indexes the associated seed in Figure 16 and the associated seed-cluster set in Figure 19.

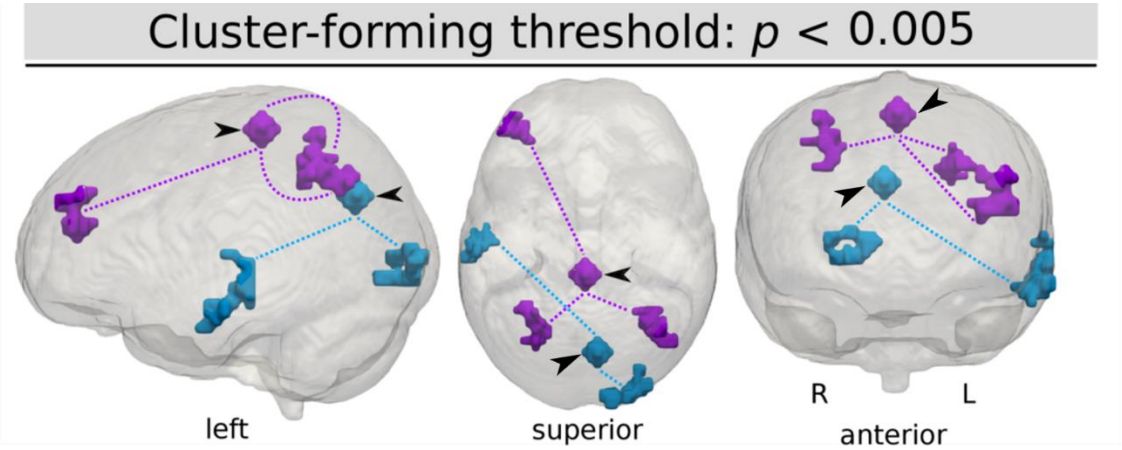

Figure 19: Glass-brain renderings of seeds (indicated by a black arrow tip) and clusters, for the results detailed in Table 11 and Figure 18 (regions revealing significantly increased connectivity to a seed in HIV+ compared to uninfected children, where seeds were placed at coordinates revealing significant between-group differences at age 7 years). All clusters of between-group differences in connectivity to the same seed, along with the seed itself, are filled with the same colour, which indexes the seed in Figure 16: purple = somatosensory network, at age 7 years; blue = posterior DMN, at age 7 years. Dotted lines indicate seed-cluster connections, but in no way represent the anatomical path of the connection.

7.4 ICA-revealed associations of within-network connectivity with immune measures

Among HIV+ children, two distinct left cerebellar regions (lobules 7 and 8) showed greater functional integration into the cerebellar network with increasing CD4%, one (lobule 8) only with CD4% in infancy and the other (lobule 7) with both CD4% in infancy and at age 9 years. *Post hoc* testing revealed significant correlations of average within-network FC in each region with age at scanning, indicating a potential confounding effect of age in this analysis. We motivated against controlling for age (Section 6.5.1); however, to be conservative, we repeated the analysis in the cerebellar network while controlling for age voxelwise. The effect of early immune health on FC in lobule 8 disappeared, but effects of early and current immune health in lobule 7 remained. We here present and discuss details for clusters revealed by the age-adjusted model. Results produced by the unadjusted model are given in Appendix E.

Table 12 presents the locations and volumes of the clusters of immune effect, and values of the *post hoc* correlation of immune measures with average FC scores over the cluster region. The clusters are anatomically depicted at their peak *Z*-scores in Figure 20. Also shown are scatter plots of FC against immune health measures, and the distribution of cluster-averaged FC scores for the HIV+ group.

Additionally, the distributions of FC scores over the cluster regions for the uninfected groups are shown for comparison purposes. We found no effect of $CD4^+$ count, neither in infancy nor at age 9 years, on within-network FC in any of the networks. Neither did we find an effect of $CD4^+$:$CD8^+$ ratio in infancy.

Table 12: Size and peak coordinates of two nearby regions showing significant association of immune health with functional integration into the cerebellar network (obtained using ICA). Also given are correlations of the immune measure with the average functional connectivity (FC) over the cluster (all are positive). Cluster labels (A, B) correspond with those in Figure 20.

ICA-generated network	Cluster anatomical location[a]	Cluster peak coordinates (MNI, LPI) *x*	*y*	*z*	Cluster volume (mm^3)	Correlation[b] of immune measure with FC averaged over the cluster region (r)	Cluster label
CD4% in infancy (at age 6–8 weeks) associated with within-network FC at age 9 years							
Cluster-forming threshold: $p < 0.005$							
Cerebellar (CER)	Left cerebellar hemisphere: crus1 and crus2 (lobule 7) in the mid and lateral regions	-26	-72	-34	1026	0.545	A
CD4% at scan (at age 9 years) associated with within-network FC at age 9 years							
Cluster-forming threshold: $p < 0.005$							
Cerebellar (CER)	Left cerebellar hemisphere: crus1 and crus2 (lobule 7) in the mid and lateral regions	-39	-63	-44	513	0.617	B

ICA, independent component analysis; **MNI**, Montreal Neurological Institute 152 atlas; **LPI**, left-posterior-inferior; **FC**, [resting state] functional connectivity.
HIV-, HIV-uninfected; **HIV+,** HIV-infected.
[a] Based on cluster overlap in Haskins pediatric atlas.
[b] Values are Pearson correlation coefficients.

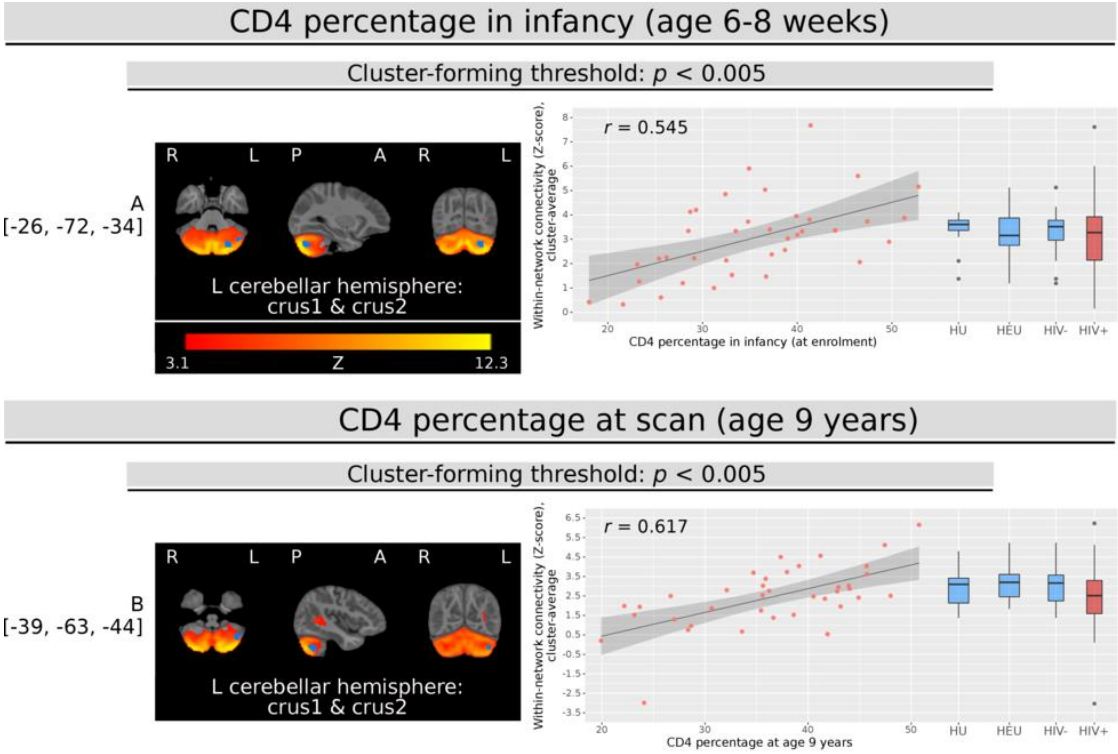

Figure 20: ***(Left)*** *Two nearby clusters (blue) within the cerebellar resting state network (hot colours) where better immune health, both at enrolment and at age 9 years, is associated with increasing within-network connectivity at age 9 years. A cluster-forming threshold of p < 0.005 was combined with an associated cluster-size threshold to yield a corrected cluster significance of p < 0.05 (two-sided). The network's group map is thresholded at Z > 3. The saturation levels for the network's heatmap are the 2nd and 98th percentiles of non-zero Z-score values.* ***(Right)*** *Plots of the average connectivity Z-scores in the cluster region against the associated immune health measure. Alongside are distributions of connectivity Z-scores, averaged over the cluster region, for the various groups. The alphabetic cluster labels in the left margin (A, B) reference the cluster details in Table 12. Coordinates under the cluster labels are those of the peak correlation, in MNI standard space, using left-posterior-inferior (LPI) convention.* ***L****, left;* ***R****, right.*

The immune effects only survive at the less severe cluster-forming threshold ($p < 0.005$). The peak coordinates for the effect of early and the effect of current immune health, while nearby, are not identical. The former is in crus 1 of left lobule 7, and the latter in crus 2 of the same lobule. The clusters showing a relation to the two measures do, however, partially overlap.

7.5 Other exploratory analyses

Effect of treatment timing (ICA pipeline)

We found no regions within ICA-generated RSNs showing effects of age at ART initiation at age 9 years: neither among HIV+ children whose ART was not interrupted (*N*=20), nor among interrupted children (*N*=20), nor among all HIV+ children (N=40).

HIV-exposed uninfected (HEU) vs HIV-unexposed uninfected (HU) (ICA pipeline)

When compared to unexposed children, HEU children had a single region, the right primary visual cortex, of reduced functional integration into the medial visual network (at both $p < 0.001$ and $p < 0.005$ cluster-forming thresholds). No other RSNs revealed significant between-group differences in within-network connectivity. Table 13 gives the coordinates of the peak FC difference, as well as the group means of FC scores averaged over the cluster regions for both significance levels. The cluster is shown overlaid on the medial visual network in Figure 21, together with boxplots of each group's distribution of cluster-averaged FC scores. *Post hoc* testing revealed no significant association of cluster-averaged FC with scan age ($p > 0.4$)

Table 13: Size and peak coordinates of a region in the medial visual network having significantly lower within-network connectivity (obtained using ICA) in HIV-exposed uninfected (HEU) children compared to HIV-unexposed uninfected (HU) children. Also given are group means of the cluster-averaged FC (Z-scores).

		Cluster peak coordinates (MNI, LPI)				**Group means (SD) of average FC Z-scores over cluster region**	
ICA-generated network	**Cluster anatomical location**[a]	*x*	*y*	*z*	**Cluster volume (mm^3)**	HU	HEU
Cluster-forming threshold: $p < 0.005$							
Visual network, medial (medVN)	R primary visual cortex (anterior end of pericalcarine sulcus)	15	-72	17	999	5.71 (1.45)	2.93 (1.23)
Cluster-forming threshold: $p < 0.001$							
Visual network, medial (medVN)	R primary visual cortex (anterior end of pericalcarine sulcus)	15	-72	17	243	6.12 (1.56)	2.93 (1.62)

ICA, independent component analysis; **MNI**, Montreal Neurological Institute 152 atlas; **LPI**, left-posterior-inferior; **FC**, [resting state] functional connectivity.
HU, HIV-unexposed uninfected; **HEU,** HIV-exposed uninfected.
[a] Based on cluster overlap in the Haskins pediatric atlas.

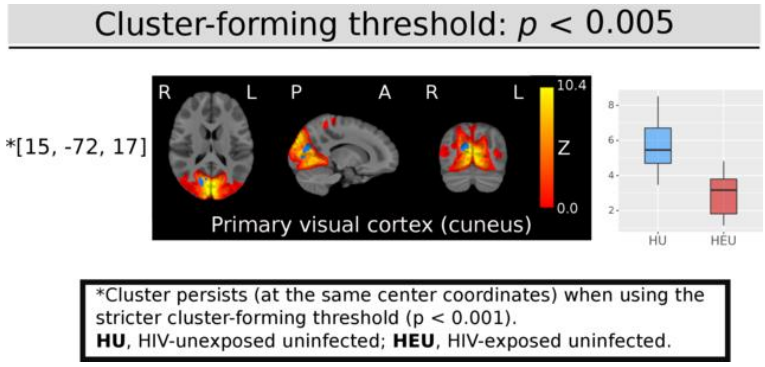

Figure 21: ***(Left)*** *One cluster (shown in blue) within the medial visual network (hot colours) demonstrated lower within-network connectivity in HIV-exposed uninfected (HEU) children compared to unexposed (HU) children. Cluster-forming thresholds of p < 0.001 and p < 0.005 were combined with cluster-size thresholds to yield a corrected cluster significance of p < 0.05 (two-sided). The network's group map is thresholded at Z > 3. The saturation levels for the network's heatmap are the 2nd and 98th percentiles of non-zero Z-score values.* ***(Right)*** *Distributions (median, with 25% and 75% quartiles as hinges, and whiskers extending to the most extreme value that is no further from the hinge than 1.5 times the interquartile range) of connectivity Z-scores, averaged over the cluster region, for the HIV+ and uninfected groups. Coordinates under the cluster labels are those of the peak between-group difference, in MNI standard space, using left-posterior-inferior (LPI) convention.*

8 Discussion

8.1 A caution on qualitative comparisons

At various points in the following discussion, as part of exploring different interpretations of our results at age 9 years, we compare them to published results acquired from the same cohort at age 7 years. Such comparisons are made with the view to attributing the differences between the two result sets to differences in age, or to age-parameterised effects of HIV/ART.

In the least, this makes the assumption that the demographics of the two samples are similar. This is largely true: the percentage of uninfected children (7 years : 9 years = 40% : 38%), perinatally-unexposed controls (7 years : 9 years = 56% : 50%) and males (7 years : 9 years = 36% : 44%), correspond well; so too do $CD4^+$ percentages at scanning (7 years : 9 years = 36% : 37%). The percentage of virologically suppressed (at scanning) HIV+ children does, however, differ somewhat (7 years : 9 years = 74% : 97%).

However, it must be cautioned that all such comparisons are merely qualitative. They do not quantitatively account for between-subject variance when considering the within-subject variance of connectivity with age. Therefore, the various speculations explored here would need to be later investigated through formal voxelwise longitudinal analysis.

8.2 ICA-generated resting state networks: reliability and developmental trajectory

Eleven of the 12 RSNs corresponded well with components identified among adults in the Functional Connectomes Project (Biswal et al. 2010), indicating reasonable reliability of the decomposition. The remaining network is here labelled as the 'anterior prefrontal cortex' network (Figure 9: aPFC). The RSNs largely concord with published adult networks – an observation also made at age 7 years in our cohort (Toich et al. 2017) – indicating that functional networks are reliably observable and already well-formed at this age. In support of this hypothesis, Thornburgh et al. (2017) observed all major networks canonically described in adults in a cohort of typically-developing 6–7-year-olds. This supports the feasibility of longitudinal analysis of large scale functional architectures through childhood and adolescence. Nevertheless, differences do exist between pediatric and adult RSNs.

While primary sensory and motor networks display robust functional organisation, higher cognitive networks can be incomplete or fragmented (Thornburgh et al. 2017; De Bie et al. 2012). In the paragraphs that follow, we discuss some of the noteworthy spatial characteristics of our observed ICA-generated RSNs, in light of those observed at age 7 years (Figure 8) in the same cohort (Toich et al. 2017), in other pediatric ICA studies, and in adults. Templates of RSN group-maps at age 7 years were available for this cohort, facilitating slice-by-slice qualitative comparisons where necessary.

8.2.1 Default mode network

We observed the DMN as two separate components, sharing a common precuneus node. The anterior component had extensive coactivation in the PFC, while the posterior had more extensive coactivation in the precuneus and lateral parietal cortices. Anterior-posterior fractionation of the DMN is consistently observed in children (Muetzel et al. 2016; De Bie et al. 2012), and concords with a lack of anterior-posterior connectivity between DMN regions in ROI-based studies (Power et al. 2010). Conversely, adults present a single integrated network. A third ventral DMN component was observed at age 7 years, but not at age 9 years, though some of its posterior-cingulate and (para)hippocampal features appear to be integrated into the posterior DMN at age 9 years. The absence of a separate ventral component at age 9 years may indicate movement towards a more mature, integrated DMN. Alternatively, the ventral DMN may be a transitory network supporting an age-specific function in younger childhood.

8.2.2 Control and attention networks

The network here labelled as the 'anterior prefrontal cortex' network (Figure 9: aPFC), having extensive coactivation at the frontal pole above the orbits, resembles a frontopolar RSN identified in a study of healthy children of age five to eight years (De Bie et al. 2012). Lacking posterior coactivation, the study postulated that it was an immature precursor of the adult cingulo-opercular network identified by Dosenbach et al. (2007) using ROI-based techniques. The cingulo-opercular network plays a key role in top-down control on the temporal scale of entire task sets. In contrast to this younger sample, the associated RSN in our study included posterior coactivation in the paracentral

and inferior parietal lobules, possibly indicating greater anterior-posterior integration with age. However, it lacks the expected dorsal anterior cingulate region that is key to Dosenbach's cingulo-opercular network[30]. Therefore, our aPFC component (and perhaps also that observed in the younger sample) more likely corresponds with the 'ventral attention system' that was defined by Fox et al. (2006) using both seed-based and ICA techniques, which is focused in the right ventral frontal regions and the right temporoparietal junction in healthy adults. This system reorients attention in response to goal-relevant stimuli. We predict that the bilateral aPFC component at age 9 years will become right-lateralised in later years.

At age 7 years, such inferior frontopolar coactivation is conjoined into the dorsal frontoparietal network (Figure 8: PAR). This may indicate an imperfect separation, at the younger age, of the more ventral systems managing cognitive control signalling and attention reorientation, from the more dorsal systems supporting information manipulation and executive functions such as working memory (for further details on how these functions map across RSNs and anatomy, see Section 5.7.2). Frontopolar coactivation at age 7 years was also less extensive[31]. Increased coactivation in frontopolar regions at age 9 years is consistent with the observation by Thornburgh and colleagues (2017) that the PFC, as well as association areas, are more greatly connected in later development, whereas primary sensory and motor cortices are favoured in younger children.

The left-lateralised dorsal frontoparietal network (Figure 9: L-PAR) appears alone in our sample. Speech and language cognition is uniquely associated with this network, consistent with the left-lateralisation of language function (Smith et al. 2009). In adults, it is often (Shirer et al. 2015; Calhoun et al. 2008) but not always (Zuo et al. 2010) accompanied by a symmetrical contralateral network. In

[30] The anterior cingulate, which along with the insulae/frontal opercula forms a core of cognitive control signalling (Ham et al. 2013; Menon & Uddin 2010; Dosenbach et al. 2007), is not absent in our decomposition, but is present in the salience network component, as is typical.

[31] Ventral frontal activation was also observed in the ventral DMN at age 7 years, a network not observed at age 9 years. However, it is not plausible that this coactivation could combine with that observed in the frontoparietal network to explain the greater frontopolar coactivation at age 9 years, since DMN networks are anticorrelated with all task positive networks (Popa et al. 2009; Fox et al. 2005), including the frontoparietal network.

5–8-year old children, De Bie et al. (2012) also only observe a left-lateralised frontoparietal system. The frontoparietal network in our own cohort at age 7 years was symmetrical and bilateral. Subsequent lateralisation is indicative of normal development.

However, the inclusion of sensorimotor cortex in the frontoparietal network at age 9 years is peculiar, as these systems are anticorrelated in adults (Doucet et al. 2011). The sparsity of pediatric ICA studies with a narrow age range makes it difficult to discern whether entanglement of these systems at this age is normal, indicative of a delayed but conventional development trajectory, or an abnormal trajectory. The former two options are at least plausible, given lack of functional separation between anatomically adjacent regions in children (Fair et al. 2009). It will be informative to study how the RSN evolves through the adolescent years.

8.2.3 Visual networks

Visual, sensory and motor networks tend to exhibit mature functional organisation already in early childhood (De Bie et al. 2012). We observed two separate visual networks at age 9 years (Figure 9: latVN, medVN), similarly to age 7 years. The split into a medial and lateral visual network is observed in other pediatric studies (Thornburgh et al. 2017), and remains in adulthood (Smith et al. 2009; Beckmann et al. 2005).

There is strong concordance between the medial and visual networks observed at age 7 and 9 years in our cohort. However, one striking difference is the inclusion of dorsal somatosensory regions (posterior paracentral lobule and dorsal-most postcentral gyrus) into the medial visual network at age 9 years (not shown). While somatosensory and visual systems are positively correlated (Doucet et al. 2011), they normally appear well-separated in ICA decompositions. Similar integration of somatosensory areas into visual networks has been observed in normal aging of adults (Biswal et al. 2010: Figure S2), indicating that it may be a late-manifesting mode of FC disruption in our cohort (which is largely HIV+ or perinatally-exposed) rather than of typical FC development through childhood. Further studies employing voxelwise longitudinal analysis to investigate development of visual networks in HIV+ and uninfected children would be informative.

8.2.4 Motor and somatosensory networks

ICA typically revels a separate motor network in children (Thornburgh et al. 2017), while primary and supplementary motor cortex is integrated with the somatosensory cortex in adults into a single sensorimotor[33] network (Biswal et al. 2010; Smith et al. 2009). The somatosensory network at age 9 years (Figure 9: SSN), as at 7 years, includes the dorsal-most portion of the precentral gyrus (seat of the primary motor cortex), but not the ventrolateral portions of the gyrus or the SMA (supplementary motor cortex). While these regions appeared as a separate motor network at age 7 years, no such network was observed at age 9 years. This may simply be an effect of sampling variation, rather than a feature of the population under investigation. In a study investigating robustness of ICA decompositions in children, the motor network demonstrated lower resampling stability than many other common networks (Muetzel et al. 2016). Alternatively, the lack of a separate motor network may indicate gradual integration into a sensorimotor network. However, we did not observe marked expansion of the somatosensory network to include additional motor areas at age 9 years compared to age 7 years.

At any rate, motor coordination has apparently not been disrupted in our generally asymptomatic cohort (Laughton et al. 2017), although missed motor development milestones are often reported in progressive HIV encephalopathy (Van Rie et al. 2007).

8.2.5 Cerebellar network

A notable feature is the presence of a separate cerebellar network (Figure 9: CER), which was not observed at age 7 years. Such a network is often (Thornburgh et al. 2017; Muetzel et al. 2016) but not always (De Bie et al. 2012) indicated in children. Conversely, it is consistently revealed in adults (Biswal et al. 2010; Smith et al. 2009). The presence of this component at age 9 years may indicate progression towards more robust FC organisation of cerebellar systems and cerebrocerebellar loops.

[33] Also called 'somatomotor.'

8.2.6 Temporoparietal network

The separate temporal lobe component – here labelled as the 'temporoparietal network' (Figure 9,Table 5: TPN) – interestingly does not include the primary auditory cortex (Brodmann area 41), though it includes the auditory and visual-auditory association cortices (superior temporal sulcus). The primary auditory cortex is, however, present in the salience network, which extends further posteriorly in the medial/superior temporal and insular cortex than seems to be typical in adults (Seeley et al. 2007). This lack of functional segregation between nearby auditory and attention-related regions is consistent with previous findings describing an anatomically-local arrangement of FC in children, as opposed to an emphasis on connectivity of anatomically-segregated but functionally related regions in adults (Fair et al. 2009). We have discussed similar lack of segregation in the frontoparietal network (Section 8.2.2).

8.2.7 Types of functional connections evidenced by networks

In concordance with De Bie et al. (2012), we note established subcortico-cortical and long-range cortico-cortical connections at this age. This is evidenced by several RSNs having spatial extents that overlap both subcortical and cortical anatomy (aDMN, SAL, SSN, L-PAR, BGN) and both anterior and posterior anatomy (aDMN, pDMN, DAN, L-PAR, aPFC), respectively (Figure 9).

8.3 HIV+ vs. uninfected functional connectivity comparisons

We discuss significant differences in FC between HIV+ and uninfected (perinatally-exposed and unexposed combined) children as revealed by ICA (Section 8.3.1) and SCA (Sections 8.3.2, 8.3.3, 8.3.4) pipelines.

8.3.1 ICA-revealed within-network differences

Against hypothesis I (Section 3), we found no HIV-related intra-network FC differences within any ICA-generated RSNs at age 9 years. The analysis at age 7 years (Toich et al. 2017) produced the same null result. This may be a consequence of within-network connectivity not being sufficiently robust at this age. There is a strong line of evidence suggesting that within-network connectivity increases towards adulthood, while between-network connectivity decreases (Fair et al. 2009; Stevens et al. 2009). Though the spatial topographies of ICA-generated RSNs largely resemble those of adult networks

already in childhood (Thornburgh et al. 2017) – an observation also made in our own cohort at ages 7 and 9 years (Figure 8, Figure 9) – graph theory indicates that functional integration, especially within anatomically-distributed networks, continues into young adulthood (Fair et al. 2009). That is, while we may observe initial allocation of brain regions to networks in early childhood, the strength with which regions are functionally integrated into those networks likely develops more slowly throughout adolescence.

8.3.2 Functional connectivity with seeds related to neuropsychological domains

We found partial support for the hypothesis that brain regions underpinning neuropsychological domains that are impaired in perinatally HIV-infected children would have FC that differs between HIV+ and uninfected children (Hypothesis III, Section 3). One of the two seeds associated with planning, specifically the seed located in the left precentral gyrus in a region involved with movement of the trunk (Plan1), and both seeds associated with visual perception (Vis1: right visual association cortex, Vis2: left superior parietal lobule) had connections demonstrating greater FC in HIV+ compared to uninfected children (Table 7). This may suggest that FC abnormalities contribute to deficits in these neuropsychological domains in HIV+ children. This causal proposition assumes that the neuropsychological deficits observed at ages 5 and 7 years, according to which we selected our seeds, have persisted in some form to age 9 years, when we measure these significant FC differences. Analysis of neuropsychological measures acquired at age 9 years are not yet complete. A proposition of opposite causality is also possible: that the observed FC abnormalities, rather than forming part of the origin of neuropsychological deficits, indicate neuroplastic reconfiguration targeting the resolution of these deficits. Our finding of FC increases in HIV+ children gives credence to this interpretation.

Impairment or delayed neurodevelopment of visuospatial perception in perinatally HIV-infected children has been previously described, at least in the pre-ART era (Birn et al. 2006; Tardieu et al. 1995; Boivin et al. 1995; Diamond 1987). Previous rs-fMRI studies also suggest susceptibility of visual function to HIV infection. For example, in an ICA analysis of early HIV infection in adults, only the lateral visual network showed reduced functional integration in the HIV+ group (Wang et al. 2011).

Within-network FC was reduced in the left inferior parietal cortex of this network, suggesting reduced integration of parietal cortex with visual association cortex. Further, the FC abnormality was predictive of poorer visual-motor coordination in HIV+ adults (Wang et al. 2011). It is striking that in our analysis, both visual perception seeds likewise revealed parietal-occipital FC that differed between HIV+ and uninfected children. Correspondence with results seen in adults may indicate that these FC abnormalities are an age-independent effect of early HIV infection, rather than being indicative of atypical or delayed neurodevelopment.

Impairment in executive functioning, of which the 'planning' construct forms part, and which is strongly associated with real-world outcomes such as academic achievement, has been inconclusively investigated in the very limited set of cognitive studies in pediatric HIV+ literature (Laughton et al. 2017; Nichols, Chernoff, Malee, Sirois, Woods, et al. 2016; Merkle 2015). It is a neuropsychological domain that does, however, show impairment in HIV+ adults, even in the post-ART era (Heaton et al. 2011). In fact, a shift is described from cognitive slowing, motor deficits and verbal deficits in the pre-ART era, to executive function and learning deficits in the post-ART era (Heaton et al. 2011).

With a limited body of pediatric neuroimaging literature, the relationship between neuroimaging markers and cognitive impairment in children is still largely unexplored. Worse cognitive performance (cognitive proficiency, working memory, processing speed) has been related to smaller grey matter volumes in the bilateral precentral and the left middle frontal gyri (among 10 investigated regions) in perinatally-infected youth (Lewis-de los Angeles et al. 2017). In our analysis, the left precentral gyrus was the seed selected for the planning domain, and had functional connections with medial frontal (paracentral lobule, SMA, ventromedial PFC), medial parietal (precuneus), left insula, and basal ganglia (left putamen) regions that differed significantly between HIV+ and uninfected children. Taken together, these two sets of results might suggest that that abnormal precentral FC in HIV+ youth arises from grey matter insults in this region and contributes to impaired cognitive function. In another study among perinatally infected youth, some functional connections of the medial PFC and the posterior

cingulate (two key nodes of the DMN) that were significantly modulated by disease severity were found to predict processing speed scores (Herting et al. 2015). The performance-predictive connection for the medial PFC was with a right inferior frontal region, while in our analysis it was the medial PFC's connectivity with the precentral gyrus 'planning' seed (Table 7: Plan1) that differed between HIV+ and uninfected children. However, the same study did describe lowered FC of the medial PFC to the precentral gyrus with greater HIV disease severity, supporting this connection's vulnerability to infection, if not its involvement in cognition.

It is striking that only two of the six regions having abnormal FC with the planning and visual perceptions seeds in HIV+ children are in the frontal lobe, and that both of these are medial. The remainder are in the posterior (parieto-occipital) cortex or in the striatum (basal ganglia). The visual perception seeds themselves are posterior, and the planning seed is dorsomedial within the precentral gyrus. DTI studies indicate that white matter bundles mature asynchronously in the postnatal period, with progression from a posterior-to-anterior and central-to-peripheral direction (Dubois et al. 2014). This might suggest that the planning- and visual perception-related FC abnormalities arise from CNS insults (HIV- or ART-mediated) during early, rather than later, development. Whether FC alterations themselves arise early and persist, or later, we cannot speculate. We do note that none of these six functional connections that differ significantly between HIV+ and uninfected children at age 9 years correspond directly with such connections observed at age 7 years[34], suggesting delayed FC alterations.

For all regions showing significantly differing FC with the planning and visual perception seeds between HIV+ and uninfected children, the HIV+ group had greater positive BOLD correlations (Figure

[34] There are, however, rough similarities. Like the 'left precentral gyrus (Plan 1 seed) ↔ left insula / transverse temporal gyrus' connection at age 9 years, the 'right postcentral gyrus ↔ superior/middle temporal gyrus' connection at age 7 years involves a region near the central sulcus and a temporal region. An ipsilateral 'occipital ↔ parietal' connection is implicated at both ages: between the right lateral occipital lobe (Vis1 seed) and the right angular gyrus at age 9 years, and between the right occipital pole / inferolateral occipital lobe and the right precuneus at age 7 years. The same connection at age 7 years similarly bears some resemblance to the 'left occipital pole ↔ left superior parietal lobule (Vis2 seed)' connection implicated at age 9 years.

11). The uninfected group has either lesser positive or near-zero BOLD correlations. Three interpretations might be posited for this phenomenon.

Firstly, greater FC in the HIV+ group might indicate connections to regions not typically engaged in neural systems subserving the neuropsychological domain of interest, and indicate recruitment of atypical brain regions. Of the six regions having significant between-group differences in FC with the planning and visual perception seeds, five lie largely outside areas consistently activated in fMRI tasks testing the associated neuropsychological domains, where these domain-related areas are mapped by automated meta-analyses (Figure 11). Of these, four lie immediately adjacent to the domain-related areas. This supports the proposition that recruitment (either immature, or insult-induced) underlies the higher correlations in HIV+ children, since recovering stroke patients recruit the function specifically of regions adjacent or contralateral to those damaged (Carpenter et al. 2000). Chang et al. have shown that HIV+ adults demonstrate abnormally expansive functional activation compared to controls in some attention tasks (2001; 2004).

The second possible explanation is that functional connections between the implicated regions have been submitted to functional pruning in uninfected children, and that their presence in HIV+ children is an indicator of immature functional organisation. Rs-fMRI studies indicate that through childhood development, the strength of short-range functional connections decrease, while the strength of long range connections between regions that are functionally-related in adults simultaneously increase (Uddin et al. 2010; Power et al. 2010; Fair et al. 2009; Supekar et al. 2009). The functional pruning of short-range connections is posited to be underpinned by synaptic pruning (Power et al. 2010), which takes place throughout the first twenty years of life (Huttenlocher 1979). Further evidence for functional pruning is that the spatial extents of RSNs tend to become reduced towards adulthood (Littow 2010), and that brain activation patterns for a given task tend to become less diffuse and more focal with age (Durston et al. 2006). All connections with the planning and visual perception seeds

showing significant HIV-related increases here were relatively short-range. There are no connections between parietal/occipital and frontal regions, for instance.

Finally, a combination of the previous two hypotheses is also plausible: connections not typically associated with a cognitive function in adults are nevertheless present in children, and are the targets for functional pruning in typical development. That is, these connections are not necessarily indicative of recruitment following damage to neural systems, but may be indicative of immature and perhaps inefficient systems.

8.3.3 Functional connectivity with seeds in the structural core

Our results lend partial support to the hypothesis that the connectivity of seeds in the structural core is particularly vulnerable to HIV and/or ART (Hypothesis II, Section 3). Two of the four tested seeds showed significant between-group differences in their connectivity. These connections involved six different target regions (Table 9). Against our expectation, all BOLD correlations were greater in the HIV+ group compared to the uninfected group. The left premotor cortex had increased FC to the medial visual network seed (right peristriate cuneus) in HIV+ children, while left ventrolateral PFC, left precentral gyrus, left intraparietal sulcus, left premotor/pre-SMA and bilateral visual association cortices had increased FC to the temporoparietal network seed (right angular gyrus). Of the latter seed's five implicated connections, three of these (to the left ventrolateral PFC, left precentral gyrus, and the left premotor/pre-SMA) bear some similarity to an 'inferior parietal ↔ frontal' connection showing HIV-related differences at age 7 years (specifically, that between the right inferior parietal lobule and the right middle frontal gyrus). The directionality at age 7 years was, however, different, with HIV+ children having lower FC than uninfected children.

All significant regions lay well outside of the RSN at the peak of which the associated seeds were placed (Figure 14), indicating that the affected connections are between- rather than within-network connections. Since nodes of the structural core have hub-like properties in graphs of structural connectivity (Hagmann et al. 2008), it is perhaps not surprising that they would be well-positioned to reveal group differences in between-network connectivity.

Since between-network connectivity appears to reduce through adolescence and young adulthood, stronger between-network connectivity in HIV+ children may be an indicator of immature functional organisation, and hence delayed or impaired neurodevelopment. In a sample of 100 subjects aged 12 to 30, Stevens et al. (2009) combined Granger causality estimates and graph theory to investigate how causal influences between ICA-revealed RSNs change with age. It was found that both the number (in- and out-degree) and strength of between-network influences decreased with age. The greater changes occurred during adolescence, as opposed to young adulthood. It was posited that reduction in between-network influences are paralleled with increased within-network FC, and that these processes subserve more independent network dynamics for the purposes of increased processing flexibility.

It is interesting that all six regions showing HIV-related differences in FC to the two seeds lie within or on the border of the left-lateralised frontoparietal network observed in our cohort (Figure 9: L-PAR). As a proviso, we cannot go so far as to suggest that these regions have exclusive membership to this network, since networks overlap spatially[35]. We have previously mentioned that the frontoparietal network unexpectedly included sensorimotor regions in its spatial extent (Section 8.2.2). Abnormal connectivity within this network may have implications for executive functions such as working memory, attention and cognitive control (Seeley et al. 2007). Since the entire cohort (HIV+ and uninfected children) were input to MELODIC for the estimation of RSN group-maps, we posited that the atypical spatial profile of this group-map at age 9 years may be an HIV-related effect. While the ICA pipeline revealed no significant FC differences within the RSN (Sections 7.3.1, 8.3.1) we wished to explore if the null result was for lack of power. To obtain separate HIV+ and uninfected group maps for the network, we performed two one-sample t-tests on subject-specific maps estimated by dual regression, thus revealing for each group the spatial features surviving variance between individuals.

[35] There is no one-to-one mapping of brain regions to RSNs. While probabilistic ICA is optimised for spatial orthogonality of estimated RSNs, spatial overlap of networks is by no means prohibited (Beckmann et al. 2005).

Visual inspection reveals some differences in the spatial profiles of the thresholded statistical maps of the two groups (Figure 22). The evolution of this network through adolescence will be informative.

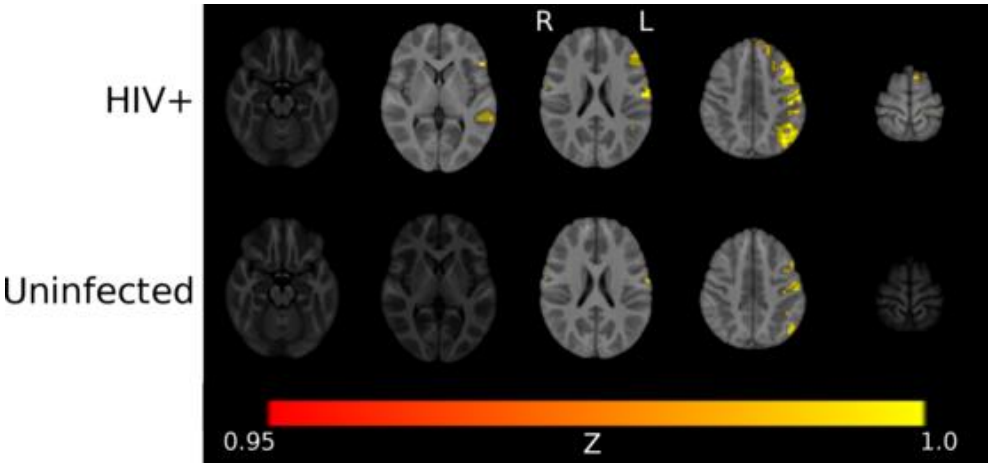

Figure 22: Separate mean spatial maps for the HIV+ and uninfected groups, obtained by performing one-sample t-tests on subject-specific maps estimated by dual regression, and controlling the family-wise error rate at 5% through correction for multiple voxel comparisons.

The left-lateralisation of regions showing HIV-related differences in FC to the right-lateralised temporoparietal network seed (right angular gyrus) is striking (Figure 15). Given that the connections are interhemispheric, one may postulate abnormal (abnormally strong, perhaps) corpus callosum structural connectivity. While corpus callosum disruption is frequently reported in adult HIV, no such disruption has been observed in our cohort at ages 5 or 7 years, perhaps due to early ART initiation (Jankiewicz et al. 2017; Ackermann et al. 2016). Conversely, abnormalities in the inferior longitudinal fasciculus and inferior fronto-occipital fasciculus were observed at both ages 5 and 7 years. Damage to the latter tract might correspond with HIV-related differences in the FC of the premotor area to the extrastriate cuneus (visual network seed)[36], although the directionality of the result (with greater FC in the HIV+ group) is then unexpected. Overall, there is limited correspondence of our FC results with structural connectivity disruptions previously observed in our cohort.

[36] While the center of the seed is marginally in the right hemisphere (Table 8), it includes the cuneus bilaterally.

8.3.4 Functional connectivity with seeds revealing HIV-related differences at age 7 years

We hypothesised that when retesting at age 9 years seeds that revealed significant between-group differences at age 7 years (Toich et al. 2016), a portion of previously-observed FC abnormalities would persist, while some would resolve; we additionally expected some new connections to be implicated at age 9 years (Hypothesis IV, Section 3). Differences in the FC profile of HIV- and/or ART-related effects between the two ages were more considerable than expected. Only one connection was implicated at both ages (discussed hereafter). If nothing else, this suggests that the effect of HIV and ART on FC are parameterised by the stage of neurodevelopment. Cross-sectional studies with samples of narrow age range are therefore essential to a better understanding of neurodevelopment in the post-ART era, and should be complemented rather than substituted by longitudinal processing pipelines.

The seed placed in the precuneus of the posterior DMN showed greater FC to the right occipital pole and left temporal middle temporal gyrus in HIV+ compared to uninfected children at age 9 years (Table 11). However, only the connection with the occipital pole emerged in the analysis at age 7 years. The connection showed decreased FC in HIV+ children at age 7 years, but increased FC at age 9. The occipital regions involved in this connection at the two ages are, however, adjacent rather than overlapping[37], possibly suggesting compensatory recruitment at age 9 years of regions suffering loss of integration at age 7 years or younger (Carpenter et al. 2000). We have discussed the hypothesis of recruitment in some detail in Section 8.3.2.

At age 9 years, the paracentral lobule seed of the somatosensory network showed increased FC with the bilateral intraparietal sulcus and the left frontal pole (Table 11). Functional integration (within-network FC) of the intraparietal sulcus into the frontoparietal network in young adults appears to have a unique influence on executive performance. Stronger correlations of these regions with the lower-order somatosensory network in HIV+ children may indicate lack of independence between sensory

[37] Cluster center at age 7 years, in MNI coordinates, left-posterior-inferior convention: $17, -88, -13$; at age 9 years: $21, -100, -7$.

and working memory modules (systems for information processing), with possible consequences of reduced response flexibility to stimuli (Stevens et al. 2009). Indeed, Doucet and colleagues (2011) show that these two 'modules' are normally anticorrelated in healthy adults, with communication mediated by a salience/control module that is positively correlated with both[38]. At age 7 years, the same somatosensory seed investigated here showed *lower* FC with the dorsal anterior cingulate, an anchor of the salience RSN (Seeley et al. 2007), in HIV+ compared to uninfected children. It is thus possible that having suffered impaired communication with the mediating salience/control module, the sensory module has increased direct communication with the working memory module, at the possible expense of loss of independence.

We have already alluded to the literature's observations that between-network influences tend to decrease towards adulthood (Stevens et al. 2009), and that the spatial extent of RSNs tend to become more reduced (Littow 2010). The fact that all the regions showing increased FC to the posterior DMN and somatosensory network seeds in HIV+ children lie on the boundary of, or outside of, the spatial extent of the seed networks (Figure 18) may indicate immature functional organisation. However, it should be noted that here the boundaries of the networks were defined based on their appearance at age 9 years, while seeds associated with these networks were taken from network peaks at age 7 years. While the seed for the somatosensory network is well seated within the extent of the somatosensory network observed at age 9 years, the seed for the posterior DMN lies on the periphery of the associated network at age 9 years (Figure 16). Thus, the above speculations are tentative for the posterior DMN seed's results.

8.4 ICA-revealed associations of within-network connectivity with immune measures

We hypothesised that poor immune health in infancy, but not current immune health, would predict lowered ICA-revealed within-network FC in early-maturing RSNs (Hypothesis V, Section 3). Indeed, we

[38] For additional discussion on observations revealed by the hierarchical clustering of RSNs performed by Doucet and colleagues (2011), see Section 5.7.2.

found a positive association of CD4% at enrolment (age 6–8 weeks) with intra-network connectivity in the cerebellar network – specifically in the crura of the left lobule 7 (Table 12).

With this association observed among HIV+ children, we then wished to explore if weaker, rather than stronger, FC in this region is abnormal. This we did by comparing the distribution of within-network FC (in the immune-correlated regions) of the HIV+ group with that of the uninfected groups. The median *Z*-scores for all groups (HIV+, uninfected[39], HEU, HU) are similar (Figure 20 boxplots). This is expected, as ICA revealed no significant effect of continued HIV-infection or perinatal exposure in these regions. Positioning of the interquartile range of FC for the HU subgroup or aggregate uninfected group in or above the 50-75% quartile in the HIV+ group, would give an intuitive indication that lower FC in the implicated regions is abnormal. For the cluster showing a relation with CD4% in infancy (Figure 20A), the positioning gives reasonable evidence that this is so. That is, HIV+ subjects with greater FC scores, which in turn are predicted by higher CD4%, better conform to the distribution of connectivity scores among uninfected subjects. The evidence is only marginal for the cluster modelling the effect of current CD4% (Figure 20B).

Cerebellar FC is under dynamic development in infancy, with intra-cerebellum resting state correlations present as early as 27 weeks postmenstrual age (Smyser et al. 2010). Against our hypothesis, we did not observe susceptibility of other early-maturing RSNs, such as visual and somatosensory networks (Fransson et al. 2007), to effects of immune health. As a possible explanation for this, the process of neural migration uncharacteristically continues beyond birth in the cerebellum, making it especially susceptible to perinatal and postnatal brain insults (Ciesielski & Knight 1994). Our primary conclusion is that early immune health can have long term consequences on FC, even if only in cerebellar development.

At age 7 years, infant immune health in the same cohort was found to predict within-network FC in right-lateralised regions of the basal ganglia network, somatosensory network (medial and lateral

[39] That is, HEU and HU combined.

parietal lobe), and salience network (inferior frontal gyrus, insula) (Toich et al. 2017). At that age, poorer immune health was associated with greater FC, which was attributed to delayed synaptic pruning. In an MR spectroscopy study of a basal ganglia voxel in the same cohort at age 5 years, Mbugua et al. (2016) found lower $CD4^+$:$CD8^+$ at enrolment (age 6–8 weeks) to be associated with lower metabolite levels indicative of neuronal integrity, despite early ART and viral load suppression. This observation lends support to the connectivity correlate in the basal ganglia network observed at age 7 years. The abovementioned immune-correlated RSNs at age 7 years were revealed by ICA at age 9 years as well (Section 8.2), but they did not reveal significant results in the correlation analysis with immune measures in this study. This discrepancy may indicate that functional consequences of poor early immunity have resolved in these regions by age 9 years. At age 7 years, ICA generated no separate cerebellar RSN, excluding the possibility of finding an association there.

Against our hypothesis, a marker of current immune heathy (CD4%) also had a positive association with within-network FC at age 9 years. The association was again in the crura (lobule 7) of the left cerebellar hemisphere. In addition to protracted postnatal neural migration, the cerebellum also exhibits protracted morphometric development through childhood, reaching its peak total volume later than the cerebrum – at approximately 11.8 years in girls, and 15.5 years in boys (Tiemeier et al. 2010). Thus, the FC maturation of this structure may still be susceptible to physiological factors at age 9 years such as poor immune health. At age 7 years, no relationships of current immune health with FC in ICA-generated RSNs were identified, though the cerebellar network was not observed at this age (Figure 8).

Other studies investigating associations of current immune health with FC in HIV+ subjects have been conducted, to the authors knowledge, only among adult cohorts. They therefore provide limited insight into the developmental propositions discussed in the previous paragraphs. For completeness, we add that Thomas et al. (2013) found no association of current immune health ($CD4^+$ count) or HIV RNA viral load with FC among HIV+ adults.

Traditionally, the cerebellum has been identified with fine motor control (Clark et al. 2010b). However, burgeoning evidence suggests that the cerebellum, and particularly the lateral cerebellar hemispheres (in which we observe our immune correlates), may also modulate higher cognitive functions (Schmahmann 1991). From the clinicopathological evidence, impairment in executive functions, spatial processing, and language processing have been observed in patients with posterior lobule and vermis lesions of the cerebellum (Schmahmann & Sherman 1998). The neuroimaging literature identifies language, executive, and emotional processing functions with crus I (lobule 7) of the cerebellum (Stoodley & Schmahmann 2009), the same anatomical region overlapping with our immune-correlated clusters (Figure 20). In our HIV+ cohort, deficits in visual perception (together with the learning and planning executive functions) have been observed (Laughton et al. 2017; Merkle 2015). Our results may indicate that part of these neuropsychological deficits are linked to disruption of cerebrocerebellar loops mediated by lowered immune health in critical developmental periods.

8.5 Other exploratory analyses

Effect of treatment timing (ICA pipeline)

That we found no effect on timing of ART initiation on FC at age 9 years, may indicate that timing effects resolve in later development if treatment is initiated before a certain critical age. In our sample, all but one HIV+ child initiated treatment before 40 weeks. While neurodevelopment outcomes were poorer at age 11 months for those children in our cohort in the deferred treatment arm (Laughton et al. 2012), neurodevelopmental differences between early and deferred arms appeared to resolve by age 5 years (Laughton et al. 2017).

HIV-exposed uninfected (HEU) vs HIV-unexposed uninfected (HU) (ICA pipeline)

We previously posited that lower within-network connectivity in childhood might explain the lack of observed HIV-related differences in ICA-revealed within-network connectivity (Section 8.3.1). It is then perhaps not surprising that the only effect of perinatal HIV-/ART- exposure was observed in the

primary visual cortex of the medial visual network (Table 13), a region and network undergoing early functional maturation (Fransson et al. 2007). Given early maturation, it is also consistent that this region demonstrates reduced FC in the presence of perinatal insults to the neuronal environment. Conversely, despite early maturation, we would not expect to simultaneous observe an effect of continuous HIV-infection and cumulative ART exposure, as half of our control group is perinatally exposed (Table 4). Thus, lack of between-group differences in this region for the ICA analysis investigating the effect of infection status (Sections 7.3.1, 8.3.1) is not surprising.

8.6 Vulnerability to HIV of functional connectivity in visual regions

It appears that disruption to within-network and between-network FC of visual cortex is a persisting or late-arising effect of perinatal and/or cumulative HIV/ART exposure. In addition to the ICA-revealed effect of exposure in the medial visual network (Section 8.5: 'HEU vs HU'), five of the 17 seed-based connections revealing HIV-related differences involved a seed or target cluster in the occipital lobe (Table 7, Table 9, Table 11), of which at least three were between-network connections. A further two connections involve a seed or cluster in the (right) angular gyrus (Table 7, Table 9), a region which integrates and perceives multimodal information, including visual; one involves a seed in the (left) superior parietal lobule (Table 7), which forms part of the dorsal ("where") visual stream; and one involves a cluster in the posterior portion of the intraparietal sulcus (Table 11), which receives input from both the dorsal and ventral visual streams (Clark et al. 2010c). As previously discussed (Section 8.3.2), visual perception deficits in perinatally HIV+ children have been described in the literature (Birn et al. 2006; Tardieu et al. 1995; Boivin et al. 1995; Diamond 1987) and in our own cohort (Laughton et al. 2017).

Our results come alongside an adult study suggesting predilection of HIV-effects for visual networks in early HIV infection (Wang et al. 2011), and a recent abstract finding that the lateral occipital network is one of three RSNs having spatial profiles significantly different from controls in perinatally infected HIV+ young adults (Sarma et al. 2017).

9 Limitations

The methods we employed to investigate our primary research questions impose limitations on the strength of the conclusions that we can draw from our results. Foremost, while we employed two-sided testing and controlled for multiple comparisons at the voxel level, we did not control for multiple testing across seeds (in SCA) or RSNs (in ICA). The largely exploratory approach adopted was in line with the project objectives (Section 0), and is perhaps suitable to a dissertation, but does require that apparently significant results be verified in follow-up studies.

Secondly, our discussion was based on results obtained at a cluster-forming threshold of $p < 0.005$. For completeness, we also included results at the more conservative threshold of $p < 0.001$, which were more limited in number, but not all null. Recently, there has been much controversy surrounding the severity of cluster-forming threshold that is required to produce (when combined with cluster-extent thresholds) an empirical FPR near to the nominal 5% FPR (Eklund et al. 2016). Nevertheless, a threshold of $p < 0.005$ shows adequate error rate control when using the mixed ACF[40] modelling recently implemented in AFNI (Cox et al. 2017), as we have done here.

Thirdly, since 75% of HIV+ children in our sample initiated treatment by 23 weeks of age, and all within 18 months of birth, we are not able to separate the effects of HIV-infection from the potential effects of ART such as neurotoxicity (Robertson et al. 2012) or abnormal metabolism (Vigano et al. 2010). Furthermore, the fact that half of the infected subjects had a non-zero period of treatment interruption (median of 41 weeks) may have had an impact on some of our results. However, we have reason to believe that this impact is limited. For the analyses investigating the effect of immune health at enrolment (before allocation to treatment arm), or perinatal exposure to HIV/ART, we of course expect no effect. In analysing the effect of timing of treatment initiation, we employed models (Section 6.5.1) that should largely eliminate confounding effects of treatment interruption. What

[40] Autocorrelation function.

remains are the analyses investigating the effect of current immune health, and those comparing the HIV-infected/ART and HIV-uninfected groups.

With the former analysis, the only confounding effect could be that which is not mediated by current immune health (or virologic status, since all but one had a supressed viral load): that is, either persisting effects of historical viremia/immunosuppression, or variance in ART-mediated neurotoxicity. However, a parallel study among the same cohort found that effects of treatment interruption on neurodevelopmental outcomes had largely resolved by age 5 years (Laughton et al. 2017). With the latter analysis (HIV-infected vs HIV-uninfected), the principal problem of treatment interruption is that it frustrates attempts to differentiate the effects of HIV-infection and ART-mediated neurotoxicity. But with regards the group difference, we expect little confounding, since the weight of the literature indicates that HIV-infection has a larger effect on brain development than ART-mediated neurotoxicity, and so the portion of the treatment interruption effect that is not mediated by HIV processes (namely, treatment toxicity) should be comparatively small.

Fourthly, our control sample was limited in size (12 HEU and 12 HU children), to some extent reducing statistical power for investigating HIV-related effects, but most especially reducing power for investigating the effect of perinatal exposure (to HIV/ART) among uninfected children. However, these two investigations are not independent. Where both perinatal exposure and cumulative exposure to HIV/ART impact the same functional connections with the same directionality, the ability to detect significant effects of HIV-infection with reference to a partially-exposed uninfected group, is reduced (as we have briefly suggested in Section 8.5). Where the directionality is opposite, effects of HIV-infection may be exaggerated. A larger control group, facilitating appropriately powered comparisons between unexposed uninfected (HU) and exposed uninfected (HEU) children, or equivalently, comparisons between HIV+ and uninfected children stratified on exposure in the control group, are needed to more carefully interpret our results.

Fifthly, while HIV+ and uninfected children were initially (in infancy) recruited from the same isiXhosa community, current socioeconomic variables and other environmental and biological factors were not considered in the present analysis (these measures were largely unavailable). The neuropsychological literature indicates that consideration of such factors, while complex, would be invaluable. For example, it has been suggested that poor behavioural outcomes may be partially misattributed to HIV-infection, since stressors such as exposure to poverty or trauma, familial mental illness, and ongoing parental drug use can together be more predictive than infection status (Mellins et al. 2003). Further, neurodevelopmental delays associated with HIV-infection and exposure appear to be exacerbated in resource-poor settings (Le Doare et al. 2012).

Sixthly, our group RSN templates were acquired by inputting the whole sample's data (both HIV+ and uninfected children) into group ICA (MELODIC), rather than inputting just that of the uninfected subsample. Inputting the whole sample's data produced a markedly more robust ICA decomposition, with fewer noise-indicative spatial features and more components corresponding to standard RSNs. However, had we adopted the latter approach, we may have had more power to detect HIV-related intra-network FC differences in the subject-specific maps subsequently acquired by dual regression (at the cost of a smaller set of non-artefactual components within which to perform analyses).

Finally, our analysis was restricted to measures of a single imaging modality, though results were cross-referenced with other modalities employed in the literature. The striking convergence of structural and functional connectivity (Damoiseaux & Greicius 2009) suggests that pipelines simultaneously leveraging rs-fMRI and DTI measures may detect HIV-related abnormalities with greater sensitivity and specificity. Our group is currently exploring such methods.

10 Conclusion

Despite early ART and early virologic suppression, vertically infected HIV+ children demonstrate instances of abnormal FC at age 9 years compared to age-matched controls. We found no HIV-related differences in functional integration into ICA-generated RSNs, perhaps as a result of within-network FC not being sufficiently robust at this age. However, in a seed-based correlation analysis, seeds placed in the structural core (Hagmann et al. 2008), in regions implicated in HIV-related between-group differences at age 7 years (Toich et al. 2017), and in regions associated with neuropsychological domains (planning, visual perception) impaired in our cohort, had connections demonstrating greater FC in HIV+ compared to uninfected children. These were all likely between-network connections. This may indicate neurodevelopmental delay, since the strength of between-network influences decreases towards adulthood, while within-network integration increases. That none of the connections found to have reduced FC in HIV+ compared to uninfected children at age 7 years were again implicated at age 9 years, suggests that observed neurobiological abnormalities point to delayed maturation of RSNs rather than permanent disruption.

In addition, we found that poorer immune health, both current and in infancy, was associated with lowered functional integration of lobule 7 into the cerebellum network at age 9 years. In agreement with a large body of literature in the post-ART era, this signifies that immunocompromise in early stages of childhood can have longstanding effects despite later effective management of immune health and viral load. Earlier treatment was not associated with FC outcomes at age 9 years, though this result may be confounded by a limited range of treatment timing (all subjects initiated ART before 18 months) and a subset of subjects having their treatment interrupted (for varying periods).

We observed a predilection of the effects of perinatal and/or cumulative HIV/ART exposure for regions associated with visual function. Visual perception and visual recognition memory have been found to be susceptible to HIV in children, and the vulnerability of visual RSNs in recently-infected adults and perinatally infected young adults has been recently described.

The neurobiological alterations described here may contribute to cognitive problems in HIV+ youth and require further investigation. Particularly, directly investigating correlations of FC with neuropsychological measures in HIV+ children could shed light on the cognitive significance of particular HIV-related FC abnormalities. While the cross-sectional analysis conducted here at age 9 years (and previously at age 7 years) allows us to investigate age-parameterised effects of HIV and or ART, a multimodal longitudinal analysis will be informative for examining hypotheses of neurodevelopmental delay.

Works cited

Ackermann, C. et al., 2016. Early antiretroviral therapy in HIV-infected children is associated with diffuse white matter structural abnormality and corpus callosum sparing. In *American Journal of Neuroradiology*. American Journal of Neuroradiology, pp. 2363–2369. Available at: http://www.ncbi.nlm.nih.gov/pubmed/27538904 [Accessed September 28, 2017].

Ackermann, C. et al., 2014. White matter signal abnormalities in children with suspected HIV-related neurologic disease on early combination antiretroviral therapy. *The Pediatric infectious disease journal*, 33(8), pp.e207-12. Available at: http://www.ncbi.nlm.nih.gov/pubmed/24595047 [Accessed July 18, 2016].

Akay, C. et al., 2014. Antiretroviral drugs induce oxidative stress and neuronal damage in the central nervous system. *Journal of NeuroVirology*, 20(1), pp.39–53. Available at: http://link.springer.com/10.1007/s13365-013-0227-1 [Accessed June 30, 2018].

Allen, E.A. et al., 2011. A baseline for the multivariate comparison of resting-state networks. *Frontiers in systems neuroscience*, 5(February), p.2. Available at: http://www.ncbi.nlm.nih.gov/pubmed/21442040 [Accessed August 21, 2017].

Allen, E.A. et al., 2014. Tracking whole-brain connectivity dynamics in the resting state. *Cerebral Cortex*, 24(3), pp.663–676. Available at: https://oup.silverchair-cdn.com/oup/backfile/Content_public/Journal/cercor/24/3/10.1093_cercor_bhs352/1/bhs352.pdf?Expires=1509626071&Signature=CMt7JQqu5tfuXmSmIohdqhZVcJXqWITpIEoJ7nkgB~3K~G~gcY0S~32br9KcgYtUAiSIfYEoSIGAb3hEfN1HAbvk9oit8IYsxNpqUwFqteEQmrV [Accessed November 1, 2017].

Anastos, K. et al., 2002. Risk of progression to aids and death in women infected with hiv-1 initiating highly active antiretroviral treatment at different stages of disease. *Archives of Internal Medicine*, 162(17), pp.1973–1980. Available at: +.

Andrews-Hanna, J.R., Reidler, J.S., Huang, C., et al., 2010. Evidence for the default network's role in spontaneous cognition. *Journal of neurophysiology*, 104(1), pp.322–35. Available at: http://www.pubmedcentral.nih.gov/articlerender.fcgi?artid=2904225&tool=pmcentrez&rendertype=abstract.

Andrews-Hanna, J.R., Reidler, J.S., Sepulcre, J., et al., 2010. Functional-Anatomic Fractionation of the Brain's Default Network. *Neuron*, 65(4), pp.550–562. Available at: http://ac.els-cdn.com/S0896627310000966/1-s2.0-S0896627310000966-main.pdf?_tid=18259c06-8651-11e7-ada6-00000aab0f02&acdnat=1503307031_2a42968921ed8cbdd30bc6aad01bc4f9 [Accessed August 21, 2017].

Andronikou, S. et al., 2014. Correlating brain volume and callosal thickness with clinical and laboratory indicators of disease severity in children with HIV-related brain disease. *Child's Nervous System*, 30(9), pp.1549–1557. Available at: https://doi.org/10.1007/s00381-014-2434-3.

Ann, H.W. et al., 2016. Characteristics of Resting-State Functional Connectivity in HIV-Associated Neurocognitive Disorder. *Plos One*, 11(4), p.e0153493. Available at: http://dx.plos.org/10.1371/journal.pone.0153493 [Accessed June 16, 2016].

Anthony, K.B. et al., 2003. Incomplete CD4 T cell recovery in HIV-1 infection after 12 months of highly active antiretroviral therapy is associated with ongoing increased CD4 T cell activation

and turnover. *J Acquir Immune Defic Syndr*, 33(2), pp.125–133. Available at: http://www.ncbi.nlm.nih.gov/pubmed/12794543.

Van Arnhem, L.A. et al., 2013. Neurologic Abnormalities in HIV-1 Infected Children in the Era of Combination Antiretroviral Therapy S. J. Buch, ed. *PLoS ONE*, 8(5), p.e64398. Available at: http://dx.plos.org/10.1371/journal.pone.0064398 [Accessed June 13, 2016].

Arthurs, O.J. et al., 2000. Linear coupling between functional magnetic resonance imaging and evoked potential amplitude in human somatosensory cortex. *Neuroscience*, 101(4), pp.803–806.

Arthurs, O.J. & Boniface, S., 2002. How well do we understand the neural origins of the fMRI BOLD signal? *Trends in Neurosciences*, 25(1), pp.27–31.

Astafiev, S. V et al., 2003. Functional organization of human intraparietal and frontal cortex for attending, looking, and pointing. *The Journal of neuroscience : the official journal of the Society for Neuroscience*, 23(11), pp.4689–99. Available at: http://www.ncbi.nlm.nih.gov/pubmed/12805308 [Accessed November 6, 2017].

Attwell, D. & Iadecola, C., 2002. The neural basis of functional brain imaging signals. *Trends in Neurosciences*, 25(12), pp.621–625. Available at: http://www.sciencedirect.com/science/article/pii/S0166223602022646.

Austin, P.C. & Steyerberg, E.W., 2015. The number of subjects per variable required in linear regression analyses. *Journal of Clinical Epidemiology*, 68(6), pp.627–636. Available at: http://linkinghub.elsevier.com/retrieve/pii/S0895435615000141 [Accessed March 6, 2017].

Badri, M., Lawn, S.D. & Wood, R., 2006. Short-term risk of AIDS or death in people infected with HIV-1 before antiretroviral therapy in South Africa: a longitudinal study. *The Lancet*, 368(9543), pp.1254–1259. Available at: http://www.sciencedirect.com/science/article/pii/S0140673606691174.

Banks, W.A., Ercal, N. & Otamis Price, T., 2006. The Blood-Brain Barrier in NeuroAIDS. *Current HIV Research*, 4, pp.0–0. Available at: https://pdfs.semanticscholar.org/4493/75789b2ff65ba96233a8ec006fe5fd6a6cea.pdf [Accessed November 21, 2017].

Barber, A.D. et al., 2013. Developmental changes in within- and between-network connectivity between late childhood and adulthood. *Neuropsychologia*, 51(1), pp.156–167. Available at: https://ac.els-cdn.com/S0028393212004782/1-s2.0-S0028393212004782-main.pdf?_tid=d9803288-b27c-11e7-9a77-00000aab0f26&acdnat=1508163675_45afbbb403808ab81c6dfd3fde10f1a5 [Accessed October 16, 2017].

Beckmann et al., 2009. Group comparison of resting-state FMRI data using multi-subject ICA and dual regression. *NeuroImage*, 47(Suppl 1), p.S148. Available at: http://web.mit.edu/fsl_v5.0.8/fsl/doc/wiki/attachments/DualRegression/CB09.pdf [Accessed July 18, 2016].

Beckmann, C.F. et al., 2005. Investigations into resting-state connectivity using independent component analysis. *Philosophical transactions of the Royal Society of London. Series B, Biological sciences*, 360(1457), pp.1001–13. Available at: http://www.ncbi.nlm.nih.gov/pubmed/16087444 [Accessed December 4, 2016].

Beckmann, C.F. & Smith, S.M., 2004. Probabilistic Independent Component Analysis for Functional Magnetic Resonance Imaging. *IEEE Transactions on Medical Imaging*, 23(2), pp.137–152.

Available at: http://ieeexplore.ieee.org/lpdocs/epic03/wrapper.htm?arnumber=1263605 [Accessed July 29, 2016].

Bennett, D.E. et al., 2006. The World Health Organization ' s global strategy for prevention and assessment of HIV drug resistance , Geneva, Switzerland. *Antiviral Therapy 13 Suppl 2:1–13*, pp.1–13. Available at: http://www.who.int/hiv/pub/toolkits/WHO_HIVDR_strategy.pdf [Accessed November 14, 2017].

Bhattacharyya, P.K. & Lowe, M.J., 2004. Cardiac-induced physiologic noise in tissue is a direct observation of cardiac-induced fluctuations. *Magnetic Resonance Imaging*, 22(1), pp.9–13. Available at: http://www.sciencedirect.com/science/article/pii/S0730725X03003102?via%3Dihub [Accessed November 9, 2017].

Bianciardi, M. et al., 2009. Sources of functional magnetic resonance imaging signal fluctuations in the human brain at rest: a 7 T study. *Magnetic Resonance Imaging*, 27(8), pp.1019–1029. Available at: https://ac.els-cdn.com/S0730725X09000599/1-s2.0-S0730725X09000599-main.pdf?_tid=4d6193a8-c51b-11e7-97b6-00000aacb35d&acdnat=1510210852_f53b3e3498be34c9458ce2b958109771 [Accessed November 9, 2017].

De Bie, H.M.A. et al., 2012. Resting-state networks in awake five- to eight-year old children. *Human Brain Mapping*, 33(5), pp.1189–1201. Available at: http://onlinelibrary.wiley.com/doi/10.1002/hbm.21280/full [Accessed June 5, 2017].

Birn, R.M. et al., 2006. Separating respiratory-variation-related fluctuations from neuronal-activity-related fluctuations in fMRI. *NeuroImage*, 31(4), pp.1536–1548. Available at: http://www.sciencedirect.com/science/article/pii/S1053811906001248 [Accessed February 11, 2016].

Biswal, B. et al., 1995. Functional connectivity in the motor cortex of resting human brain using echo-planar MRI. *Magnetic Resonance in Medicine*, 34(4), pp.537–541.

Biswal, B.B. et al., 2010. Toward discovery science of human brain function. Supporting Information. *Proceedings of the National Academy of Sciences of the United States of America*, 107(10), pp.4734–9. Available at: http://www.pnas.org/cgi/doi/10.1073/pnas.0911855107 [Accessed July 5, 2016].

Blakemore, S.J. & Choudhury, S., 2006. Development of the adolescent brain: Implications for executive function and social cognition. *Journal of Child Psychology and Psychiatry and Allied Disciplines*, 47(3–4), pp.296–312. Available at: http://doi.wiley.com/10.1111/j.1469-7610.2006.01611.x [Accessed April 4, 2017].

Blumberg, B.M., Gelbard, H.A. & Epstein, L.G., 1994. HIV-1 infection of the developing nervous system: central role of astrocytes in pathogenesis. *Virus Research*, 32(2), pp.253–267. Available at: http://www.sciencedirect.com/science/article/pii/0168170294900442.

Boivin, M.J. et al., 1995. A preliminary evaluation of the cognitive and motor effects of pediatric HIV infection in Zairian children. *Health psychology : official journal of the Division of Health Psychology, American Psychological Association*, 14(1), pp.13–21. Available at: http://content.ebscohost.com/ContentServer.asp?T=P&P=AN&K=1995-18127-001&S=L&D=pdh&EbscoContent=dGJyMNLe80Sep7c4zdnyOLCmr0%2BeprNSr6i4TbaWxWXS&ContentCustomer=dGJyMPPZ8oTn2LmF39%2FsU%2BPe7Yvy [Accessed October 19, 2017].

Bourgeois, J.P. & Rakic, P., 1993. Changes of synaptic density in the primary visual cortex of the macaque monkey from fetal to adult stage. *The Journal of neuroscience : the official journal of*

the Society for Neuroscience, 13(7), pp.2801–2820. Available at: http://www.jneurosci.org/content/jneuro/13/7/2801.full.pdf [Accessed October 12, 2017].

Braver, T.S. et al., 1997. A Parametric Study of Prefrontal Cortex Involvement in Human Working Memory. *NeuroImage*, 5(1), pp.49–62. Available at: https://ac.els-cdn.com/S1053811996902475/1-s2.0-S1053811996902475-main.pdf?_tid=7a2ed6c0-b4d1-11e7-8a97-00000aacb35f&acdnat=1508419925_6106376383f6383eae068b26c1b60a5c [Accessed October 19, 2017].

Bressler, S.L. et al., 2008. Top-Down Control of Human Visual Cortex by Frontal and Parietal Cortex in Anticipatory Visual Spatial Attention. *Journal of Neuroscience*, 28(40), pp.10056–10061. Available at: http://www.ncbi.nlm.nih.gov/pubmed/18829963 [Accessed October 25, 2017].

Brinkman, K. et al., 1998. Adverse effects of reverse transcriptase inhibitors: mitochondrial toxicity as common pathway. *AIDS (London, England)*, 12(May), pp.1735–1744.

Buxton, R.B., 2009. Relaxation and Contrast in MRI. In *Introduction to Functional Magnetic Resonance Imaging: Principles and Techniques*. Cambridge University Press, pp. 147–172. Available at: https://books.google.co.za/books?hl=en&lr=&id=vqkgAwAAQBAJ&oi=fnd&pg=PP8&dq=Introduction+to+functional+magnetic+resonance+imaging+principles+and+techniques+Buxton&ots=4pfmtbTTl8&sig=jgXSn9J7OMWAYZJHOpjLeMo0gPU [Accessed August 6, 2016].

Calhoun, V.D., Kiehl, K.A. & Pearlson, G.D., 2008. Modulation of temporally coherent brain networks estimated using ICA at rest and during cognitive tasks. *Human Brain Mapping*, 29(7), pp.828–838. Available at: http://doi.wiley.com/10.1002/hbm.20581 [Accessed August 22, 2017].

Calhoun, V.D., Liu, J. & Adali, T., 2009. A review of group ICA for fMRI data and ICA for joint inference of imaging, genetic, and ERP data. *NeuroImage*, 45(1 Suppl), pp.S163-72. Available at: http://www.ncbi.nlm.nih.gov/pubmed/19059344 [Accessed July 5, 2016].

Canestri, A. et al., 2010. Discordance Between Cerebral Spinal Fluid and Plasma HIV Replication in Patients with Neurological Symptoms Who Are Receiving Suppressive Antiretroviral Therapy. *Clinical Infectious Diseases*, 50(5), pp.773–778. Available at: https://academic.oup.com/cid/article-lookup/doi/10.1086/650538 [Accessed December 2, 2017].

Caniglia, E.C. et al., 2014. Antiretroviral penetration into the CNS and incidence of AIDS-defining neurologic conditions. *Neurology*, 83(2), pp.134–141. Available at: http://www.neurology.org/content/83/2/134.abstract.

Carpenter, P. a, Just, M. a & Reichle, E.D., 2000. Working memory and executive function: evidence from neuroimaging. *Current opinion in neurobiology*, 10(2), pp.195–199.

Carvalhal, A. et al., 2016. Central nervous system penetration effectiveness of antiretroviral drugs and neuropsychological impairment in the Ontario HIV Treatment Network Cohort Study. *Journal of NeuroVirology*, 22(3), pp.349–357. Available at: https://doi.org/10.1007/s13365-015-0404-5.

Cauli, B. et al., 2004. Cortical GABA Interneurons in Neurovascular Coupling: Relays for Subcortical Vasoactive Pathways. *Journal of Neuroscience*, 24(41), pp.8940–8949. Available at: http://www.jneurosci.org/content/24/41/8940.

Chan, R.C.K. et al., 2008. Assessment of executive functions: Review of instruments and identification of critical issues. *Archives of Clinical Neuropsychology*, 23(2), pp.201–216. Available at: http://www.sciencedirect.com/science/article/pii/S0887617707001928 [Accessed

October 17, 2017].

Chang, L. et al., 2004. Adaptation of the attention network in human immunodeficiency virus brain injury. *Annals of Neurology*, 56(2), pp.259–272.

Chang, L. et al., 2001. Neural correlates of attention and working memory deficits in HIV patients. *Neurology*, 57(6), pp.1001–1007. Available at: http://www.neurology.org/cgi/doi/10.1212/WNL.57.6.1001 [Accessed June 13, 2017].

Chen, B.R. et al., 2014. A Critical Role for the Vascular Endothelium in Functional Neurovascular Coupling in the Brain. *Journal of the American Heart Association*, 3(3). Available at: http://jaha.ahajournals.org/content/3/3/e000787.

Chen, B.R. et al., 2011. High-speed vascular dynamics of the hemodynamic response. *NeuroImage*, 54(2), pp.1021–1030. Available at: http://www.sciencedirect.com/science/article/pii/S1053811910012176.

Chen, S. et al., 2008. Group independent component analysis reveals consistent resting-state networks across multiple sessions. *Brain Research*, 1239, pp.141–151. Available at: http://www.ncbi.nlm.nih.gov/pubmed/18789314 [Accessed November 10, 2017].

Chiappini, E. et al., 2009. Five-year follow-up of children with perinatal HIV-1 infection receiving early highly active antiretroviral therapy. *BMC infectious diseases*, 9, p.140. Available at: http://www.ncbi.nlm.nih.gov/pubmed/19709432 [Accessed November 22, 2017].

Chiriboga, C.A. et al., 2005. Incidence and prevalence of HIV encephalopathy in children with HIV infection receiving highly active anti-retroviral therapy (HAART). *The Journal of pediatrics*, 146(3), pp.402–407. Available at: https://ac.els-cdn.com/S002234760400959X/1-s2.0-S002234760400959X-main.pdf?_tid=1f987dae-cec8-11e7-af9c-00000aab0f01&acdnat=1511274638_3cadb18aa9ed1a7b65029a88431d8f64 [Accessed November 21, 2017].

CHIVA, 2017. *Standards of Care for Infants, Children, and Young People with HIV*, Available at: https://www.chiva.org.uk/files/8015/0642/1695/CHIVA_STANDARDS_2017.pdf.

Chumbley, J.R. & Friston, K.J., 2009. False discovery rate revisited: FDR and topological inference using Gaussian random fields. *NeuroImage*, 44(1), pp.62–70. Available at: http://ac.els-cdn.com/S1053811908006472/1-s2.0-S1053811908006472-main.pdf?_tid=58b753f0-7769-11e7-b46c-00000aab0f02&acdnat=1501668180_ae8afa2eddaace9201243752859fda0f [Accessed August 2, 2017].

Churchill, M. & Nath, A., 2013. Where does HIV hide? A focus on the central nervous system. *Current opinion in HIV and AIDS*, 8(3), pp.165–9. Available at: http://www.ncbi.nlm.nih.gov/pubmed/23429501.

Ciesielski, K.T. et al., 1997. Cerebellar hypoplasia and frontal lobe cognitive deficits in disorders of early childhood. *Neuropsychologia*, 35(5), pp.643–655. Available at: https://ac.els-cdn.com/S0028393296001194/1-s2.0-S0028393296001194-main.pdf?_tid=5202239a-ae79-11e7-8736-00000aab0f27&acdnat=1507722355_954c7e8b26ff43cc63939220b2f9933b [Accessed October 11, 2017].

Ciesielski, K.T. & Knight, J.E., 1994. Cerebellar abnormality in autism: A nonspecific effect of early brain damage? *Acta Neurobiologiae Experimentalis*, 54(2), pp.151–154. Available at: http://www.hurri.ane.pl/pdf/5418.pdf [Accessed October 11, 2017].

Clark, D.L., Boutros, N.N. & Mendez, M.F., 2010a. Frontal lobe. In *The brain and behavior: an introduction to behavioral neuroanatomy*. Cambridge University Press, pp. 84–121.

Clark, D.L., Boutros, N.N. & Mendez, M.F., 2010b. Gross anatomy of the brain. In *The brain and behavior: an introduction to behavioral neuroanatomy*. Cambridge University Press, pp. 4–13.

Clark, D.L., Boutros, N.N. & Mendez, M.F., 2010c. Occipital and parietal lobes. In *The brain and behavior: an introduction to behavioral neuroanatomy*. Cambridge University Press, pp. 33–58.

Condon, B. et al., 1987. MR relaxation times of cerebrospinal fluid. *Journal of computer assisted tomography*, 11(2), p.203. Available at: http://www.ncbi.nlm.nih.gov/pubmed/3819116 [Accessed August 5, 2016].

Cooper, D.A. et al., 1988. Characterization of T lymphocyte responses during primary infection with human immunodeficiency virus. *J Infect Dis*, 157. Available at: https://doi.org/10.1093/infdis/157.5.889.

Cooper, E.R. et al., 1998. Encephalopathy and progression of human immunodeficiency virus disease in a cohort of children with perinatally acquired human immunodeficiency virus infection. *The Journal of Pediatrics*, 132(5), pp.808–812. Available at: http://www.sciencedirect.com/science/article/pii/S0022347698703087.

Corbetta, M., 2012. Functional connectivity and neurological recovery. *Developmental Psychobiology*, 54(3), pp.239–253. Available at: http://doi.wiley.com/10.1002/dev.20507 [Accessed November 13, 2017].

Corbetta, M. et al., 2000. Voluntary orienting is dissociated from target detection in human posterior parietal cortex. *Nature neuroscience*, 3(3), pp.292–7. Available at: http://www.nature.com/doifinder/10.1038/73009 [Accessed November 6, 2017].

Corbetta, M., Patel, G. & Shulman, G.L., 2008. The Reorienting System of the Human Brain: From Environment to Theory of Mind. *Neuron*, 58(3), pp.306–324. Available at: http://www.ncbi.nlm.nih.gov/pubmed/18466742 [Accessed November 5, 2017].

Cordes, D. et al., 2000. Mapping functionally related regions of brain with functional connectivity MR imaging. *American Journal of Neuroradiology*, 21(9), pp.1636–1644. Available at: http://www.ncbi.nlm.nih.gov/pubmed/11039342 [Accessed November 6, 2017].

La Corte, V. et al., 2016. Cognitive decline and reorganization of functional connectivity in healthy aging: The pivotal role of the salience network in the prediction of age and cognitive performances. *Frontiers in Aging Neuroscience*, 8(AUG), p.204. Available at: http://journal.frontiersin.org/Article/10.3389/fnagi.2016.00204/abstract [Accessed November 10, 2017].

Cotton, M.F. et al., 2013. Early time-limited antiretroviral therapy versus deferred therapy in South African infants infected with HIV: Results from the children with HIV early antiretroviral (CHER) randomised trial. *The Lancet*, 382(9904), pp.1555–1563.

Cox, R.W., 1996. AFNI: Software for Analysis and Visualization of Functional Magnetic Resonance Neuroimages. *Computers and Biomedical Research*, 29(3), pp.162–173. Available at: http://linkinghub.elsevier.com/retrieve/pii/S0010480996900142 [Accessed July 4, 2016].

Cox, R.W. et al., 2017. FMRI Clustering in AFNI: False-Positive Rates Redux. *Brain Connectivity*, 7(3), pp.152–171. Available at: http://online.liebertpub.com/doi/pdf/10.1089/brain.2016.0475 [Accessed August 1, 2017].

Cox, R.W. & Jesmanowicz, A., 1999. Real-time 3D image registration for functional MRI. *Magnetic Resonance in Medicine*, 42(6), pp.1014–1018. Available at: http://doi.wiley.com/10.1002/%28SICI%291522-2594%28199912%2942%3A6%3C1014%3A%3AAID-MRM4%3E3.0.CO%3B2-F [Accessed August

8, 2016].

Crinion, J. et al., 2007. Spatial normalization of lesioned brains: Performance evaluation and impact on fMRI analyses. *NeuroImage*, 37(3), pp.866–875.

Cysique, L.A. & Brew, B.J., 2011. Prevalence of non-confounded HIV-associated neurocognitive impairment in the context of plasma HIV RNA suppression. *Journal of NeuroVirology*, 17(2), pp.176–183. Available at: http://link.springer.com/10.1007/s13365-011-0021-x [Accessed October 30, 2017].

Dabis, F. & Ekpini, E.R., 2002. HIV-1/AIDS and maternal and child health in Africa. *Lancet*, 359(9323), pp.2097–2104. Available at: http://www.sciencedirect.com/science/article/pii/S0140673602089092 [Accessed November 13, 2017].

Dalakas, M.C., Semino-Mora, C. & Leon-Monzon, M., 2001. Mitochondrial Alterations with Mitochondrial DNA Depletion in the Nerves of AIDS Patients with Peripheral Neuropathy Induced by 2'3'-Dideoxycytidine (ddC). *Laboratory Investigation*, 81, p.1537. Available at: http://dx.doi.org/10.1038/labinvest.3780367.

Damoiseaux, J.S. et al., 2006. Consistent resting-state networks across healthy subjects. *Proceedings of the National Academy of Sciences of the United States of America*, 103(37), pp.13848–53. Available at: http://www.ncbi.nlm.nih.gov/pubmed/16945915 [Accessed August 22, 2017].

Damoiseaux, J.S. & Greicius, M.D., 2009. Greater than the sum of its parts: a review of studies combining structural connectivity and resting-state functional connectivity. *Brain Structure and Function*, 213(6), pp.525–33. Available at: https://link-springer-com.ezproxy.uct.ac.za/content/pdf/10.1007%2Fs00429-009-0208-6.pdf [Accessed October 22, 2017].

Davey, C.E. et al., 2013. Filtering induces correlation in fMRI resting state data. *NeuroImage*, 64(1), pp.728–740.

Davey, R.T. et al., 1999. HIV-1 and T cell dynamics after interruption of highly active antiretroviral therapy (HAART) in patients with a history of sustained viral suppression. *Proceedings of the National Academy of Sciences*, 96(26), pp.15109–15114. Available at: http://www.pnas.org/content/96/26/15109.abstract.

Depas, G. et al., 1995. Functional brain imaging in HIV-1-infected children born to seropositive mothers. *Journal of nuclear medicine : official publication, Society of Nuclear Medicine*, 36(12), pp.2169–2174. Available at: http://www.ncbi.nlm.nih.gov/pubmed/8523099 [Accessed July 18, 2016].

Desimone, R. & Duncan, J., 1995. Neural Mechanisms of Selective Visual Attention. *Annual Review of Neuroscience*, 18(1), pp.193–222. Available at: http://www.annualreviews.org/doi/10.1146/annurev.ne.18.030195.001205 [Accessed November 6, 2017].

Diamond, G.W., 1987. Characterization of Cognitive Functioning HIV Infection in a Subgroup of Children with Congenital. *Archives of Clinical Neuropsychology*, 2(3), pp.245–256. Available at: https://academic.oup.com/acn/article-lookup/doi/10.1093/arclin/2.3.245 [Accessed October 19, 2017].

Didier, N. et al., 2002. HIV-1-induced production of endothelin-1 in an in vitro model of the human blood–brain barrier. *NeuroReport*, 13(9). Available at: http://journals.lww.com/neuroreport/Fulltext/2002/07020/HIV_1_induced_production_of_en

dothelin_1_in_an_in.22.aspx.

Van Dijk, K.R.A., Sabuncu, M.R. & Buckner, R.L., 2012. The influence of head motion on intrinsic functional connectivity MRI. *NeuroImage*, 59(1), pp.431–438.

Diniz, L.M.O. et al., 2011. Impact of HAART on growth and hospitalization rates among HIV-infected children. *Jornal de Pediatria*, 87(2), pp.131–137. Available at: http://jped.com.br/conteudo/Ing_resumo.asp?varArtigo=2167&cod=&idSecao=1.

Divi, R.L. et al., 2010. Progressive mitochondrial compromise in brains and livers of primates exposed in utero to nucleoside reverse transcriptase inhibitors (NRTIs). *Toxicological Sciences*, 118(1), pp.191–201. Available at: http://www.ncbi.nlm.nih.gov/pubmed/20702595 [Accessed July 3, 2018].

Le Doare, K., Bland, R. & Newell, M.-L., 2012. Neurodevelopment in Children Born to HIV-Infected Mothers by Infection and Treatment Status. *PEDIATRICS*, 130(5), pp.e1326–e1344. Available at: http://www.ncbi.nlm.nih.gov/pubmed/23118140 [Accessed October 19, 2017].

Donald, K.A. et al., 2015. HIV Encephalopathy: pediatric case series description and insights from the clinic coalface. *AIDS Research and Therapy*, 12(1), p.2. Available at: http://www.aidsrestherapy.com/content/12/1/2 [Accessed July 18, 2016].

Dosenbach, N.U.F. et al., 2007. Distinct brain networks for adaptive and stable task control in humans. *Proceedings of the National Academy of Sciences of the United States of America*, 104(26), pp.11073–8. Available at: http://www.ncbi.nlm.nih.gov/pubmed/17576922 [Accessed August 23, 2017].

Doucet, G. et al., 2011. Brain activity at rest: a multiscale hierarchical functional organization. *Journal of Neurophysiology*, 105(6), pp.2753–2763. Available at: http://jn.physiology.org/content/jn/105/6/2753.full.pdf [Accessed November 1, 2017].

Dubois, J. et al., 2014. The early development of brain white matter: A review of imaging studies in fetuses, newborns and infants. *Neuroscience*, 276, pp.48–71.

Durston, S. et al., 2006. A shift from diffuse to focal cortical activity with development: Commentary. *Developmental Science*, 9(1), pp.1–20. Available at: http://doi.wiley.com/10.1111/j.1467-7687.2005.00454.x [Accessed October 19, 2017].

Edén, A. et al., 2010. HIV-1 Viral Escape in Cerebrospinal Fluid of Subjects on Suppressive Antiretroviral Treatment. *The Journal of Infectious Diseases*, 202(12), pp.1819–1825. Available at: +.

Egger, M. et al., 2002. Prognosis of HIV-1-infected patients starting highly active antiretroviral therapy: a collaborative analysis of prospective studies. *The Lancet*, 360(9327), pp.119–129. Available at: http://www.sciencedirect.com/science/article/pii/S0140673602094114.

Eisenhut, M., 2013. An update on HIV in children. *Paediatrics and Child Health (United Kingdom)*, 23(3), pp.109–114. Available at: http://dx.doi.org/10.1016/j.paed.2012.06.003.

Eisfeld, C. et al., 2013. CSF Penetration by Antiretroviral Drugs. *CNS Drugs*, 27(1), pp.31–55. Available at: https://doi.org/10.1007/s40263-012-0018-x.

Eklund, A., Nichols, T.E. & Knutsson, H., 2016. Cluster failure: Why fMRI inferences for spatial extent have inflated false-positive rates. *Proceedings of the National Academy of Sciences of the United States of America*, 113(28), pp.7900–5. Available at: http://www.ncbi.nlm.nih.gov/pubmed/27357684 [Accessed February 13, 2017].

Ellis, R.J. et al., 2000. Cerebrospinal fluid HIV RNA originates from both local CNS and systemic

sources. *Neurology*, 54(4), pp.927–936. Available at: http://n.neurology.org/content/54/4/927.

Epstein, L.G. et al., 1986. Neurologic Manifestations of Human Immunodeficiency Virus Infection in Children. *Pediatrics*, 78(4), pp.678–687. Available at: http://pediatrics.aappublications.org/content/78/4/678.

Ernst, T. et al., 2002. Abnormal brain activation on functional MRI in cognitively asymptomatic HIV patients. *Neurology*, 59(9), pp.1343–1349. Available at: http://www.neurology.org/cgi/doi/10.1212/01.WNL.0000031811.45569.B0 [Accessed June 16, 2016].

Ewings, E.L. et al., 2000. Genotoxic and functional consequences of transplacental zidovudine exposure in fetal monkey brain mitochondria. *J Acquir Immune Defic Syndr*, 24(2), pp.100–105. Available at: http://www.ncbi.nlm.nih.gov/pubmed/10935684 [Accessed July 14, 2018].

Fair, D.A. et al., 2009. Functional brain networks develop from a "local to distributed" organization. *PLoS Computational Biology*, 5(5), p.e1000381. Available at: http://www.ncbi.nlm.nih.gov/pubmed/19412534 [Accessed July 8, 2016].

Farrant, K. & Uddin, L.Q., 2015. Asymmetric development of dorsal and ventral attention networks in the human brain. *Developmental Cognitive Neuroscience*, 12, pp.165–174. Available at: http://www.sciencedirect.com/science/article/pii/S1878929315000262 [Accessed June 2, 2017].

Filippi, C.G. et al., 2001. Diffusion Tensor Imaging of Patients with HIV and Normal-appearing White Matter on MR Images of the Brain. *American Journal of Neuroradiology*, 22(2), pp.277–283. Available at: http://www.ajnr.org/content/22/2/277.

Filippini, N. et al., 2009. Distinct patterns of brain activity in young carriers of the APOE-epsilon4 allele. *Pnas*, 106(17), pp.7209–7214. Available at: http://www.ncbi.nlm.nih.gov/pubmed/19357304 [Accessed December 8, 2016].

Finn, E.S. et al., 2015. Functional connectome fingerprinting: identifying individuals using patterns of brain connectivity. *Nature Neuroscience*, 18(11), pp.1664–1671. Available at: http://www.nature.com/doifinder/10.1038/nn.4135 [Accessed November 10, 2017].

Finzi, D. et al., 1999. Latent infection of CD4+ T cells provides a mechanism for lifelong persistence of HIV-1, even in patients on effective combination therapy. *Nature Medicine*, 5, p.512. Available at: http://dx.doi.org/10.1038/8394.

Fischl, B., Sereno, M.I. & Dale, A.M., 1999. Cortical surface-based analysis. II: Inflation, flattening, and a surface-based coordinate system. *Neuroimage*, 9(2), pp.195–207. Available at: https://surfer.nmr.mgh.harvard.edu/ftp/articles/fischl99b-recon2.pdf [Accessed July 8, 2016].

Foster, C. et al., 2017. Paediatric European Network for Treatment of AIDS Treatment Guideline 2016 update: antiretroviral therapy recommended for all children living with HIV. *HIV Medicine*, 18(2), pp.133–134. Available at: http://doi.wiley.com/10.1111/hiv.12399 [Accessed November 26, 2017].

Fox, M.D. et al., 2006. Spontaneous neuronal activity distinguishes human dorsal and ventral attention systems. *Proceedings of the National Academy of Sciences*, 103(26), pp.10046–10051. Available at: http://www.ncbi.nlm.nih.gov/pubmed/16788060 [Accessed July 18, 2016].

Fox, M.D. et al., 2005. The human brain is intrinsically organized into dynamic, anticorrelated functional networks. *Proceedings of the National Academy of Sciences*, 102(27), pp.9673–9678. Available at: http://www.pnas.org.ezproxy.uct.ac.za/content/102/27/9673.full.pdf [Accessed November 3, 2017].

Fransson, P. et al., 2007. Resting-state networks in the infant brain. *Proceedings of the National Academy of Sciences of the United States of America*, 104(39), pp.15531–15536. Available at: http://www.pnas.org/content/104/39/15531.full.pdf [Accessed October 11, 2017].

Fries, P., 2005. A mechanism for cognitive dynamics: Neuronal communication through neuronal coherence. *Trends in Cognitive Sciences*, 9(10), pp.474–480. Available at: http://www.sciencedirect.com/science/article/pii/S1364661305002421?via%3Dihub [Accessed November 13, 2017].

Gabiano, C. et al., 1992. Mother-to-child transmission of human immunodeficiency virus type 1: risk of infection and correlates of transmission. *Pediatrics*, 90(3), pp.369–374. Available at: http://pediatrics.aappublications.org/content/pediatrics/90/3/369.full.pdf [Accessed August 9, 2017].

Garvie, P.A. et al., 2014. Discordance of Cognitive and Academic Achievement Outcomes in Youth With Perinatal HIV Exposure. *The Pediatric Infectious Disease Journal*, 33(9), pp.e232–e238. Available at: http://content.wkhealth.com/linkback/openurl?sid=WKPTLP:landingpage&an=00006454-201409000-00014.

Gongvatana, A. et al., 2009. White matter tract injury and cognitive impairment in human immunodeficiency virusinfected individuals. *Journal of NeuroVirology*, 15(2), pp.187–195. Available at: https://doi.org/10.1080/13550280902769756.

Gotts, S.J. et al., 2012. Fractionation of social brain circuits in autism spectrum disorders. *Brain*, 135(9), pp.2711–2725. Available at: http://www.ncbi.nlm.nih.gov/pubmed/22791801 [Accessed July 1, 2016].

Gotts, S.J. et al., 2013. The perils of global signal regression for group comparisons: a case study of Autism Spectrum Disorders. *Frontiers in Human Neuroscience*, 7(July), p.356. Available at: http://journal.frontiersin.org/article/10.3389/fnhum.2013.00356/abstract [Accessed July 28, 2016].

Gourlay, A. et al., 2013. Barriers and facilitating factors to the uptake of antiretroviral drugs for prevention of mother-to-child transmission of HIV in sub-Saharan Africa: A systematic review. *Journal of the International AIDS Society*, 16(1), p.18588. Available at: http://www.ncbi.nlm.nih.gov/pubmed/23870277 [Accessed November 13, 2017].

Greenland, S., 2008. Invited commentary: Variable selection versus shrinkage in the control of multiple confounders. *American Journal of Epidemiology*, 167(5), pp.523–529. Available at: https://academic.oup.com/aje/article-lookup/doi/10.1093/aje/kwm355 [Accessed March 1, 2017].

Greenland, S., Mansournia, M.A. & Altman, D.G., 2016. Sparse data bias: a problem hiding in plain sight. *Bmj*, 22(3), p.i1981. Available at: http://www.ncbi.nlm.nih.gov/pubmed/17504780 [Accessed March 3, 2017].

Greicius, M.D. et al., 2003. Functional connectivity in the resting brain: a network analysis of the default mode hypothesis. *Proceedings of the National Academy of Sciences of the United States of America*, 100(1), pp.253–8. Available at: http://www.ncbi.nlm.nih.gov/pubmed/12506194 [Accessed August 21, 2017].

Guha, A. et al., 2016. Intrinsic network connectivity abnormalities in HIV-infected individuals over age 60. *Journal of NeuroVirology*, 22(1), pp.80–87. Available at: http://link.springer.com/10.1007/s13365-015-0370-y [Accessed June 28, 2016].

Gusnard, D.A., Raichle, M.E. & Raichle, M.E., 2001. Searching for a baseline: functional imaging and the resting human brain. *Nature reviews. Neuroscience*, 2(10), pp.685–694. Available at: http://www.nature.com/doifinder/10.1038/35094500 [Accessed July 18, 2016].

Hagmann, P. et al., 2008. Mapping the structural core of human cerebral cortex K. J. Friston, ed. *PLoS Biology*, 6(7), pp.1479–1493. Available at: http://dx.plos.org/10.1371/journal.pbio.0060159 [Accessed August 28, 2017].

Ham, T. et al., 2013. Cognitive Control and the Salience Network: An Investigation of Error Processing and Effective Connectivity. *Journal of Neuroscience*, 33(16), pp.7091–7098. Available at: http://www.jneurosci.org/content/jneuro/33/16/7091.full.pdf [Accessed November 1, 2017].

He, B.J. et al., 2008. Electrophysiological correlates of the brain's intrinsic large-scale functional architecture. *Proceedings of the National Academy of Sciences*, 105(41), pp.16039–16044. Available at: http://www.pnas.org/content/105/41/16039.full.pdf [Accessed November 13, 2017].

Heaton, R.K. et al., 2011. HIV-associated neurocognitive disorders before and during the era of combination antiretroviral therapy: Differences in rates, nature, and predictors. *Journal of NeuroVirology*, 17(1), pp.3–16. Available at: http://link.springer.com/10.1007/s13365-010-0006-1 [Accessed October 19, 2017].

Herting, M.M. et al., 2015. Default Mode Connectivity in Youth With Perinatally Acquired HIV. *Medicine*, 94(37), p.e1417. Available at: http://content.wkhealth.com/linkback/openurl?sid=WKPTLP:landingpage&an=00005792-201509030-00013 [Accessed June 16, 2016].

Van den Heuvel, M.P., Stam, C.J., et al., 2009. Efficiency of functional brain networks and intellectual performance. *The Journal of neuroscience : the official journal of the Society for Neuroscience*, 29(23), pp.7619–7624. Available at: http://www.ncbi.nlm.nih.gov/pubmed/19515930 [Accessed November 10, 2017].

Van den Heuvel, M.P., Mandl, R.C.W., et al., 2009. Functionally linked resting-state networks reflect the underlying structural connectivity architecture of the human brain. *Human Brain Mapping*, 30(10), pp.3127–3141. Available at: http://doi.wiley.com/10.1002/hbm.20737 [Accessed August 22, 2017].

Van den Heuvel, M.P. & Hulshoff Pol, H.E., 2010. Exploring the brain network: A review on resting-state fMRI functional connectivity. *European Neuropsychopharmacology*, 20(8), pp.519–534. Available at: http://dx.doi.org/10.1016/j.euroneuro.2010.03.008.

Hillman, E.M.C., 2014. Coupling Mechanism and Significance of the BOLD Signal: A Status Report. *Annual Review of Neuroscience*, 37(1), pp.161–181. Available at: http://www.annualreviews.org.ezproxy.uct.ac.za/doi/pdf/10.1146/annurev-neuro-071013-014111 [Accessed November 6, 2017].

HIV Paediatric Prognostic Markers Collaborative Study Group, 2006. Predictive value of absolute CD4 cell count for disease progression in untreated HIV-1-infected children. *AIDS*, 20(9). Available at: http://journals.lww.com/aidsonline/Fulltext/2006/06120/Predictive_value_of_absolute_CD4_cell_count_for.10.aspx.

HIV Paediatric Prognostic Markers Collaborative Study Group, 2003. Short-term risk of disease progression in HIV-1-infected children receiving no antiretroviral therapy or zidovudine monotherapy: a meta-analysis. *The Lancet*, 362(9396), pp.1605–1611. Available at: http://www.sciencedirect.com/science/article/pii/S0140673603147939.

Hoare, J. et al., 2012. A diffusion tensor imaging and neurocognitive study of HIV-positive children who are HAART-na??ve “slow progressors.” *Journal of NeuroVirology*, 18(3), pp.205–212. Available at: http://link.springer.com/10.1007/s13365-012-0099-9 [Accessed June 13, 2016].

Hoare, J. et al., 2015. Clinical associations of white matter damage in cART-treated HIV-positive children in South Africa. *Journal of NeuroVirology*, 21(2), pp.120–128. Available at: http://link.springer.com/10.1007/s13365-014-0311-1 [Accessed November 27, 2017].

Hofman, F.M. et al., 1999. HIV-1 tat protein induces the production of interleukin-8 by human brain-derived endothelial cells. *Journal of Neuroimmunology*, 94(1), pp.28–39. Available at: http://www.sciencedirect.com/science/article/pii/S0165572898001982.

Holroyd, C.B. et al., 2004. Dorsal anterior cingulate cortex shows fMRI response to internal and external error signals. *Nature Neuroscience*, 7(5), pp.497–498. Available at: http://dare.ubvu.vu.nl/bitstream/handle/1871/17407/Holroyd?sequence=2 [Accessed November 1, 2017].

Huttenlocher, P.R., 1979. Synaptic density in human frontal cortex - Developmental changes and effects of aging. *Brain Research*, 163(2), pp.195–205. Available at: http://www.sciencedirect.com/science/article/pii/0006899379903494 [Accessed October 12, 2017].

Imamichi, H. et al., 2001. Human Immunodeficiency Virus Type 1 Quasi Species That Rebound after Discontinuation of Highly Active Antiretroviral Therapy Are Similar to the Viral Quasi Species Present before Initiation of Therapy. *The Journal of Infectious Diseases*, 183(1), pp.36–50. Available at: +.

Ipser, J.C. et al., 2015. HIV Infection Is Associated with Attenuated Frontostriatal Intrinsic Connectivity: A Preliminary Study. *Journal of the International Neuropsychological Society*, 21(3), pp.203–213. Available at: http://www.journals.cambridge.org/abstract_S1355617715000156 [Accessed June 16, 2016].

Iqbal, Z. et al., 2016. Pilot assessment of brain metabolism in perinatally HIV-Infected youths using accelerated 5D echo planar J-Resolved spectroscopic imaging. *PLoS ONE*, 11(9), pp.1–18.

Izbudak, I. et al., 2013. Perinatally HIV-infected youth presenting with acute stroke: Progression/evolution of ischemic disease on neuroimaging. *Journal of Neuroradiology*, 40(3), pp.172–180.

Jankiewicz, M. et al., 2017. White Matter Abnormalities in Children with HIV Infection and Exposure. *Frontiers in Neuroanatomy*, 11, p.88. Available at: http://journal.frontiersin.org/article/10.3389/fnana.2017.00088/full [Accessed October 22, 2017].

Janssen, R.S. et al., 1992. Epidemiology of human immunodeficiency virus encephalopathy in the United States. *Neurology*, 42(8), p.1472. Available at: http://www.neurology.org/content/42/8/1472.abstract.

Janssen, R.S. et al., 1991. Nomenclature and research case definitions for neurologic manifestations of human immunodeficiency virus-type 1 (HIV-1) infection. *Neurology*, 41(6), pp.778–785.

Jenkinson, M., 2009. Registration, atlases and cortical flattening. In P. Jezzard et al., eds. *Functional Magnetic Resonance Imaging: An Introduction to Methods*. Oxford: Oxford University Press, pp. 271–294.

Jeremy, R.J. et al., 2005. Neuropsychological Functioning and Viral Load in Stable Antiretroviral Therapy-Experienced HIV-Infected Children. *Pediatrics*, 115(2), pp.380–387. Available at:

http://pediatrics.aappublications.org/cgi/doi/10.1542/peds.2004-1108.

Jo, H.J. et al., 2013. Effective preprocessing procedures virtually eliminate distance-dependent motion artifacts in resting state FMRI. *Journal of Applied Mathematics*, 2013, pp.1–9. Available at: http://www.hindawi.com/journals/jam/2013/935154/ [Accessed August 6, 2016].

Jo, H.J. et al., 2010. Mapping sources of correlation in resting state FMRI, with artifact detection and removal. *NeuroImage*, 52(2), pp.571–582.

Joanes, D.N. & Gill, C.A., 1998. Comparing measures of sample skewness and kurtosis. *Journal of the Royal Statistical Society: Series D (The Statistician)*, 47(1), pp.183–189. Available at: http://doi.wiley.com/10.1111/1467-9884.00122 [Accessed November 16, 2017].

Jones, L.L. et al., 2009. Is puberty starting earlier in urban South Africa? *American Journal of Human Biology*, 21(3), pp.395–397. Available at: http://doi.wiley.com/10.1002/ajhb.20868 [Accessed October 12, 2017].

Kamangar, F., 2012. Confounding Variables in Epidemiologic Studies: Basics and Beyond. , 15(8).

Kaufman, A.S. & Kaufman, N.L., 2004. *Kaufman Assessment Battery for Children Second Edition*, Circle Pines, MN.

Kaul, M., Garden, G.A. & Lipton, S.A., 2001. Pathways to neuronal injury and apoptosis in HIV-associated dementia. *Nature*, 410, p.988. Available at: http://dx.doi.org/10.1038/35073667.

Kelly, R.E. et al., 2010. Visual inspection of independent components: Defining a procedure for artifact removal from fMRI data. *Journal of Neuroscience Methods*, 189(2), pp.233–245. Available at: http://ac.els-cdn.com/S0165027010001627/1-s2.0-S0165027010001627-main.pdf?_tid=b70b4350-713b-11e7-8963-00000aacb361&acdnat=1500988876_86363859a3674d7b31d9045e3515e093 [Accessed July 25, 2017].

Kim, H.-Y., 2013. Statistical notes for clinical researchers: assessing normal distribution (2) using skewness and kurtosis. *Restorative Dentistry & Endodontics*, 38(1), p.52. Available at: http://www.ncbi.nlm.nih.gov/pubmed/23495371 [Accessed November 15, 2017].

Kim, H., Daselaar, S.M. & Cabeza, R., 2010. Overlapping brain activity between episodic memory encoding and retrieval: Roles of the task-positive and task-negative networks. *NeuroImage*, 49(1), pp.1045–1054. Available at: https://ac-els-cdn-com.ezproxy.uct.ac.za/S1053811909008489/1-s2.0-S1053811909008489-main.pdf?_tid=9a3d1f3c-c069-11e7-9e29-00000aacb362&acdnat=1509694725_67215d2e7b25c9265f90dd3d182f9c94 [Accessed November 3, 2017].

Koekkoek, S. et al., 2008. Neurocognitive function profile in HIV-infected school-age children. *European Journal of Paediatric Neurology*, 12(4), pp.290–297.

Koppensteiner, H. & Wu, L., 2012. Macrophages and their relevance in Human Immunodeficiency Virus Type I infection. *Retrovirology*, 9(1), p.82. Available at: http://retrovirology.biomedcentral.com/articles/10.1186/1742-4690-9-82 [Accessed November 13, 2017].

Van der Kouwe, A.J.W. et al., 2008. Brain morphometry with multiecho MPRAGE. *NeuroImage*, 40(2), pp.559–569. Available at: http://www.sciencedirect.com/science/article/pii/S1053811907011457 [Accessed October 26, 2017].

Koyama, M.S. et al., 2011. Resting-state functional connectivity indexes reading competence in children and adults. *The Journal of neuroscience : the official journal of the Society for Neuroscience*, 31(23), pp.8617–24. Available at: http://www.jneurosci.org/content/jneuro/31/23/8617.full.pdf [Accessed November 13, 2017].

Kuafman, A.S. et al., 2005. *Essentials of KABC-II assessment. Vol. 94*, Hoboken, New Jersey: John Wiley & Sons. Available at: https://scholar.google.co.za/scholar?hl=en&as_sdt=0%2C5&q=Kaufman%2C+A.+S.%2C+Lichtenberger%2C+E.+O.%2C+Fletcher-Janzen%2C+E.%2C+%26+Kaufman%2C+N.+L.+%282005%29.+Essentials+of+KABC-II+assessment.+Hoboken%2C+New+Jersey%3A+John+Wiley+%26+Sons&btnG= [Accessed October 25, 2017].

Kuritzkes, D.R. et al., 1999. Lamivudine in combination with zidovudine, stavudine, or didanosine in patients with HIV-1 infection. A randomized, double-blind, placebo-controlled trial. *AIDS*, 13(6). Available at: http://journals.lww.com/aidsonline/Fulltext/1999/04160/Lamivudine_in_combination_with_zidovudine,.9.aspx.

Laird, A.R. et al., 2011. Behavioral interpretations of intrinsic connectivity networks. *Journal of cognitive neuroscience*, 23(12), pp.4022–4037.

Laughton, B. et al., 2012. Early antiretroviral therapy improves neurodevelopmental outcomes in infants. *AIDS (London, England)*, 26(13), pp.1685–90. Available at: http://www.ncbi.nlm.nih.gov/pubmed/22614886 [Accessed December 8, 2016].

Laughton, B. et al., 2017. Five year Neurodevelopment Outcomes of perinatally HIV-infected children on early limited or deferred continuous antiretroviral therapy. Manuscript submitted for publication.

Lee, M.H., Smyser, C.D. & Shimony, J.S., 2013. Resting-state fMRI: a review of methods and clinical applications. *AJNR Am J Neuroradiol*, 34, pp.1866–1872. Available at: http://www.ncbi.nlm.nih.gov/pubmed/22936095 [Accessed July 26, 2016].

Letendre, S. et al., 2008. Validation of the CNS Penetration-Effectiveness rank for quantifying antiretroviral penetration into the central nervous system. *Archives of neurology*, 65(1), pp.65–70. Available at: http://archneur.jamanetwork.com/article.aspx?doi=10.1001/archneurol.2007.31 [Accessed November 21, 2017].

Lewis-de los Angeles, C.P. et al., 2017. Lower total and regional grey matter brain volumes in youth with perinatally-acquired HIV infection: Associations with HIV disease severity, substance use, and cognition. *Brain, Behavior, and Immunity*, 62, pp.100–109. Available at: https://ac.els-cdn.com/S088915911730003X/1-s2.0-S088915911730003X-main.pdf?_tid=5f66f47e-b3d4-11e7-9755-00000aacb35d&acdnat=1508311218_ae7f76789b3a469e7da356b556c622be [Accessed October 18, 2017].

Lewis, C.M. et al., 2009. Learning sculpts the spontaneous activity of the resting human brain. *Proceedings of the National Academy of Sciences*, 106(41), pp.17558–17563. Available at: httpwww.pnas.orgcontent1064117558.abstract.

Lewis, W. & Dalakas, M., 1995. Mitochondrial toxicity of antiviral drugs. *Nature medicine*, 1(5), p.417.

Lindsey, J.C. et al., 2007. Neurodevelopmental functioning in HIV-infected infants and young children before and after the introduction of protease inhibitor-based highly active antiretroviral

therapy. *Pediatrics*, 119(3), pp.e681–e693.

Littow, 2010. Age-related differences in functional nodes of the brain cortex - a high model order group ICA study. *Frontiers in Systems Neuroscience*, 4. Available at: http://www.ncbi.nlm.nih.gov/pubmed/20953235 [Accessed October 13, 2017].

Liu, F. et al., 2013. Abnormal amplitude low-frequency oscillations in medication-naive, first-episode patients with major depressive disorder: A resting-state fMRI study. *Journal of Affective Disorders*, 146(3), pp.401–406.

Lobato, M.N. et al., 1995. Encephalopathy in children with perinatally acquired human immunodeficiency virus infection. *The Journal of Pediatrics*, 126(5), pp.710–715. Available at: http://www.sciencedirect.com/science/article/pii/S0022347695703977.

Logothetis, N.K. et al., 2001. Neurophysiological investigation of the basis of the fMRI signal. *Nature*, 412, pp.1–8. Available at: http://dx.doi.org/10.1038/35084005.

Logothetis, N.K. & Wandell, B.A., 2004. Interpreting the BOLD Signal. *Annual Review of Physiology*, 66(1), pp.735–769. Available at: http://www.annualreviews.org.ezproxy.uct.ac.za/doi/pdf/10.1146/annurev.physiol.66.082602.092845 [Accessed November 6, 2017].

De Luca, M. et al., 2006. fMRI resting state networks define distinct modes of long-distance interactions in the human brain. *NeuroImage*, 29(4), pp.1359–1367. Available at: http://ac.els-cdn.com/S1053811905006257/1-s2.0-S1053811905006257-main.pdf?_tid=5f8b86de-7385-11e7-b4d8-00000aacb360&acdnat=1501240413_89b15390bc5b86781d915a9d3a009ad3 [Accessed July 28, 2017].

Luiz, D.M. et al., 2006. *Griffiths Mental Development Scales–Extended Revised. Two to eight years. Administration manual*, Oxford, UK.

Lundgren, J.D. et al., 1994. Comparison of long-term prognosis of patients with AIDS treated and not treated with zidovudine. *Journal of the American Medical Association*, 271(14), pp.1088–1092. Available at: http://jama.jamanetwork.com/article.aspx?doi=10.1001/jama.1994.03510380044035 [Accessed November 25, 2017].

Madhi, S.A. et al., 2010. Effect of HIV infection status and anti-retroviral treatment on quantitative and qualitative antibody responses to pneumococcal conjugate vaccine in infants. *The Journal of infectious diseases*, 202(3), pp.355–61. Available at: http://www.ncbi.nlm.nih.gov/pubmed/20583920 [Accessed June 30, 2016].

Malee, K.M. et al., 2011. Mental health functioning among children and adolescents with perinatal HIV infection and perinatal HIV exposure. *AIDS Care*, 23(12), pp.1533–1544. Available at: http://www.tandfonline.com/doi/abs/10.1080/09540121.2011.575120.

Mantini, D. et al., 2007. Electrophysiological signatures of resting state networks in the human brain. *Proceedings of the National Academy of Sciences of the United States of America*, 104(32), pp.13170–5. Available at: http://www.ncbi.nlm.nih.gov/pubmed/17670949 [Accessed November 6, 2017].

Marra, C.M. et al., 2009. Impact of combination antiretroviral therapy on cerebrospinal fluid HIV RNA and neurocognitive performance. *AIDS*, 23(11). Available at: http://journals.lww.com/aidsonline/Fulltext/2009/07170/Impact_of_combination_antiretroviral_therapy_on.8.aspx.

Martin, S.C. et al., 2006. Cognitive functioning in school-aged children with vertically acquired HIV

infection being treated with highly active antiretroviral therapy (HAART). *Developmental neuropsychology*, 30(2), pp.633–57. Available at: http://www.tandfonline.com/doi/abs/10.1207/s15326942dn3002_1 [Accessed November 24, 2017].

Mathiesen, C. et al., 2004. Modification of activity-dependent increases of cerebral blood flow by excitatory synaptic activity and spikes in rat cerebellar cortex. *The Journal of Physiology*, 512(2), pp.555–566. Available at: https://doi.org/10.1111/j.1469-7793.1998.555be.x.

Mbugua, K.K. et al., 2016. HIV-associated CD4+/CD8+ depletion in infancy is associated with neurometabolic reductions in the basal ganglia at age 5 years despite early antiretroviral therapy. *AIDS*, 30(9), pp.1353–1362. Available at: http://content.wkhealth.com/linkback/openurl?sid=WKPTLP:landingpage&an=00002030-201606010-00005 [Accessed September 28, 2017].

McCoig, C. et al., 2002. Effect of combination antiretroviral therapy on cerebrospinal fluid HIV RNA, HIV resistance, and clinical manifestations of encephalopathy. *The Journal of pediatrics*, 141(1), pp.36–44.

McNamee, R., 2003. Confounding and confounders. *Occupational and environmental medicine*, 60(3), pp.227–234. Available at: http://www.ncbi.nlm.nih.gov/pubmed/12598677 [Accessed March 1, 2017].

Mellins, C.A. et al., 2003. High Rates of Behavioral Problems in Perinatally HIV-Infected Children Are Not Linked to HIV Disease. *Pediatrics*, 111(2).

Melrose, R.J. et al., 2008. Compromised fronto-striatal functioning in HIV: An fMRI investigation of semantic event sequencing. *Behavioural Brain Research*, 188(2), pp.337–347.

Menon, V. & Uddin, L.Q., 2010. Saliency, switching, attention and control: a network model of insula function. *Brain Structure and Function*, pp.1–13.

Merkle, V., 2015. *The Cognitive Development of HIV-infected and -uninfected Children in South Africa (Unpublished master's thesis)*. Julius Maximilian University of Würzburg.

Molfese, P.J. et al., 2015. The Haskins Pediatric Brain Atlas. In *OHBM*. Available at: https://ww4.aievolution.com/hbm1501/index.cfm?do=abs.viewAbs&abs=3559 [Accessed July 4, 2016].

Moore, A.L. et al., 2003. Virologic, immunologic, and clinical response to highly active antiretroviral therapy: the gender issue revisited. *Journal of acquired immune deficiency syndromes (1999)*, 32(4), pp.452–61. Available at: http://www.ncbi.nlm.nih.gov/pubmed/12640206 [Accessed August 9, 2017].

Muetzel, R.L. et al., 2016. Resting-state networks in 6-to-10 year old children. *Human Brain Mapping*, 37(12), pp.4286–4300. Available at: http://doi.wiley.com/10.1002/hbm.23309 [Accessed October 13, 2017].

Murphy, K., Birn, R.M. & Bandettini, P.A., 2013. Resting-state fMRI confounds and cleanup. *NeuroImage*, 80, pp.349–359. Available at: https://ac.els-cdn.com/S1053811913003170/1-s2.0-S1053811913003170-main.pdf?_tid=87823db2-c525-11e7-9cad-00000aacb35f&acdnat=1510215243_b8f5d04a46e45f588334a94e9de268f1 [Accessed November 9, 2017].

Musielak, K.A. & Fine, J.G., 2015. An Updated Systematic Review of Neuroimaging Studies of Children and Adolescents with Perinatally Acquired HIV. *Journal of Pediatric Neuropsychology*. Available at: http://link.springer.com/10.1007/s40817-015-0009-1.

Nagarajan, R. et al., 2012. Neuropsychological function and cerebral metabolites in HIV-infected youth. *Journal of Neuroimmune Pharmacology*, 7(4), pp.981–990. Available at: http://link.springer.com/10.1007/s11481-012-9407-7 [Accessed July 18, 2016].

Nicastri, E. et al., 2005. Gender differences in clinical progression of HIV-1-infected individuals during long-term highly active antiretroviral therapy. *Aids*, 19(6), pp.577–583. Available at: http://www.ncbi.nlm.nih.gov/pubmed/15802976%5Cnhttp://ovidsp.tx.ovid.com/ovftpdfs/FPDDNCFBEGFHGD00/fs046/ovft/live/gv023/00002030/00002030-200504080-00006.pdf.

Nichols, S.L. et al., 2015. Executive Functioning in Children and Adolescents With Perinatal HIV Infection. *The Pediatric infectious disease journal*, 34(9), pp.969–75. Available at: http://www.ncbi.nlm.nih.gov/pubmed/26376309%5Cnhttp://www.pubmedcentral.nih.gov/articlerender.fcgi?artid=PMC4761421.

Nichols, S.L., Chernoff, M.C., Malee, K.M., Sirois, P.A., Woods, S.P., et al., 2016. Executive functioning in children and adolescents with perinatal HIV infection and perinatal HIV exposure. *Journal of the Pediatric Infectious Diseases Society*, 5, pp.S15–S23.

Nichols, S.L., Chernoff, M.C., Malee, K.M., Sirois, P.A., Williams, P.L., et al., 2016. Learning and Memory in Children and Adolescents With Perinatal HIV Infection and Perinatal HIV Exposure. *The Pediatric Infectious Disease Journal*, 35(6), pp.649–654. Available at: http://insights.ovid.com/crossref?an=00006454-201606000-00011.

Nielsen, A.N. & Lauritzen, M., 2004. Coupling and uncoupling of activity-dependent increases of neuronal activity and blood flow in rat somatosensory cortex. *The Journal of Physiology*, 533(3), pp.773–785. Available at: https://doi.org/10.1111/j.1469-7793.2001.00773.x.

O'Gorman, M.R.G. & Zijenah, L.S., 2008. CD4 T cell measurements in the management of antiretroviral therapy--A review with an emphasis on pediatric HIV-infected patients. *Cytometry. Part B, Clinical cytometry*, 74 Suppl 1(September 2007), pp.S19–S26. Available at: http://doi.wiley.com/10.1002/cyto.b.20398 [Accessed November 22, 2017].

O'Mahony, S.M. et al., 2005. Efavirenz Induces Depressive-Like Behaviour, Increased Stress Response and Changes in the Immune Response in Rats. *Neuroimmunomodulation*, 12(5), pp.293–298. Available at: https://www.karger.com/DOI/10.1159/000087107.

Ortega, M., Brier, M.R. & Ances, B.M., 2015. Effects of HIV and combination antiretroviral therapy on cortico-striatal functional connectivity. *AIDS (London, England)*, 29(January), pp.703–12. Available at: http://www.ncbi.nlm.nih.gov/pubmed/25849834 [Accessed June 16, 2016].

Palella, F.J. et al., 1998. Declining Morbidity and Mortality among Patients with Advanced Human Immunodeficiency Virus Infection. *New England Journal of Medicine*, 338(13), pp.853–860. Available at: http://dx.doi.org/10.1056/NEJM199803263381301.

Panel on Antiretroviral Therapy and Medical Management of HIV-Infected Children, Guidelines for the use of antiretroviral agents in pediatric HIV infection. Available at: http://aidsinfo.nih.gov/guidelines [Accessed November 26, 2017].

Paul, R.H. et al., 2007. Proton MRS and Neuropsychological Correlates in AIDS Dementia Complex: Evidence of Subcortical Specificity. *The Journal of Neuropsychiatry and Clinical Neurosciences*, 19(3), pp.283–292. Available at: http://neuro.psychiatryonline.org/doi/pdf/10.1176/jnp.2007.19.3.283 [Accessed October 30, 2017].

Peppiatt, C.M. et al., 2006. Bidirectional control of CNS capillary diameter by pericytes. *Nature*, 443, p.700. Available at: http://dx.doi.org/10.1038/nature05193.

Persaud, D. et al., 2000. A stable latent reservoir for HIV-1 in resting CD4(+) T lymphocytes in infected children. *Journal of Clinical Investigation*, 105(7), pp.995–1003. Available at: http://www.ncbi.nlm.nih.gov/pmc/articles/PMC377486/.

Poole, V.N. et al., 2016. Intrinsic functional connectivity predicts individual differences in distractibility. *Neuropsychologia*, 86, pp.176–182. Available at: http://www.sciencedirect.com/science/article/pii/S0028393216301397?via%3Dihub#bib49 [Accessed November 10, 2017].

Popa, D., Popescu, A.T. & Pare, D., 2009. Contrasting Activity Profile of Two Distributed Cortical Networks as a Function of Attentional Demands. *Journal of Neuroscience*, 29(4), pp.1191–1201. Available at: http://www.ncbi.nlm.nih.gov/pubmed/19176827 [Accessed November 3, 2017].

Poppe, A.B. et al., 2013. Toward a neurometric foundation for probabilistic independent component analysis of fMRI data. *Cognitive, affective & behavioral neuroscience*, 13(3), pp.641–59. Available at: http://link.springer.com/10.3758/s13415-013-0180-8 [Accessed November 23, 2016].

Power, J.D. et al., 2014. Methods to detect, characterize, and remove motion artifact in resting state fMRI. *NeuroImage*, 84, pp.320–341.

Power, J.D. et al., 2012. Spurious but systematic correlations in functional connectivity MRI networks arise from subject motion. *NeuroImage*, 59(3), pp.2142–2154.

Power, J.D. et al., 2010. The Development of Human Functional Brain Networks. *Neuron*, 67(5), pp.735–748. Available at: http://linkinghub.elsevier.com/retrieve/pii/S0896627310006276 [Accessed August 28, 2017].

Price, R.W. & Spudich, S., 2008. Antiretroviral Therapy and Central Nervous System HIV Type 1 Infection. *The Journal of Infectious Diseases*, 197(Supplement_3), pp.S294–S306. Available at: +.

Pruim, R.H.R. et al., 2015. Evaluation of ICA-AROMA and alternative strategies for motion artifact removal in resting state fMRI. *NeuroImage*, 112, pp.278–287.

Raichle, M.E. et al., 2001. A default mode of brain function. *Proceedings of the National Academy of Sciences of the United States of America*, 98(2), pp.676–82. Available at: http://www.ncbi.nlm.nih.gov/pubmed/11209064 [Accessed August 21, 2017].

Raichle, M.E., 2015. The Brain's Default Mode Network. *Annual Review of Neuroscience*, 38(1), pp.433–447. Available at: http://www.ncbi.nlm.nih.gov/pubmed/25938726 [Accessed November 3, 2017].

Reineberg, A.E. et al., 2015. Resting-state networks predict individual differences in common and specific aspects of executive function. *NeuroImage*, 104, pp.69–78. Available at: https://ac.els-cdn.com/S1053811914007873/1-s2.0-S1053811914007873-main.pdf?_tid=5c1c8e32-c61c-11e7-873c-00000aacb35d&acdnat=1510321265_e7ce4abda2eba264349f7944d80a3a4d [Accessed November 10, 2017].

Van Rie, A. et al., 2007. Neurologic and neurodevelopmental manifestations of pediatric HIV/AIDS: A global perspective. *European Journal of Paediatric Neurology*, 11(1), pp.1–9.

Robertson, K., Liner, J. & Meeker, R.B., 2012. Antiretroviral neurotoxicity. *Journal of NeuroVirology*, 18(5), pp.388–399. Available at: http://link.springer.com/10.1007/s13365-012-0120-3 [Accessed July 7, 2016].

Rogers, B.P. et al., 2007. Assessing functional connectivity in the human brain by fMRI. *Magnetic*

Resonance Imaging, 25(10), pp.1347–1357. Available at: http://www.sciencedirect.com.ezproxy.uct.ac.za/science/article/pii/S0730725X07002238 [Accessed November 9, 2017].

Rosazza, C. & Minati, L., 2011. Resting-state brain networks: Literature review and clinical applications. *Neurological Sciences*, 32(5), pp.773–785. Available at: https://link.springer.com/content/pdf/10.1007%2Fs10072-011-0636-y.pdf [Accessed November 1, 2017].

Rytty, R. et al., 2013. GroupICA dual regression analysis of resting state networks in a behavioral variant of frontotemporal dementia. *Frontiers in human neuroscience*, 7(August), p.461. Available at: http://www.ncbi.nlm.nih.gov/pubmed/23986673 [Accessed December 4, 2016].

Saad, Z.S. et al., 2012. Trouble at rest: how correlation patterns and group differences become distorted after global signal regression. *Brain Connect*, 2(1), pp.25–32.

Sacktor, N. et al., 2010. Longitudinal psychomotor speed performance in human immunodeficiency virus-seropositive individuals: impact of age and serostatus. *Journal of neurovirology*, 16(5), pp.335–341. Available at: https://link.springer.com/content/pdf/10.3109/13550284.2010.504249.pdf [Accessed November 24, 2017].

Sala-Llonch, R. et al., 2012. Brain connectivity during resting state and subsequent working memory task predicts behavioural performance. *Cortex*, 48(9), pp.1187–1196. Available at: www.sciencedirect.com [Accessed November 10, 2017].

Sarma, M.K. et al., 2014. Regional brain gray and white matter changes in perinatally HIV-infected adolescents. *NeuroImage: Clinical*, 4(Supplement C), pp.29–34. Available at: http://www.sciencedirect.com/science/article/pii/S2213158213001423.

Sarma, M.K. et al., 2017. Resting State Brain Networks in Perinatally HIV-infected Adult Youths. *International Society for Magnetic Resonance in Medicine, 26th Annual Meeting*. Available at: http://dev.ismrm.org/2017/1698.html [Accessed October 31, 2017].

Sato, J.R. et al., 2015. Decreased centrality of subcortical regions during the transition to adolescence: A functional connectivity study. *NeuroImage*, 104, pp.44–51. Available at: http://www.sciencedirect.com/science/article/pii/S1053811914008052 [Accessed April 4, 2017].

Satterthwaite, T.D. et al., 2013. An improved framework for confound regression and filtering for control of motion artifact in the preprocessing of resting-state functional connectivity data. *NeuroImage*, 64(1), pp.240–256.

Satterthwaite, T.D. et al., 2012. Impact of in-scanner head motion on multiple measures of functional connectivity: Relevance for studies of neurodevelopment in youth. *NeuroImage*, 60(1), pp.623–632.

Schmahmann, J.D., 1991. An Emerging Concept: The Cerebellar Contribution to Higher Function. *Archives of Neurology*, 48(11), p.1178. Available at: http://archneur.jamanetwork.com/article.aspx?doi=10.1001/archneur.1991.00530230086029 [Accessed October 13, 2017].

Schmahmann, J.D., 2005. Cognition, emotion and the cerebellum. *Brain*, 129(2), pp.290–292. Available at: http://academic.oup.com/brain/article/129/2/290/292272/Cognition-emotion-and-the-cerebellum [Accessed October 13, 2017].

Schmahmann, J.D. & Sherman, J.C., 1998. The cerebellar cognitive affective syndrome. *Brain*, 121(4),

pp.561–579. Available at: https://watermark.silverchair.com/1210561.pdf?token=AQECAHi208BE49Ooan9kkhW_Ercy7Dm3ZL_9Cf3qfKAc485ysgAAAe4wggHqBgkqhkiG9w0BBwagggHbMIIB1wIBADCCAdAGCSqGSIb3DQEHATAeBglghkgBZQMEAS4wEQQMLbaixplcybB0Pma-AgEQgIIBoblaaiKsusaebHY6WFg0F_NgApNGRh91NGcJfscq_tWRjfw [Accessed October 13, 2017].

Schmithorst, V.J. & Holland, S.K., 2004. Comparison of Three Methods for Generating Group Statistical Inferences from Independent Component Analysis of Functional Magnetic Resonance Imaging Data. *Journal of Magnetic Resonance Imaging*, 19(3), pp.365–368. Available at: http://doi.wiley.com/10.1002/jmri.20009 [Accessed November 10, 2017].

Seeley, W.W. et al., 2007. Dissociable intrinsic connectivity networks for salience processing and executive control. *The Journal of neuroscience : the official journal of the Society for Neuroscience*, 27(9), pp.2349–2356. Available at: http://www.jneurosci.org/cgi/doi/10.1523/JNEUROSCI.5587-06.2007 [Accessed July 18, 2016].

Shah, A. et al., 2016. Neurotoxicity in the Post-HAART Era: Caution for the Antiretroviral Therapeutics. *Neurotoxicity Research*, 30(4), pp.677–697. Available at: https://link-springer-com.ezproxy.uct.ac.za/content/pdf/10.1007%2Fs12640-016-9646-0.pdf [Accessed November 22, 2017].

Shannon, B.J. et al., 2011. Premotor functional connectivity predicts impulsivity in juvenile offenders. *Proceedings of the National Academy of Sciences*, 108(27), pp.11241–11245. Available at: http://www.ncbi.nlm.nih.gov/pubmed/21709236 [Accessed November 3, 2017].

Sheffield, J.M. & Barch, D.M., 2016. Cognition and resting-state functional connectivity in schizophrenia. *Neuroscience and Biobehavioral Reviews*, 61, pp.108–120. Available at: https://ac.els-cdn.com/S0149763415003048/1-s2.0-S0149763415003048-main.pdf?_tid=5a55ba9a-c614-11e7-a311-00000aacb362&acdnat=1510317818_7c60eef4a4836913cc395f83bd6cb61e [Accessed November 10, 2017].

Shehzad, Z. et al., 2009. The resting brain: Unconstrained yet reliable. *Cerebral Cortex*, 19(10), pp.2209–2229. Available at: https://academic.oup.com/cercor/article-lookup/doi/10.1093/cercor/bhn256 [Accessed August 2, 2017].

Shirer, W.R. et al., 2015. Optimization of rs-fMRI Pre-processing for Enhanced Signal-Noise Separation, Test-Retest Reliability, and Group Discrimination. *NeuroImage*, 117, pp.67–79.

Shulman, G.L. et al., 1997. Common Blood Flow Changes across Visual Tasks: II. Decreases in Cerebral Cortex. *Journal of Cognitive Neuroscience*, 9(5), pp.648–663. Available at: http://www.mitpressjournals.org/doi/10.1162/jocn.1997.9.5.648 [Accessed November 2, 2017].

Shulman, G.L. et al., 2010. Right hemisphere dominance during spatial selective attention and target detection occurs outside the dorsal frontoparietal network. *The journal of neuroscience*, 30(10), pp.3640–3651. Available at: http://www.jneurosci.org/cgi/doi/10.1523/JNEUROSCI.4085-09.2010 [Accessed July 1, 2016].

SMART Study Group, 2006. CD4+ Count–Guided Interruption of Antiretroviral Treatment. *New England Journal of Medicine*, 355(22), pp.2283–2296. Available at: http://www.nejm.org/doi/abs/10.1056/NEJMoa062360 [Accessed November 26, 2017].

Smith, D. V. et al., 2014. Characterizing individual differences in functional connectivity using dual-regression and seed-based approaches. *NeuroImage*, 95, pp.1–12.

Smith, R. et al., 2012. Impact of HIV Severity on Cognitive and Adaptive Functioning During Childhood and Adolescence. *The Pediatric Infectious Disease Journal*, 31(6), pp.592–598. Available at: http://content.wkhealth.com/linkback/openurl?sid=WKPTLP:landingpage&an=00006454-201206000-00012.

Smith, S.M. et al., 2004. Advances in functional and structural MR image analysis and implementation as FSL. In *NeuroImage*. pp. S208–S219.

Smith, S.M. et al., 2009. Correspondence of the brain's functional architecture during activation and rest. *Proceedings of the National Academy of Sciences of the United States of America*, 106(31), pp.13040–5. Available at: http://www.pnas.org/cgi/doi/10.1073/pnas.0905267106 [Accessed June 27, 2016].

Smith, S.M. et al., 2013. Resting-state fMRI in the Human Connectome Project. *NeuroImage*, 80, pp.144–168. Available at: http://www.ncbi.nlm.nih.gov/pubmed/23702415 [Accessed August 7, 2016].

Smith, S.M., 2006. The pathogenesis of HIV infection: stupid may not be so dumb after all. *Retrovirology*, 3(1), p.60. Available at: https://retrovirology.biomedcentral.com/track/pdf/10.1186/1742-4690-3-60?site=retrovirology.biomedcentral.com [Accessed November 13, 2017].

Smurzynski, M. et al., 2011. Effects of central nervous system antiretroviral penetration on cognitive functioning in the ALLRT cohort. *AIDS*, 25(3). Available at: http://journals.lww.com/aidsonline/Fulltext/2011/01280/Effects_of_central_nervous_system_antiretroviral.10.aspx.

Smyser, C.D. et al., 2010. Longitudinal analysis of neural network development in preterm infants. *Cerebral Cortex*, 20(12), pp.2852–2862. Available at: http://www.cercor.oxfordjournals.org/cgi/doi/10.1093/cercor/bhq035 [Accessed August 15, 2016].

Sokoloff, L., 1981. Relationships among local functional activity, energy metabolism, and blood flow in the central nervous system. *Fed Proc*, 40(8), pp.2311–2316. Available at: http://www.ncbi.nlm.nih.gov/pubmed/7238911 [Accessed July 28, 2018].

Sole-Padulles, C. et al., 2016. Intrinsic connectivity networks from childhood to late adolescence: Effects of age and sex. *Developmental Cognitive Neuroscience*, 17, pp.35–44. Available at: http://www.sciencedirect.com/science/article/pii/S1878929315300670 [Accessed April 4, 2017].

Sridharan, D., Levitin, D.J. & Menon, V., 2008. A critical role for the right fronto-insular cortex in switching between central-executive and default-mode networks. *Proceedings of the National Academy of Sciences*, 105(34), pp.12569–12574. Available at: http://www.ncbi.nlm.nih.gov/pubmed/18723676 [Accessed November 5, 2017].

Starck, T. et al., 2013. Resting state fMRI reveals a default mode dissociation between retrosplenial and medial prefrontal subnetworks in ASD despite motion scrubbing. *Frontiers in human neuroscience*, 7(November), p.802. Available at: http://www.ncbi.nlm.nih.gov/pubmed/24319422 [Accessed August 11, 2016].

Stebbing, J., Gazzard, B. & Douek, D.C., 2004. Where Does HIV Live? *New England Journal of Medicine*, 350(18), pp.1872–1880. Available at: http://www.nejm.org/doi/pdf/10.1056/NEJMra032395 [Accessed November 13, 2017].

Stevens, M.C., Pearlson, G.D. & Calhoun, V.D., 2009. Changes in the interaction of resting-state neural networks from adolescence to adulthood. *Human Brain Mapping*, 30(8), pp.2356–2366. Available at: http://doi.wiley.com/10.1002/hbm.20673 [Accessed October 20, 2017].

Stevenson, M., 2003. HIV-1 pathogenesis. *Nature Medicine*, 9(7), pp.853–860. Available at: http://www.nature.com/doifinder/10.1038/nm0703-853 [Accessed November 13, 2017].

Stoodley, C.J. & Schmahmann, J.D., 2009. Functional topography in the human cerebellum: A meta-analysis of neuroimaging studies. *NeuroImage*, 44(2), pp.489–501. Available at: https://ac.els-cdn.com/S1053811908009725/1-s2.0-S1053811908009725-main.pdf?_tid=4de582d2-afed-11e7-8c70-00000aacb35e&acdnat=1507882121_3de640b1df024239f156391ad189978b [Accessed October 13, 2017].

Streck, E.L. et al., 2008. Effects of the HIV treatment drugs nevirapine and efavirenz on brain creatine kinase activity. *Metabolic Brain Disease*, 23(4), pp.485–492. Available at: https://doi.org/10.1007/s11011-008-9109-2.

Supekar, K., Musen, M. & Menon, V., 2009. Development of Large-Scale Functional Brain Networks in Children K. J. Friston, ed. *PLoS Biology*, 7(7), p.e1000157. Available at: http://dx.plos.org/10.1371/journal.pbio.1000157 [Accessed October 17, 2017].

Tabachnick, B.G. & Fidell, L.S., 2014. A Guide to Statistical Techniques. In *Using Multivariate Statistics*. Harlow, Essex: Pearson Education Limited.

Taha, T.E. et al., 2005. Gender differences in perinatal HIV acquisition among African infants. *Pediatrics*, 115(2), pp.e167-72. Available at: http://pediatrics.aappublications.org/content/pediatrics/115/2/e167.full.pdf [Accessed August 10, 2017].

Takano, T. et al., 2005. Astrocyte-mediated control of cerebral blood flow. *Nature Neuroscience*, 9, p.260. Available at: http://dx.doi.org/10.1038/nn1623.

Talairach, J. & Tournoux, P., 1988. *Co-Planar Stereotaxis Atlas of the Human Brain*, G. Thieme. Available at: https://books.google.co.za/books?id=ssEbmvfcJT8C.

Tallini, Y.N. et al., 2007. Propagated Endothelial Ca2+ Waves and Arteriolar Dilation In Vivo. *Circulation Research*, 101(12), pp.1300–1309. Available at: http://circres.ahajournals.org/content/101/12/1300.

Tardieu, M. et al., 1995. Cognitive assessment of school-age children infected with maternally transmitted human immunodeficiency virus type 1. *The Journal of pediatrics*, 126(Cdc), pp.375–379. Available at: https://ac.els-cdn.com/S0022347695704515/1-s2.0-S0022347695704515-main.pdf?_tid=30866dc2-b4ad-11e7-9575-00000aacb361&acdnat=1508404340_8f8434f96b9a8515adb9865c38a2ecac [Accessed October 19, 2017].

Tardieu, M. et al., 2000. HIV-1-related encephalopathy in infants compared with children and adults. *Neurology*, 54(5), pp.1089–1095. Available at: http://www.neurology.org/content/54/5/1089.

Tassiopoulos, K. et al., 2016. Following young people with perinatal HIV infection from adolescence into adulthood: the protocol for PHACS AMP Up, a prospective cohort study. *BMJ Open*, 6(6), p.e011396. Available at: http://dx.doi.org/10.1136/ [Accessed November 23, 2017].

Taylor, J. et al., 1989. CD4 percentage, CD4 number, and CD4: CD8 ratio in HIV infection: which to choose and how to use. *JAIDS Journal of Acquired Immune Deficiency Syndromes*, 2(2), pp.114–124.

Thomas, J.B. et al., 2013. Pathways to neurodegeneration: Effects of HIV and aging on resting-state functional connectivity. *Neurology*, 80(13), pp.1186–1193. Available at: http://www.ncbi.nlm.nih.gov/pubmed/23446675 [Accessed June 16, 2016].

Thomas, J.B. et al., 2015. Weighted brain networks in disease: Centrality and entropy in human immunodeficiency virus and aging. *Neurobiology of Aging*, 36(1), pp.401–412. Available at: http://www.ncbi.nlm.nih.gov/pubmed/25034343 [Accessed June 16, 2016].

Thompson, L. et al., 2014. Long term effects of treatment interruptions in adults and children. In *Conference on Retroviruses and Opportunistic Infections*. Boston, MA.

Thompson, P.M. & Jahanshad, N., 2015. Novel Neuroimaging Methods to Understand How HIV Affects the Brain. *Current HIV/AIDS Reports*, 12(2), pp.289–298. Available at: http://www.ncbi.nlm.nih.gov/pubmed/25902966 [Accessed June 13, 2016].

Thornburgh, C.L. et al., 2017. Concordance of the Resting State Networks in Typically Developing, 6- to 7-Year-Old Children and Healthy Adults. *Frontiers in human neuroscience*, 11, p.199. Available at: http://www.ncbi.nlm.nih.gov/pubmed/28487641 [Accessed October 13, 2017].

Tiemeier, H. et al., 2010. Cerebellum development during childhood and adolescence: A longitudinal morphometric MRI study. *NeuroImage*, 49(1), pp.63–70. Available at: http://www.sciencedirect.com/science/article/pii/S1053811909008933 [Accessed October 10, 2017].

Toich, J. et al., 2016. Resting state functional connectivity correlates with infancy immune health in HIV-infected children. *Organization for Human Brain Mapping, 22nd Annual Meeting*. Available at: https://ww5.aievolution.com/hbm1601/index.cfm?do=abs.viewAbs&abs=1262.

Toich, J.T.. et al., 2017. Functional connectivity alterations in medial brain regions and associations with infant CD4 measures in HIV infected children on early ART: a study at age 7 years. Manuscript submitted for publication.

Tornatore, C. et al., 1994. HIV-1 infection of subcortical astrocytes in the pediatric central nervous system. *Neurology*, 44(3 Part 1), p.481. Available at: http://www.neurology.org/content/44/3_Part_1/481.abstract.

Tucker, K.A. et al., 2004. Neuroimaging in human immunodeficiency virus infection. In *Journal of Neuroimmunology*. pp. 153–162.

Uban, K.A. et al., 2015. White matter microstructure among youth with perinatally acquired HIV is associated with disease severity. *AIDS*, 29(9), pp.1035–1044. Available at: http://www.ncbi.nlm.nih.gov/pubmed/26125138 [Accessed June 10, 2018].

Uddin, L., Supekar, K. & Menon, V., 2010. Typical and atypical development of functional human brain networks: insights from resting-state FMRI. *Frontiers in systems neuroscience*, 4(May), p.21. Available at: http://www.ncbi.nlm.nih.gov/pubmed/20577585 [Accessed July 27, 2017].

UNAIDS, 2016. Fact Sheet 2016 - Latest statistics on the status of the AIDS epidemic. Available at: http://www.unaids.org/sites/default/files/media_asset/UNAIDS_FactSheet_en.pdf [Accessed November 13, 2017].

UNAIDS, 2015a. *How AIDS changed everything*, Geneva, Switzerland. Available at: http://www.unaids.org/sites/default/files/media_asset/MDG6Report_en.pdf.

UNAIDS, 2015b. *Progress report on the global plan towards the elimination of new HIV infections among children and keeping their mothers alive, 2015.*, Geneva, Switzerland. Available at: http://www.unaids.org/sites/default/files/media_asset/JC2774_2015ProgressReport_GlobalPl

an_en.pdf.

Valcour, V. et al., 2012. Central Nervous System Viral Invasion and Inflammation During Acute HIV Infection. *The Journal of Infectious Diseases*, 206(2), pp.275–282. Available at: +.

Vatansever, D., Menon, D.K. & Stamatakis, E.A., 2017. Default mode contributions to automated information processing. *Proceedings of the National Academy of Sciences*, p.201710521. Available at: http://www.ncbi.nlm.nih.gov/pubmed/29078345 [Accessed November 3, 2017].

Vella, S. et al., 2012. The history of antiretroviral therapy and of its implementation in resource-limited areas of the world. *AIDS*, 26(10), pp.1231–1241. Available at: http://content.wkhealth.com/linkback/openurl?sid=WKPTLP:landingpage&an=00002030-201206190-00012 [Accessed November 22, 2017].

Van De Ven, V.G. et al., 2004. Functional connectivity as revealed by spatial independent component analysis of fMRI measurements during rest. *Human Brain Mapping*, 22(3), pp.165–178. Available at: http://doi.wiley.com/10.1002/hbm.20022 [Accessed November 10, 2017].

Vigano, A. et al., 2010. Tenofovir disoproxil fumarate and bone mineral density: A 60-month longitudinal study in a cohort of HIV-infected youths. *Antiviral Therapy*, 15(7), pp.1053–1058.

Vincent, J. et al., 1989. Neurologic symptoms as the initial presentation of HIV infection in pediatric patients. In *Fifth International Conference on AIDS*. pp. 4–9.

Vincent, J.L. et al., 2007. Intrinsic functional architecture in the anaesthetized monkey brain. *Nature*, 447, p.83. Available at: http://dx.doi.org/10.1038/nature05758.

Violari, A. et al., 2008. Early antiretroviral therapy and mortality among HIV-infected infants. *The New England journal of medicine*, 359(21), pp.2233–2244. Available at: http://www.pubmedcentral.nih.gov/articlerender.fcgi?artid=2950021&tool=pmcentrez&rendertype=abstract [Accessed June 30, 2016].

Volberding, P.A. et al., 1995. A comparison of immediate with deferred zidovudine therapy for asymptomatic HIV-infected adults with CD4 cell counts of 500 or more per cubic millimeter. AIDS Clinical Trials Group. *New England Journal of Medicine*, 333(7), pp.401–407. Available at: http://www.nejm.org/doi/abs/10.1056/NEJM199508173330701 [Accessed November 25, 2017].

Walker, S.Y. et al., 2013. Neurocognitive function in HIV-positive children in a developing country. *International Journal of Infectious Diseases*, 17(10), pp.e862–e867. Available at: http://www.sciencedirect.com/science/article/pii/S1201971213001057?via%3Dihub [Accessed December 2, 2017].

Wang, L. et al., 2012. Alzheimer disease family history impacts resting state functional connectivity. *Annals of Neurology*, 72(4), pp.571–577. Available at: http://doi.wiley.com/10.1002/ana.23643 [Accessed July 22, 2016].

Wang, L. et al., 2006. Changes in hippocampal connectivity in the early stages of Alzheimer's disease: Evidence from resting state fMRI. *NeuroImage*, 31(2), pp.496–504.

Wang, X. et al., 2011. Abnormalities in Resting-State Functional Connectivity in Early Human Immunodeficiency Virus Infection. *Brain Connectivity*, 1(3), pp.207–217. Available at: http://www.ncbi.nlm.nih.gov/pubmed/22433049 [Accessed June 16, 2016].

Weissenbacher, A. et al., 2009. Correlations and anticorrelations in resting-state functional connectivity MRI: A quantitative comparison of preprocessing strategies. *NeuroImage*, 47(4), pp.1408–1416. Available at: https://ac-els-cdn-com.ezproxy.uct.ac.za/S105381190900487X/1-

s2.0-S105381190900487X-main.pdf?_tid=896d5c48-c51a-11e7-a5fe-00000aacb362&acdnat=1510210522_36cb5d2a6ad7e2fcd46a1beb9ba877af [Accessed November 9, 2017].

WHO, 2006a. *Antiretroviral therapy for HIV infection in adults and adolescents: recommendations for a public health approach*, World Health Organization.

WHO, 2006b. *Antiretroviral therapy of HIV infection in infants and children: towards universal access: recommendations for a public health approach*, World Health Organization.

WHO, 2016. *Consolidated guidelines on the use of antiretroviral drugs for treating and preventing HIV infection: recommendations for a public health approach*, Available at: http://apps.who.int/iris/bitstream/10665/208825/1/9789241549684_eng.pdf?ua=1 [Accessed November 13, 2017].

WHO, 2010. *PMTCT strategic vision 2010–2015 : preventing mother-to-child transmission of HIV to reach the UNGASS and Millennium Development Goals*, Available at: http://www.who.int/hiv/pub/mtct/strategic_vision.pdf [Accessed November 13, 2017].

Wiktor, S.Z., Ekpini, E. & Nduati, R.W., 1997. Prevention of mother-to-child transmission of HIV-1 infection. *AIDS (London, England)*, 11 Suppl A, pp.S79-87. Available at: https://www.popline.org/node/281400 [Accessed November 13, 2017].

Williams, P.L. et al., 2013. Pubertal onset in children with perinatal HIV infection in the era of combination antiretroviral treatment. *AIDS*, 27(12), pp.1959–1970. Available at: http://www.ncbi.nlm.nih.gov/pubmed/24145244 [Accessed October 18, 2017].

Winkler, A.M. et al., 2014. Permutation inference for the general linear model. *NeuroImage*, 92, pp.381–397. Available at: http://www.sciencedirect.com/science/article/pii/S1053811914000913 [Accessed June 14, 2017].

Wood, S. et al., 2009. The impact of AIDS diagnoses on long-term neurocognitive and psychiatric outcomes of surviving adolescents with perinatally acquired HIV. *Aids*, 23(14), pp.1859–1865. Available at: https://www.google.co.uk/#q=Wood+SM%2C+Shah+SS%2C+Steenhoff+AP%2C+Rutstein+RM.+The+impact+of+AIDS+diagnoses+on+long-term.

Wu, K. et al., 2013. Topological Organization of Functional Brain Networks in Healthy Children: Differences in Relation to Age, Sex, and Intelligence X.-N. Zuo, ed. *PLoS ONE*, 8(2), p.e55347. Available at: http://dx.plos.org/10.1371/journal.pone.0055347 [Accessed August 9, 2017].

Yadav, S.K. et al., 2017. Altered structural brain changes and neurocognitive performance in pediatric HIV. *NeuroImage: Clinical*, 14(Supplement C), pp.316–322. Available at: http://www.sciencedirect.com/science/article/pii/S2213158217300323.

Yan, C.G. et al., 2013. A comprehensive assessment of regional variation in the impact of head micromovements on functional connectomics. *NeuroImage*, 76, pp.183–201.

Yarkoni, T. et al., 2011. Large-scale automated synthesis of human functional neuroimaging data. *Nature Methods*, 8(8), pp.665–670. Available at: http://www.ncbi.nlm.nih.gov/pubmed/21706013 [Accessed May 3, 2017].

Yeo, B.T.T. et al., 2011. The organization of the human cerebral cortex estimated by intrinsic functional connectivity. *Journal of Neurophysiology*, 106(3), pp.1125–65. Available at: http://jn.physiology.org/content/106/3/1125.full.pdf+html [Accessed July 28, 2017].

Zhu, Q. et al., 2011. Resting-State Neural Activity across Face-Selective Cortical Regions Is Behaviorally Relevant. *Journal of Neuroscience*, 31(28), pp.10323–10330. Available at: http://www.ncbi.nlm.nih.gov/pubmed/21753009 [Accessed November 10, 2017].

Zidovetzki, R. et al., 1998. Human Immunodeficiency Virus Tat Protein Induces Interleukin 6 mRNA Expression in Human Brain Endothelial Cells via Protein Kinase C- and cAMP-Dependent Protein Kinase Pathways. *AIDS Research and Human Retroviruses*, 14(10), pp.825–833. Available at: https://doi.org/10.1089/aid.1998.14.825.

Zijenah, L.S. et al., 2005. T lymphocytes among HIV-infected and -uninfected infants: CD4/CD8 ratio as a potential tool in diagnosis of infection in infants under the age of 2 years. *Journal of Translational Medicine*, 3(1), p.6. Available at: https://doi.org/10.1186/1479-5876-3-6.

Zuo, X.-N. et al., 2010. Reliable Intrinsic Connectivity Networks: Test-Retest Evaluation Using ICA and Dual Regression Approach. *NeuroImage*, 49(3), pp.2163–2177.

Appendix A: Parameters passed to afni_proc.py

The afni_proc.py command forms part of the AFNI toolbox (Cox 1996). The shell variables $subjectName, $restSet, $anatSet and $atlas are respectively set for each subject's patient identification, the path of the resting state EPI data, the path of the anatomical volume, and the path of the Haskins Pediatric Brain nonlinear template version 1.0 (Molfese et al. 2015).

```
afni_proc.py                                                          \
-subj_id $subjectName                                                 \
-dsets $restSet                                                       \
-copy_anat $anatSet                                                   \
-anat_has_skull no                                                    \
-scr_overwrite                                                        \
-blocks despike tshift align tlrc volreg blur mask scale regress      \
-tcat_remove_first_trs 4                                              \
-tshift_interp -Fourier                                               \
-volreg_align_to MIN_OUTLIER                                          \
-align_opts_aea -AddEdge -save_epi_ns -giant_move -epi_strip
3dAutomask                                                            \
-tlrc_base $atlas                                                     \
-tlrc_NL_warp                                                         \
-volreg_align_to MIN_OUTLIER
-volreg_align_e2a                                                     \
-volreg_tlrc_warp                                                     \
-regress_anaticor                                                     \
-regress_bandpass 0.01 0.2                                            \
-regress_apply_mot_types demean deriv                                 \
-regress_run_clustsim no                                              \
-regress_est_blur_epits                                               \
-regress_est_blur_errts
```

Appendix B: Details of preprocessing blocks and supporting theory

This section discusses the blocks involved in the preprocessing pipeline (Figure 4 of Section 6.3.1), and motivates design decisions with supporting theory. We describe, in order, the operations performed in native (subject-specific) space, the transformation from native to standard space, and the operations performed in standard (template) space.

Preprocessing in native space

The first four EPI volumes were removed to allow for a steady state magnetisation assumption for all subsequent volumes (Gotts et al. 2012). With a flip angle of 90 degrees, the longitudinal net magnetisation is nullified with each RF pulse, such that a longitudinal steady state is reached after just one pulse. Discarding a few extra volumes additionally takes into account the effect of a having a repetition time (TR) that is short relative to the transverse relaxation time, especially the larger relaxation time of CSF (Condon et al. 1987). Without sufficient time for the transverse magnetisation to decay completely before the application of the next RF pulse, echoes of this residual magnetisation are added to the new transverse magnetisation (Buxton 2009); but after a few pulses, the effect becomes constant.

Intensity spikes (large transients) in each voxel's time course were suppressed. Suppression was proportional to the extent to which the spike violated smoothness constraints (Jo et al. 2013). The AFNI research team has qualitatively demonstrated the benefit of despiking for rigid-body motion correction (Jo et al. 2013). This benefit was also observed in our sample. Slice timing alignment was used to align the two-dimensional slices of each EPI volume to the same temporal origin by interpolation, allowing subsequent processing to treat whole volumes as having been acquired instantaneously.

Moving from native to standard space

For multi-subject analysis to be performed, it is not only required that a voxel's time course refers always to the same point in that subject's brain (that is, that motion be corrected), but that it refers to the same point in a common reference frame provided by a standard brain template, such as that proposed by Talairach and Tournoux (1988). To this end, each subject's EPI volumes underwent three transformations (which are further unpacked in the following paragraphs): within-run volume coregistration; alignment to the T1-weighted volume; and spatial normalisation to the Haskins Pediatric Brain template (Molfese et al. 2015). Though computed consecutively, these transforms were combined into a single operation to avoid multiple resampling costs. The T1 volumes were skull-stripped such that only brain matter was considered in the calculation of transforms; the outputs of this process were visually inspected, and subject-specific tuning of skull-stripping parameters was applied where necessary. Non-brain matter was likewise masked in the EPI data for the purposes of calculating transforms (using a simpler histogram-based segmentation), but the masking was not carried forward to later analyses.

Volume coregistration within each EPI run, which aligns volumes to a base volume in the series, was employed to correct for rigid-body motion (Cox & Jesmanowicz 1999). The volume with the minimum fraction of outlier voxel values was selected as the base, since it would likely be the least distorted by (rigid-body and intra-TR) motion. As the template in atlas-space is not a linear transformation of any of the subjects, a nonlinear full warping registration is needed to move the EPI volumes into this domain, an operation which requires much anatomical information to be present in the data (Jenkinson 2009). The EPI data, while being sensitive to BOLD signal changes, contains minimal anatomical information. A two-stage process is therefore adopted. Firstly, each EPI volume is aligned to that subject's skull-stripped T1 volume, imputing the anatomical information of the latter to the former. Secondly, the T1 volume is registered to the brain template and the same transformation is applied to the EPI series. For the EPI-to-T1 alignment, an affine transformation with a local Pearson

correlation cost function — evaluated over the minimum outlier EPI volume — performed best by visual inspection. Either a low dimensional affine transform or a high dimensional non-linear warping transform can be employed for the T1-to-template registration. Non-linear warping better matches local anatomical structures between subjects (Crinion et al. 2007), but is also more easily confounded by mismatch between the native brain and the template. For our sample, non-linear warping produced the most accurate and reliable registration to the template.

In all subjects, some protrusion of the occipital and frontal poles was observed in the spatially-normalised EPI relative to the template, as illustrated in Figure B-1. This was not an artefact of registration — internal structures were well registered — but rather of slight geometric distortion along this axis in the original EPI. Such distortion is frequently observed in EPI pulse sequences because of B_0 field inhomogeneities, which in turn arise from differences in magnetic susceptibility between different tissues at air/tissue interfaces (Buxton 2009; Smith et al. 2004). Because a complete B_0 field map was not acquired as part of the imaging sequence, this minor artefact was not corrected.

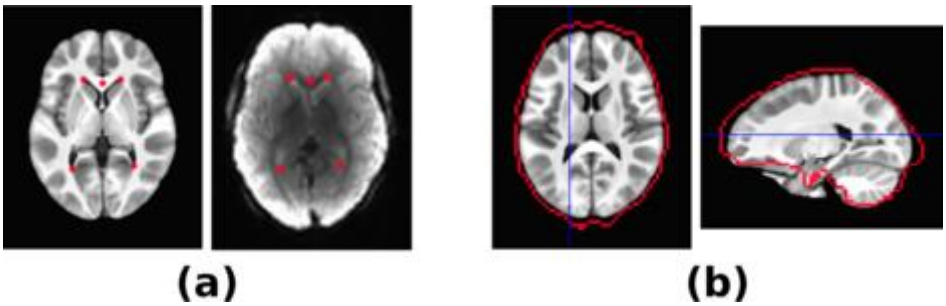

*Figure B-1: **(a)** Correspondence of a sample of landmarks (anterior pole of corpus callosum; in-slice ventricular boundaries) between the registered EPI and the template. **(b)** Outline of the registered EPI (extracted from a brain mask) superimposed on the template. While internal structures are well aligned – as seen in (a) – registration cannot (indeed, should not) accommodate exaggerated elongations along the anterior-posterior axis caused by B_0 inhomogeneity.*

<u>*Preprocessing in standard space*</u>

To improve signal to noise ratio, the registered EPI data was spatially smoothed with a Gaussian kernel of full width at half maximum (FWHM) 6 mm. The resultant volume was output as an intermediate 'partially-preprocessed' EPI dataset, employed purely for the estimation of group ICA components. To obtain a 'fully-preprocessed' dataset suitable for input to statistical analyses, nuisance regression and

temporal filtering were additionally performed in standard space to isolate, as far as possible, the neuronal signal of interest.

Mean, linear and quadratic trends were removed, to account for slow baseline signal fluctuations such as scanner drift (Jo et al. 2013). Motion realignment parameters previously estimated during volume coregistration were regressed out along with their first derivatives, ameliorating the complex secondary motion effects produced by spin-history disturbances (Pruim et al. 2015). A combination of tissue-based regression and temporal bandpass filtering was used to suppress physiological noise (resulting from respiration and heart cycle) and hardware-related artefacts, as well as to further suppress motion bias (Jo et al. 2010). While tissue-based regression generally aims to isolate confounds by extracting regionally non-specific covariance, projecting regressors out of very large regions will not effectively handle (in fact, will spread) locally fluctuating transient hardware artefacts (Jo et al. 2010). A local white matter regressor was therefore employed which at each voxel in the white matter mask is averaged over a 15 mm radius, as opposed to a regressor averaged over the entire mask (Jo et al. 2010). Regressors were not projected out of grey matter or CSF, as the signal in these regions may be correlated with the grey matter signal of interest[41]. Doing so may warp individual connectivity matrices and invalidate group contrasts (Gotts et al. 2013; Saad et al. 2012).

Temporal bandpass filtering was performed outside the interval of 0.01 Hz to 0.2 Hz. The more common lowpass limit of 0.1 Hz (Lee et al. 2013) has been relaxed to 0.2 Hz, in light of recent warnings against violating sample independence to levels where statistics computed on the signals are meaningless (Davey et al. 2013). It is worth noting that some studies, including the Human Connectome Project (Smith et al. 2013), choose to omit low pass filtering entirely (Shirer et al. 2015) — in such cases, signal content is still capped by the excitation pulse repetition time (TR), according to Nyquist criteria (the highest frequency contained being $\frac{1}{2 \cdot TR}$).

[41] This is strictly on true for non-ventricular CSF.

Every ‘partially-preprocessed’ and ‘fully-preprocessed’ 4-dimensional rs-fMRI dataset was grand-mean intensity normalised using a single multiplicative factor, as is common (Sato et al. 2015; Smith et al. 2014; Starck et al. 2013), to meet assumptions of subsequent statistical analyses.

Appendix C: Cluster-size thresholds employed in independent component analysis

Table C-1: Cluster-size thresholds calculated using AFNI's (Cox 1996) 3dClustSim module for each resting state network. This threshold is the minimum aggregate volume required for a cluster of voxels, each voxel revealing a 'significant' effect, to meet the chosen cluster-level false discovery rate of 5%. This volume is determined by a Monte Carlo simulation that is parameterised by the inherent spatial smoothness of fMRI noise in the spatial domain of each network, since we aim to exclude clusters that could have been formed by random noise alone. The spatial smoothness and cluster-size values were calculated using AFNI's new 'mixed autocorrelation function' methodology (Cox et al. 2017), which takes into consideration the deviation of the distribution of fMRI noise from the Gaussian distribution.

RSN name, abbreviated	**RSN name, full**	**Cluster-size threshold (mm^3) for a cluster-forming threshold of $p < 0.005$**	**Cluster-size threshold (mm^3) for a cluster-forming threshold of $p < 0.001$**
latVN	Lateral visual network	459	189
medVN	Medial visual network	567	243
aDMN	Anterior default mode network	432	189
pDMN	Posterior default mode network	486	216
SAL	Salience network	432	189
CER	Cerebellar network	351	162
SSN	Somatosensory network	405	189
DAN	Dorsal attention network	486	216
L-PAR	Left-lateralised frontoparietal network	513	216
TPN	Temporoparietal network	459	189
aPFC	Anterior prefrontal cortex	378	189
BGN	Basal ganglia network	297	135

RSN, resting state network.

Appendix D: Nuisance features observed in group components revealed by group independent component analysis

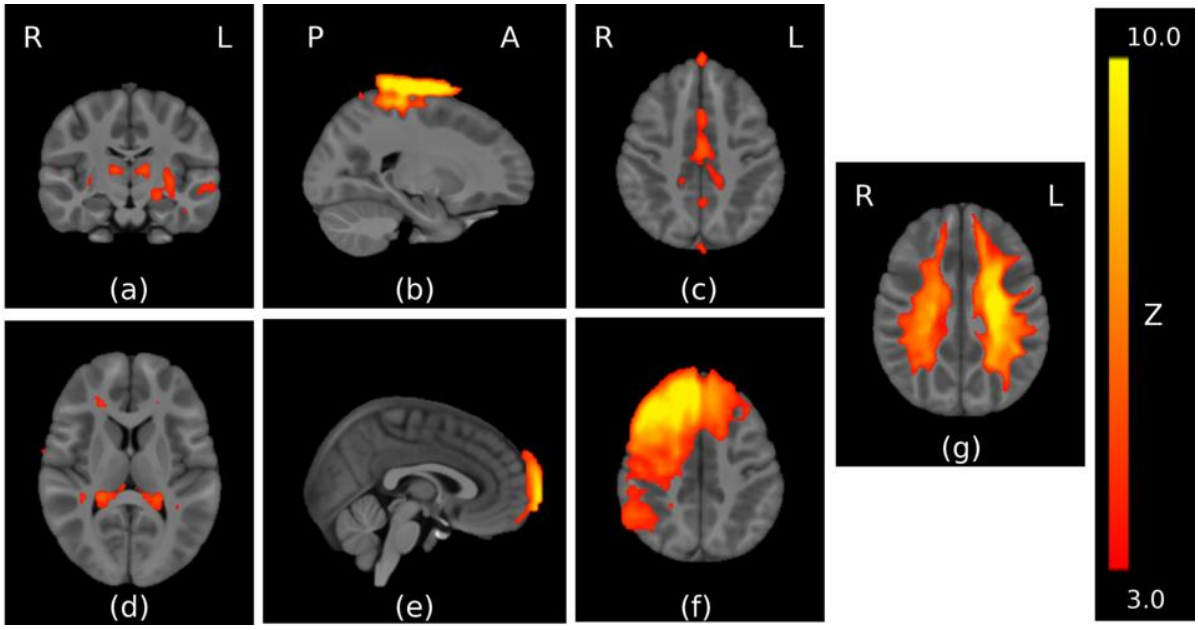

Figure D-1: Spatial characteristics typical of artefactual ICs (Kelly et al. 2010) that were observed in our group independent component analysis (ICA) decomposition. Components presenting these characteristics were excluded from later voxelwise analyses. (a) Significant contribution from a blood vessel network (BVN); specifically, from the horizontal M1-segment of the middle cerebral artery. (b) Clusters are largely peripheral or lie outside of the brain. (c) Coactivation in the sagittal sinus. (d) Coactivation in CSF. (e) Structured ring-like pattern on periphery. (f) Improbably expansive coactivation, with little regard for GM boundaries. (g) Large central WM clusters. ICs are here shown thresholded using alternative hypothesis testing at $p > 0.95$.

Appendix E: Associations of functional connectivity with immune measures, before controlling for age voxelwise

Table E-1: Size and peak coordinates of regions showing significant association of immune health with functional integration into the cerebellar network (obtained using ICA). Clusters are grouped first by the modelled immune effect, and secondly by the cluster-forming threshold. Also given are correlations of the immune measure with the average functional connectivity (FC) over the cluster (all are positive), as well as group means of the cluster-averaged functional connectivity. Cluster labels (A – C) correspond with those in Figure E-1.

ICA-generated network	Cluster anatomical location[a]	Cluster peak coordinates (MNI, LPI) *x*	*y*	*z*	Cluster volume (mm^3)	Correlation[b] of immune measure with FC averaged over the cluster region (r)	Cluster label
CD4% in infancy (at age 6–8 weeks) associated with within-network FC at age 9 years							
Cluster-forming threshold: $p < 0.005$							
Cerebellar (CER)	L cerebellar hemisphere: crus1 and crus2 (lobule 7) in the mid and lateral regions	**-36**	**-63**	**-44**	2295	0.548	A
Cerebellar (CER)	L cerebellar hemisphere: midzone of lobule 8	-26	-66	-55	675	0.335	B
Cluster-forming threshold: $p < 0.001$							
Cerebellar (CER)	L cerebellar hemisphere: crus1 and crus2 (lobule 7) in the mid and lateral regions	**-36**	**-63**	**-44**	486	0.509	A*
CD4% at scan (at age 9 years) associated with within-network RSFC at age 9 years							
Cluster-forming threshold: $p < 0.005$							
Cerebellar (CER)	L cerebellar hemisphere: crus1 and crus2 (lobule 7) in the mid and lateral regions	-39	-63	-44	864	0.628	C

ICA, independent component analysis; **MNI**, Montreal Neurological Institute 152 atlas; **LPI**, left-posterior-inferior; **FC**, [resting state] functional connectivity.
HU, HIV-unexposed uninfected; **HEU,** HIV-exposed uninfected; **HIV-**, HIV-uninfected; **HIV+,** HIV-infected.
[a] Based on cluster overlap in Haskins pediatric atlas.
[b] Values are Pearson correlation coefficients.

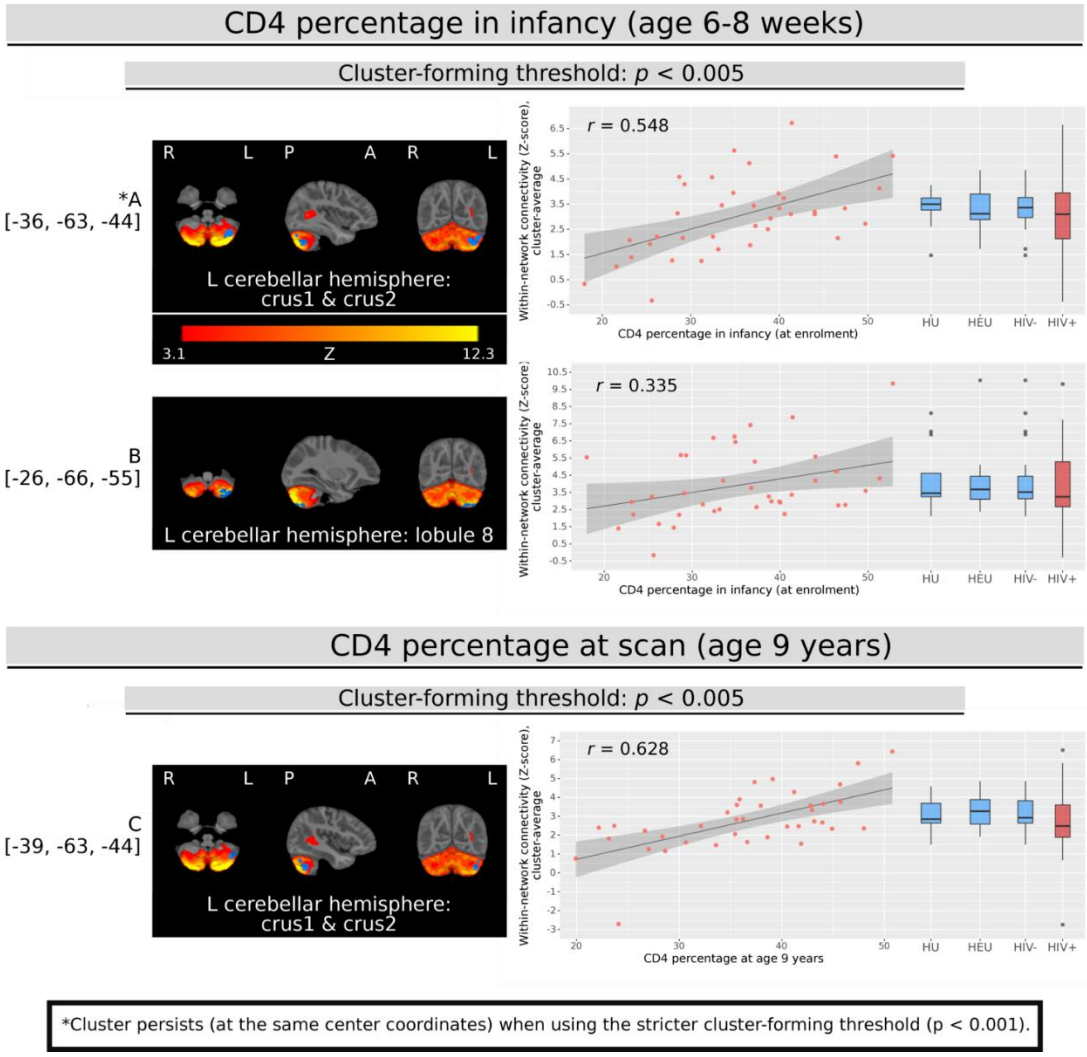

Figure E-1: ***(Left)*** *The cerebellar resting state network (hot colours) revealed clusters (blue) of significant association of within-network connectivity, as measured at age 9 years, with CD4%, as measured at both enrolment (age 6-8 weeks) and at age 9 years. Cluster-forming thresholds of p < 0.001 and p < 0.005 were combined with cluster-size thresholds to yield a corrected cluster significance of p < 0.05 (two-sided) in all cases. The network's group map is thresholded at Z > 3. The saturation levels for the network's heatmap are the 2nd and 98th percentiles of non-zero Z-score values.* ***(Right)*** *Plots of the average connectivity Z-scores in the cluster region against the associated immune health measure. Alongside are distributions of connectivity Z-scores, averaged over the cluster region, for the various groups. The alphabetic cluster labels in the left margin (A – C) reference the cluster details in Table E-1. Coordinates under the cluster labels are those of the peak association, in MNI standard space, using left-posterior-inferior (LPI) convention.*

END